P
2mi4

NASA TECHNICAL NOTE

NASA TN D-7301

NASA TN D-7301

EXPERIMENTAL VALIDATION OF A LANDING-DYNAMICS COMPUTER PROGRAM FOR LEGGED SPACECRAFT LANDERS

by John R. McGehee and Sandy M. Stubbs

Langley Research Center
Hampton, Va. 23665

NATIONAL AERONAUTICS AND SPACE ADMINISTRATION • WASHINGTON, D. C. • DECEMBER 1973

1. Report No.	2. Government Accession No.	3. Recipient's Catalog No.
NASA TN D-7301		

4. Title and Subtitle	5. Report Date
EXPERIMENTAL VALIDATION OF A LANDING-DYNAMICS COMPUTER PROGRAM FOR LEGGED SPACECRAFT LANDERS	December 1973
	6. Performing Organization Code

7. Author(s)	8. Performing Organization Report No.
John R. McGehee and Sandy M. Stubbs	L-8726
	10. Work Unit No.
	815-20-09-01

9. Performing Organization Name and Address	11. Contract or Grant No.
NASA Langley Research Center Hampton, Va. 23605	
	13. Type of Report and Period Covered
	Technical Note

12. Sponsoring Agency Name and Address	14. Sponsoring Agency Code
National Aeronautics and Space Administration Washington, D.C. 20546	

15. Supplementary Notes

16. Abstract

Validation of a landing-dynamics computer program has been accomplished by comparing analytical data with data from a limited experimental program. Agreement obtained establishes the subject landing-dynamics computer program as a reliable design tool for legged spacecraft landers.

17. Key Words (Suggested by Author(s))	18. Distribution Statement
Landing-dynamics computer program Legged spacecraft landers	Unclassified – Unlimited

19. Security Classif. (of this report)	20. Security Classif. (of this page)	21. No. of Pages	22. Price*
Unclassified	Unclassified	71	Domestic, $3.50 Foreign, $6.00

*For sale by the National Technical Information Service, Springfield, Virginia 22151

EXPERIMENTAL VALIDATION OF A LANDING-DYNAMICS COMPUTER PROGRAM FOR LEGGED SPACECRAFT LANDERS

By John R. McGehee and Sandy M. Stubbs
Langley Research Center

SUMMARY

A study, comparing data from a 3/8-scale dynamic model and an analytical model of a legged spacecraft lander, was conducted to validate experimentally a landing-dynamics computer program for such landers. The results of this study showed that good agreement was obtained between analytical and experimental center-of-gravity accelerations, primary-strut strokes, strut forces, and vehicle motions. Landing-surface characteristics significantly influence the stability characteristics and loads imposed upon the vehicle. Landing-gear unsprung mass, footpad-to-surface friction coefficients, and the presence or absence of the primary-strut deadband have significant effects on the stability characteristics of legged landers. The agreement obtained between analytical and limited experimental data established that the computer program employed in this study can be used with confidence as a design tool for legged spacecraft landers.

INTRODUCTION

The development of spacecraft for accomplishing soft landings on Mars or other planets has in the past required extensive model testing to insure the structural integrity of the landing gear and primary body structures and to assure vehicle stability for the most severe landing condition that the spacecraft is expected to encounter. Some previous spacecraft designed for soft landings have used legged-type landing gears. The results obtained from analytical studies of legged landers are presented in references 1 through 7. The analyses developed in the above studies were generally limited to a specific landing-gear design and because of project schedules were necessarily restricted in scope.

The purpose of this paper is to present comparative results obtained from analytical and experimental investigations of the landing dynamics of a legged lander to

determine the validity of the analysis of reference 8. A 3/8-scale model of an early version of the Viking spacecraft lander was used in the experimental portion of this investigation. The comprehensive analysis employed in this study includes consideration of the overall vehicle structural elastic effects on landing dynamics, variation of landing-surface characteristics, unsprung mass of the landing gear, and inverted tripod and cantilever types of landing gears (from three to five landing legs) and has an additional capability of defining loads throughout the spacecraft structure. The analysis has been programmed for operation on a digital computer. The analytical procedure and computer input-output information are presented in references 8 and 9.

SYMBOLS

Values are given in both SI and U.S. Customary Units. The measurements and calculations were made in U.S. Customary Units.

a_X, a_Y, a_Z	normal, lateral, and longitudinal acceleration, respectively, m/s^2 (ft/sec^2) or earth g units
I_X, I_Y, I_Z	mass moment of inertia about the X-, Y-, and Z-axis, respectively, $kg\text{-}m^2$ $(slug\text{-}ft^2)$
L,R	left-hand and right-hand secondary struts respectively, when externally observed with line-of-sight coincident with footpad-pivot and c.g.
P	primary strut
V_H, V_V	horizontal and vertical velocity, respectively, m/s (ft/sec)
X,Y,Z	axes
1,2,3	landing-leg designation
β	gravitational scale factor, earth gravity/Mars gravity
ζ	surface slope

λ	geometric scale factor
μ	footpad-to-surface friction coefficient

Subscripts:

gcs	gravity coordinate system
scs	surface coordinate system
vcs	vehicle coordinate system
max	maximum values

SCALING LAWS

The scale relationships pertinent to this investigation are shown in table I. These scale relationships provide for the conduct of free-body model tests in earth's gravity field and the prediction of full-scale results in Mars' gravity field. Comparison of results obtained using this scaling technique are made with data obtained using an elastic-suspension-model test procedure for simulating Martian gravity in reference 10 and good agreement was obtained. The scale factors for the quantities shown with an asterisk (table I) were chosen to provide a suitable model for small-scale testing. The geometric scale factor ($\lambda = 3/8$) was selected to allow a stiff construction, a suitable size, and a proper mass distribution and also for convenience in conducting the tests. The scale factor for stress was assigned the value of unity to permit the structural scaling of the load alleviators. The gravitational scale factor ($\beta = 8/3$) was dictated by the fact that the force of the earth's gravity field is approximately 8/3 times that of Mars. The assignment of the scaling relationships for geometry, stress, and gravitational force thus determines other pertinent scale relationships according to the laws of physics for a dynamically scaled model.

DESCRIPTION OF MODELS

The general arrangement of both the experimental and the analytical models is given in figure 1 together with the coordinate-system axes.

The 3/8-Scale Experimental Model

A 3/8-scale dynamic model of an early version of the Viking lander was tested in the experimental portion of this investigation. A photograph of the 3/8-scale experimental model is shown in figure 2 and details of the landing gear are presented in figures 3 to 6. Pertinent parameters for the 3/8-scale model are presented in table II. A description of the test model center body and landing gear follows.

Center body.- The center-body structure (see fig. 2) is a hexagonally shaped box with the upper and lower surfaces having integrally machined stiffeners. The side plates and landing-gear attachment plates are riveted to the upper and lower plates, thus completing the box structure. A cylindrical section is riveted to the upper and lower plates with the longitudinal axis coincident with the vertical axis of symmetry of the center body. This cylinder serves as a base for attaching the drop-release adaptor and the center-of-gravity accelerometer mounting plate. The center-body construction was as light as possible to allow for ballast weight for obtaining the desired mass, mass moments of inertia, and center-of-gravity location. It was also made as stiff as possible, by filling the box interior with balsa wood glued in place, in order to minimize structural elastic effects on measured data.

Landing gear.- As noted in figures 1 and 2, the landing gear consists of three legs located at 120° intervals on the center body. Each leg is an inverted-tripod arrangement consisting of one primary and two secondary struts. The primary struts contain columns of four force-staged crushable, aluminum alloy, honeycomb elements for load alleviation and energy dissipation. These struts are pinned at the center-body attachment points and at the tripod-vertex mounting blocks to permit rotation in the vertical plane to alleviate any bending loads. The pinned attachments are made with self-alining ball bearings to reduce friction and to permit limited differential stroking of the secondary struts without causing primary strut binding.

The secondary struts are stiff, tubular members which serve as stabilizing elements for the primary struts. These are attached to the center-body structure through bending-element load alleviators (see fig. 3) to limit the loads transmitted to the center body. Both secondary struts on each leg are pinned at one end to their respective load alleviators with self-alining ball bearings to permit rotation in the vertical and horizontal planes. At the other end, one of the secondary struts is rigidly attached to the tripod-vertex mounting block. The remaining secondary strut is pinned

about a single axis at the tripod vertex to permit rotation in the plane of the two secondary struts. This arrangement permits unrestricted leg rotation in the vertical plane and limited rotation of the leg in the plane containing the secondary struts.

A stiff, non-shock-absorbing footpad is rigidly attached to the tripod-vertex mounting block and the footpad design is shown in figure 4. For some landings spikes, one of which is also shown in the figure, were used in lieu of the footpads to simulate an infinite coefficient of friction by constraining the motion of the tripod vertex.

Force-stroke characteristics for the primary and secondary struts are presented in figure 5. These characteristics were determined from dynamic tests of the model primary strut, and pseudo-static tests of the model secondary-strut load alleviators.

The tension force-stroke curve for the secondary struts is assumed to have the same shape as the compression force-stroke curve. When compression is the initial loading, the tension force-stroke curve originates at the bottom of the elastic unloading curve shown typically in figure 5. This assumption neglects the effects of strain-hardening and geometric changes in the load alleviators; however, pseudo-static tests of the load alleviators, which had previously been compressively deformed, did not exhibit discernible changes in the load-stroke characteristics when loaded and plastically deformed by strut tension loads.

The unsprung mass of each landing leg, that portion of the landing-leg mass which must be rapidly decelerated and brought to rest at touchdown, consisted of the mass of the footpad, and a portion of the masses of the tripod-vertex mounting block, the secondary struts, and the primary-strut piston and piston rod.

A few model tests were conducted using a ratchet mechanism in the primary strut to eliminate the strut "deadband." The term deadband refers to the extension of the primary strut from a compressed position at essentially zero load. The ratchet mechanism employed in these tests is shown schematically in figure 6 and consisted of two spring-loaded square pawls mounted in a tube and installed in the piston rod. The pawls were restrained by the cylinder walls during the compression stroke and engaged slots in the cylinder walls during the extension strokes, thus preventing full extension of the piston rod.

Analytical Model

The scale relationships shown in table I were employed to obtain the full-scale values for defining the geometry, mass properties, and forces required as inputs to

the computer program. Values of these pertinent parameters for the analysis are given in figures 1, 3, 4, and 5 and table II.

The mass moments of inertia required as inputs to the computer program are those of the center body and the unsprung portion of the landing gear. Due to the difficulty in determining the effective unsprung-mass moments of inertia, various values of these moments of inertia were used as inputs to the computer program to determine that value which resulted in obtaining the best agreement between computed and experimental time-history data from an early experimental test. This value of unsprung inertia was used to determine the unsprung mass of each landing leg when the mass was assumed concentrated at the vertex of each tripod. Since the total vehicle inertias about the three axes of the experimental model were obtained using the bifilar pendulum method, the center-body inertias were obtained by subtracting the inertias of the unsprung mass of the landing gear from the total-vehicle inertias.

The input force-stroke characteristics of the primary struts were the full-scale values of those of the experimental model as presented in figure 5(a). For those tests in which the ratchet was used in the primary strut to remove the deadband, the tension force-stroke characteristics were represented by a linear spring whose spring rate was the same as that of the compressive unloading spring rate (dashed line in fig. 5(a)).

Because of the limit of the computer program capability the nonlinear compressive force-stroke characteristics of the secondary struts were represented by only five straight line segments as shown in figure 5(b). The representation of the tension force-stroke characteristics, again because of computer program limitations, consisted of a linear spring whose spring rate was equal in magnitude to the compressive unloading spring rate.

APPARATUS AND PROCEDURE

The test apparatus and test parameters for the experimental model are described. The input parameters required by the landing-dynamics computer program for the computations performed in the analytical investigation are also described. All values are full scale unless designated otherwise.

Experimental Test Apparatus

Drop pendulum.- A photograph of a model test setup is shown in figure 7 and a sketch illustrating operation of the drop pendulum during model launch and landing is shown in figure 8. The pendulum, with the model installed at the desired attitude, was released from a predetermined pull-back height to produce the desired horizontal velocity at the lowest point of the swing. The model was released from the pendulum carriage at the lowest point and the predetermined free-fall height produced the desired vertical velocity at model touchdown. The experimental tests were conducted in the impacting structures facility at the Langley Research Center.

Landing surface and surface friction coefficients.- The landing surface (schematically illustrated in fig. 8) was a steel-reinforced concrete slab covered with smooth plywood sheets. The plywood was anchored to the concrete surface at 0.3-m (1-ft) intervals in an effort to eliminate motions between the plywood and the concrete during a model landing. For accomplishing an investigation of the loads and motions of the model resulting from a landing in a soft soil, the landing surface was surrounded by side walls which permitted a soil depth of approximately 0.3 m (1 ft). The soil used was a black dune sand which had an angle of internal friction of approximately 32°, a mass density of 1200 kg/m^3 (2.3 slugs/ft^3), and a relative compaction factor assumed to be 0.1. The soil was not scaled to give proper full-scale Mars landing results but was used to obtain quantitative comparisons with data obtained on the hard landing surface and to permit validation of the computer program for a soft soil landing.

The friction coefficients at the footpad-surface interface, for landings on the hard surface, were determined by placing the model on the landing surface ($\zeta = 0^{\circ}$) and applying a deadweight load at the leading footpad with the line of action parallel to the landing surface. The load was systematically increased in small increments and after each added increment a force was manually applied at the center of gravity of the model to overcome static friction. When the deadweight load was sufficient to slide the model at a slow, relatively constant velocity, once the static friction was overcome, the friction coefficient was computed by dividing the deadweight load by the model weight.

A coefficient of friction of approximately 0.6 was obtained for the bare aluminum footpads sliding on the plywood surface. When a sheet of butyl rubber was attached to the footpads and a 400-grit abrasive paper attached to the landing surface, the friction

coefficient obtained between these surfaces was approximately 1.0. In order to obtain large values of resisting force between model and the landing surface, the footpads were removed and spikes having the same mass as the footpads were installed on the model. When these spikes were used during a model test, a dense fiberboard surface was installed over the plywood surface to avoid splintering of the plywood surface and thus provide greater constraint on the motion of the spike. The friction coefficent for landings made under these conditions is referred to in this paper as infinite.

Instrumentation and data reduction.- Normal, lateral, and longitudinal accelerations were measured at the model center of gravity by rigidly mounted piezoresistive strain-gage accelerometers. Stroke was measured for the primary strut of each leg using linear potentiometers. Strain gages were attached to all three struts of each leg and were calibrated to measure force. The signals from the accelerometers, potentiometers, and strain gages were transmitted through trailing cables to frequency-modulated magnetic tape recorders. The limiting flat frequency response of the accelerometers and potentiometers with the associated recording equipment was 1000 Hz. The limiting response for the strain-gage force measurements was 5000 Hz. In the process of data reduction, the acceleration and stroke data were passed through 300 Hz low-pass filters and the force data through 880 Hz low-pass filters to eliminate undesirable high-frequency structural oscillations. The data were digitized using a sample rate of 2000 samples per second and stored on tapes which were processed to obtain printouts and plots of the data.

Motion pictures (taken at 64 and 200 frames per second) were used to determine landing attitudes, touchdown velocities, and motions. A video camera, tape recorder, and receiver were used to obtain an immediate review of the test conditions and landing behavior.

Coordinate systems.- Sketches identifying coordinate systems, vehicle attitudes, and surface slopes are shown in figure 9. The three coordinate systems are used to locate the lander as a function of time. These consist of two coordinate systems fixed relative to the planet (gravity coordinate system and surface coordinate system) and one vehicle coordinate system moving with the lander, whose origin is at the vehicle center of gravity. All coordinate systems are right-handed and each has three orthogonal axes. Acceleration and velocity components have the same sense of direction as the coordinate axis along which they are defined. Compressive strut forces and strut strokes are assumed to be negative, while tension forces and strokes are assumed to be positive.

Computer Program

The analytical procedure and computer input-output information are presented in references 8 and 9. The landing-loads and motions computer program has the capability of predicting the landing dynamics of legged landers having up to five landing legs of the cantilever or inverted tripod type. Elasticity of the center-body structure and the leg structure can be included for the determination of internal and external loads and motions. The loads and stability of a legged-type lander can be determined for a lander simulated as a two-mass system (spring and damper connected center-body and unsprung masses) for hard or soil-type landing surfaces. The load alleviating primary struts may be modeled as containing crushable elements (stroke dependent) or hydraulic elements (velocity dependent) for energy absorption. For the stroke-dependent, crushable-element type of load alleviator, the deadband may be retained or removal of the deadband may be simulated. In the program the model is considered unstable when the gravity-force vector, originating at the center of gravity, intercepts the plane of the footpads outside of the triangular area bounded by the footpads.

Parameters Investigated

The experimental investigation was conducted primarily to provide data for validating landing-dynamics computer programs proposed for use in evaluating landing loads and motions of Viking lander designs. Consequently, the experimental program encompasses only a limited number of tests conducted for various touchdown and surface parameters.

Experimental test parameters.- The procedure used for establishing the model attitude for a test consisted of setting the pendulum carriage to the desired roll, pitch, and yaw angles. The roll angle is defined as the angle between the Z-axis of the vehicle coordinate system Z_{VCS} and the Z-axis of the gravity coordinate system Z_{GCS}. Similarly the pitch and yaw angles are defined as the angles between the X- and Y-axes of the vehicle coordinate system and the gravity coordinate system, respectively. The angles were set in the order of roll, pitch, and yaw. The heights of the pendulum carriage were set to obtain the desired horizontal and vertical velocities.

Landings were made at touchdown roll angles of 0°, 120°, 150°, and 180°, and a range of nominal pitch angles from 9° to -9°. With the exception of one test the yaw angle was set at 0°, although measurements show actual values of yaw angles at

touchdown varying between 1° and -1.5°. Nominal vertical touchdown velocity was 3.35 m/s (11 ft/sec) and nominal horizontal velocities were 1.2, 0, and -1.2 m/s (4, 0, and -4 ft/sec). Landings were made on surface slopes ranging from 0° to 35°. With the exception of one test, during which the model was landed on a soil surface, the landing surface was hard. Nominal friction coefficients of 0.6, 1.0, and ∞ were employed for tests conducted on the hard landing surface.

Analytical input parameters.- The input geometry, masses, mass moments of inertia, and touchdown parameters for calculations of the landing dynamics of the analytical model were determined by applying the scaling laws to the pertinent measured values obtained from the experimental model tests. The input velocities, surface slopes, friction coefficients, and attitude angles were the same for each computer run as the values measured during the corresponding experimental test. Input attitude angles were selected on the basis of film readings and observations of the experimental data. In no instance did the selected values exceed the tolerance values established for the experimental data.

RESULTS AND DISCUSSION

The data obtained in this investigation are presented in tables III and IV as maximum values of center-of-gravity accelerations, primary strut strokes, and strut forces. Also included are comments relating to the stability characteristics of the model for each test condition. Experimental and analytical data are presented as time histories of center-of-gravity accelerations, primary strut strokes, and strut forces for selected tests of the 3/8-scale experimental model. Additional experimental and analytical time-history data are included in the appendix. All data in this section are presented as full-scale values.

Experimental Model Results

The time-history data for the selected tests of the 3/8-scale experimental model are presented in figures 10 to 13. The analytical data, shown by the solid lines, will be discussed in a later section. The cases presented were selected to illustrate the effect on landing loads and motions, of friction coefficient, the removal of primary strut deadband, and changes in the landing-surface characteristics.

Effect of friction coefficient.- Figure 10 presents the data from cases 3 and 15 which represent tests in which the model impacted on leg 1 and had a horizontal velocity component directed down a 20° surface slope. The touchdown parameters for these tests were approximately the same with the exception of the footpad-to-surface friction coefficient. For case 3 the model was equipped with footpads which provided a friction coefficient of approximately 0.6 and for case 15 spikes were substituted for the footpads and provided an infinitely high friction coefficient. A comparison of figures 10(a) and 10(c) reveals that the normal accelerations a_x were greater for the test conducted at the higher friction coefficient; however, the lateral and longitudinal accelerations a_y and a_z were approximately the same for the two tests. As would be expected, because of the load alleviators in the struts, the strut forces (see figs. 10(b) and 10(d)) were about the same magnitude for each of the runs. However, the inboard (2L and 3R) secondary struts, which developed tension forces during the test conducted at $\mu = 0.6$, were subjected to compressive loads during the test at $\mu = \infty$. The normal components of these compressive forces for the test at $\mu = \infty$, added to the normal components of the other strut forces would result in a larger normal acceleration for the test at $\mu = \infty$. The primary-strut strokes for leg 1, which made initial contact with the landing surface, were about the same for both cases. The primary-strut strokes on legs 2 and 3 were greater for the low-friction case and may be attributed to greater footpad motion which results in larger leg rotations and consequently greater primary-strut stroking. A stable landing occurred for the test conducted at the lower friction coefficient and an unstable landing resulted for the test at the higher friction coefficent as shown in table III.

Effect of removing primary-strut deadband.- The effects of removing the primary-strut deadband on loads and motions are illustrated in figure 11 which presents the time-history data from cases 12 and 11, and in figure 12 which presents pitch-angle time histories to illustrate the motions of the overall vehicle. Cases 11 and 12 have the same nominal values of touchdown parameters and were conducted for a single-leg impact with the horizontal velocity component directed into the slope. The primary strut used to obtain the data for case 11 had a deadband, and the deadband was removed using a ratchet mechanism to obtain the data for case 12. The surface slope was 19° for case 11 and 30° for case 12.

The most obvious difference between the time-history data for these cases is the time duration of the compressive forces in the secondary struts of leg 1 (1R and 1L). These forces for case 11 (with deadband) were sustained for a longer time than those of

case 12 (deadband removed). This result would be expected since the compressive spring force in the primary strut would, when pitch rotation relieved the compressive loading, accelerate the unsprung mass of the leg toward the surface. Contact between the footpad and the surface would be maintained for a longer period of time, thus sustaining the secondary-strut compressive forces. When the primary-strut deadband was removed, the primary strut was physically restrained from extending, and the pitch rotation of the model lifted the footpad from the surface much sooner as shown by the shorter compressive force pulses for 1R and 1L. It should be noted that the leg-1 primary-strut compressive-force pulses were of the same duration for both of these cases.

The most significant result obtained by removing the deadband from the primary strut is the large improvement in the stability characteristics of the model. The pitch-angle time histories shown in figure 12 illustrate the improvement in stability. With the deadband in the primary strut (case 11) the model was unstable on a 19° slope. Removing the deadband from the primary strut (case 12) resulted in a stable landing of the model on a 30° slope. This improvement in stability may be attributed to two factors (1) the shorter duration of the compressive force in the secondary struts with the corresponding shorter angular impulse, and (2) the reduction in angular impulse resulting from the large inertial tension force developed in the restrained primary strut. Additional tests were conducted in an effort to remove the deadband by using honeycomb cartridges bonded to the primary-strut cylinder head and the piston in lieu of a ratchet mechanism. These tests indicated some improvement in the stability characteristics but did not show as much improvement as that obtained by using the ratchet mechanism.

Effect of changes in landing-surface characteristics.- The effect of landing-surface characteristics on the loads and motions of the model is shown by comparing case 11 of figure 11(c) with case 14 of figure 13. The model tests represented by these cases were conducted for a single-leg initial impact with the horizontal velocity component directed into a 19° surface slope. The landing surface for case 11 was a hard plywood surface where the footpad-to-surface friction coefficent was approximately 1.0 and for case 14 the landing surface was a soft soil. The experimental data obtained during the model tests on the soft soil are presented as full-scale data; however, it should be noted that this data would not be representative of a landing of a full-scale model on Mars because the particle size of the soil and the atmospheric pressure have not been scaled. The analytical data presented were obtained using 3/8-scale input values instead

of full scale to permit validation of the computer program for a soft-soil landing and for quantitative comparisons with data obtained on the hard landing surface.

The center-of-gravity accelerations, primary-strut strokes, and strut forces are considerably smaller when landing on the soil surface as opposed to the hard surface. This result is as expected since much of the model touchdown energy normally absorbed by the landing gear is now absorbed by the soil. In the leg-1 impact for case 14 (soft-soil landing) essentially all of the energy was absorbed in the soil since the force applied to the primary strut (1P) was never large enough to initiate crushing of the first-stage honeycomb. Furthermore, the secondary strut forces for leg 1 (1R and 1L) were never large enough to initiate plastic deformation of the bending-element load alleviators. The soil also absorbed a considerable amount of energy during the impacts of legs 2 and 3. The strokes for these struts during soil impact were approximately one-half those for impacts on the hard landing surface. Also the secondary struts for legs 2 and 3, for the soil landing, were not plastically deformed and therefore did not absorb energy. The preceding discussion would be generally applicable to comparisons between a hard-surface landing and landings on soil surfaces of varying degrees of softness, but the magnitudes of the parameters would vary.

The stability of the model was greatly enhanced by the soft-soil landing as shown by comparing the pitch-angle time histories for case 11 and case 14 in figure 12. The landing made on the hard surface was unstable but the soft-soil landing was very stable since the maximum pitch angle encountered was about 19° and the stability angle for these touchdown parameters was approximately 47° as shown for case 11. However, it should be noted that this vastly improved stability was obtained at the sacrifice of clearance between the center body of the model and the landing surface which could result in the center body impacting a rock and exceeding design loads.

Analytical Results

Comparison with experiment.- In addition to illustrating the effect of footpad-to-surface friction coefficient, primary-strut deadband, and landing-surface characteristics on landing loads and motions, the touchdown parameters of the selected cases presented in figures 10 to 13 are sufficiently different to demonstrate the validity of the analytical program. These cases will be employed to compare the analytical predictions with the experimental results.

The analytical prediction of the landing loads and motions for comparison with experimental results is particularly sensitive to the input values of landing-gear force-stroke characteristics and to input values of the touchdown parameters such as velocity, attitude, and footpad-to-surface friction. Prior to the analytical simulation of the test cases nominal values of the forces and strokes for the leg struts (see fig. 5) were defined and were used in all simulations as were nominal values of footpad-to-surface friction coefficients. The touchdown-attitude inputs for the analytical simulations were based on values obtained from motion-picture-film data for each test case.

An examination of the analytical and experimental time-history data presented in figures 10 to 13 and those presented in the appendix indicates that the analytical program closely predicts the time phasing of events occurring during a landing. Small errors in time phasing, illustrated typically in figure 10(c) for legs 2P and 3P, were found to be due to errors on the order of $\pm 1^{\circ}$ between actual touchdown pitch and yaw angles and the values taken from motion-picture-film data.

The maximum values of center-of-gravity accelerations, primary-strut strokes, and strut forces for the experimental and analytical data are presented in the correlation plots of figure 14. Experimental data are plotted along the ordinate as a function of analytical data plotted on the abscissa. For this type of plot, exact agreement between the experimental and analytical data would result in a straight line through the origin with a slope of unity.

Figure 14(a) presents correlation plots for maximum values of center-of-gravity accelerations and primary-strut strokes. There is some scatter of the data about the exact correlation lines which may be attributed to differences in the measured yaw angle, used as an input to the analytical program, and the actual touchdown yaw angle of the model. These differences in yaw angles and the resulting variation in the time phasing of leg impacts affect the superposition of the strut forces and, consequently, the accelerations. Considering these facts, good agreement was obtained between experimental and analytical center-of-gravity accelerations and primary-strut strokes.

Figure 14(b) relates the maximum experimental and analytical values of primary- and secondary-strut forces. The experimental compression forces for the primary struts are generally somewhat less than those obtained from the analytical program due to the fact that nominal values of force and stroke were used for the computer inputs. The tension forces shown for the primary struts in figure 14(b) for case 12 are due to

the ratchet mechanism used to prevent primary-strut re-extension. In the analytical simulation ratchets were included on all three primary struts and in the experimental investigation a ratchet was employed only on the primary strut of leg 1. The agreement in the primary-strut force levels for that leg was excellent and the agreement between the experimental and analytical secondary strut forces is good. The analytically determined tension forces in these struts are generally slightly greater than those obtained from the experimental investigation. A constant damping force (arbitrarily assigned a value of approximately 4 percent of the maximum full-scale primary-strut force (0.445 kN (100 lbf)) was included in the inputs to the computer program for the primary struts. However, an examination of the experimental time-history data for the strut forces (shown in figs. 10(d), 11(b), 11(d), and figures in the appendix) reveals that the damping in the experimental model was slightly greater than that included in the analytical program which could account for these differences.

The frequency of secondary strut oscillations was generally the same for both experimental and analytical models. (See figs. 11(b) and 11(d) and figs. A1(d) and A1(t) of the appendix.) The apparent difference in frequency for the secondary struts, as shown in figure 10(d), is due to a difference in computed and experimental spike penetration into the landing surface. For this case, the spikes used on the experimental model penetrated further and did not pull free from the surface, whereas the footpads simulated in the computer program penetrated only slightly and at a time of approximately 0.18 sec lifted off the surface allowing the secondary struts to vibrate.

Time histories of experimental and analytical pitch angles are shown in figure 12 for five cases having significantly different touchdown parameters such as friction coefficients, pitch attitudes, surface slopes, and landing-surface characteristics. An examination of these plots shows that the data obtained from the analytical program is in good agreement with the experimental data.

It has been shown by comparing experimental center-of-gravity accelerations, primary-strut strokes, strut forces, and angular motions, from tests conducted for a variety of touchdown parameters, with data obtained from the subject computer program that good agreement was obtained.

As previously noted the data presented in this paper assumes a rigid center-body structure. The subject program has the capability of including center-body structural elastic effects. Results presented in reference 11 show good agreement between

experimental data, from an earlier experimental investigation, and analytical data from the subject program, in which center-body structural elasticity was a significant parameter.

Effect of selected parameters.- The validity of the analytical program having been demonstrated, a limited parametric study was conducted. Deadbands were used in the primary struts for this study. At the time of this investigation, the surface slopes and footpad-to-surface friction coefficients which the Viking lander might encounter during a landing on the Martian surface were not well defined. Since these parameters are important in defining the stability characteristics of the lander at touchdown, it was desirable to evaluate analytically the effects of unsprung mass and footpad-to-surface friction coefficients on stability-critical surface slopes.

Computed stability-critical surface slopes are shown as a function of ratios of the unsprung mass of the landing gear to vehicle mass in figure 15. For these computations the total-vehicle mass and total mass moments of inertia were held constant. The mass and moments of inertia of the center body changed proportionately with changes in unsprung mass. The unsprung mass was also considered to be concentrated at the vertex of the leg struts. Consequently, experimental data cannot be compared with the computed data presented in this figure. Except for extremely low mass ratios, as the unsprung mass decreases (resulting in a decreasing mass ratio), the stability of the vehicle decreases as indicated by a lower slope at which the vehicle turns over. The variation is nonlinear and, as shown, the maximum rate of deterioration in stability-critical surface slope occurs between mass ratios of 0.04 and 0.06. Over the range of mass ratios between 0.12 and 0.006, the surface slope on which the model was stable decreased from 27.5° to 17.5°. At extremely low mass ratios of 0.006 to 0.001, a discontinuity developed in the stability boundary. It was observed from a comparison of the data obtained at these mass ratios that the unsprung mass accelerations computed for the mass ratio of 0.001 were approximately an order of magnitude greater than those obtained for a mass ratio of 0.006. As a result, the data for the mass ratio of 0.001 were recomputed using a time interval of 0.00005 sec instead of 0.0001 sec. The results obtained indicated that the model was stable on an 18° slope instead of the 27° slope determined from the previous computation. Since the integration time interval has such a large effect on the definition of the stability-critical surface slope at these lower mass ratios, the data for the mass ratio of 0.006 were also recomputed at this small

integration time interval (0.00005 sec). The slope at which the model was unstable for this mass ratio was not affected by the reduction in integration time interval.

The data of figure 15 indicate that the ratio of landing-gear unsprung mass to total-vehicle mass is important for determining the stability characteristics of a vehicle having a legged-type landing gear. In addition, the user of a landing-dynamics computer program which incorporates the unsprung mass of the landing gear as a variable must be aware of the effects that integration time interval may have on predicting stability characteristics of such a vehicle for small ratios of landing-gear unsprung mass to total-vehicle mass.

The stability-critical surface slopes as a function of footpad-to-surface friction coefficients are shown in figure 16. The data shown by the open symbols are computed and those shown by the filled symbols were obtained from experimental model tests. For the touchdown parameters used in the computations (see sketch in fig. 16), the data indicate that footpad-to-surface friction coefficients above approximately 0.8 have no appreciable effect on the stability-critical surface slope. For values of friction coefficients less than approximately 0.8, the surface slope at which the model becomes unstable increases with decreasing friction coefficient. The limited experimental data available for this set of touchdown parameters indicate that the computed results are valid.

CONCLUDING REMARKS

A study, comparing data from a 3/8-scale dynamic model and an analytical model of a legged spacecraft lander, was conducted to validate experimentally a landing-dynamic computer program for such landers. The results of this study showed that good agreement was obtained between analytical and experimental center-of-gravity accelerations, primary-strut strokes, strut forces, and vehicle motions. Landing-surface characteristics significantly influence the stability characteristics and loads imposed upon the vehicle. Landing on a soft surface, as opposed to landing on a hard surface, resulted in a reduction of loads applied to the model and also increased the stability of the model. The landing-gear unsprung mass, footpad-to-surface friction coefficients, and the presence or absence of the primary-strut deadband have significant effects on the stability characteristics of legged spacecraft landers. The agreement obtained between analyti-

cal and limited experimental data established that the computer program employed in this study can be used with confidence as a design tool for legged spacecraft landers.

Langley Research Center,
National Aeronautics and Space Administration,
Hampton, Va., July 30, 1973.

APPENDIX

EXPERIMENTAL AND ANALYTICAL DATA TIME HISTORIES

Comparative experimental and analytical center-of-gravity acceleration, strut-stroke, and strut-force time histories are presented in figure A1 to illustrate further the agreement between experimental and computed data for a variety of lander touchdown parameters. In addition these data are included to facilitate validation of other landing-dynamics computer programs for legged spacecraft landers.

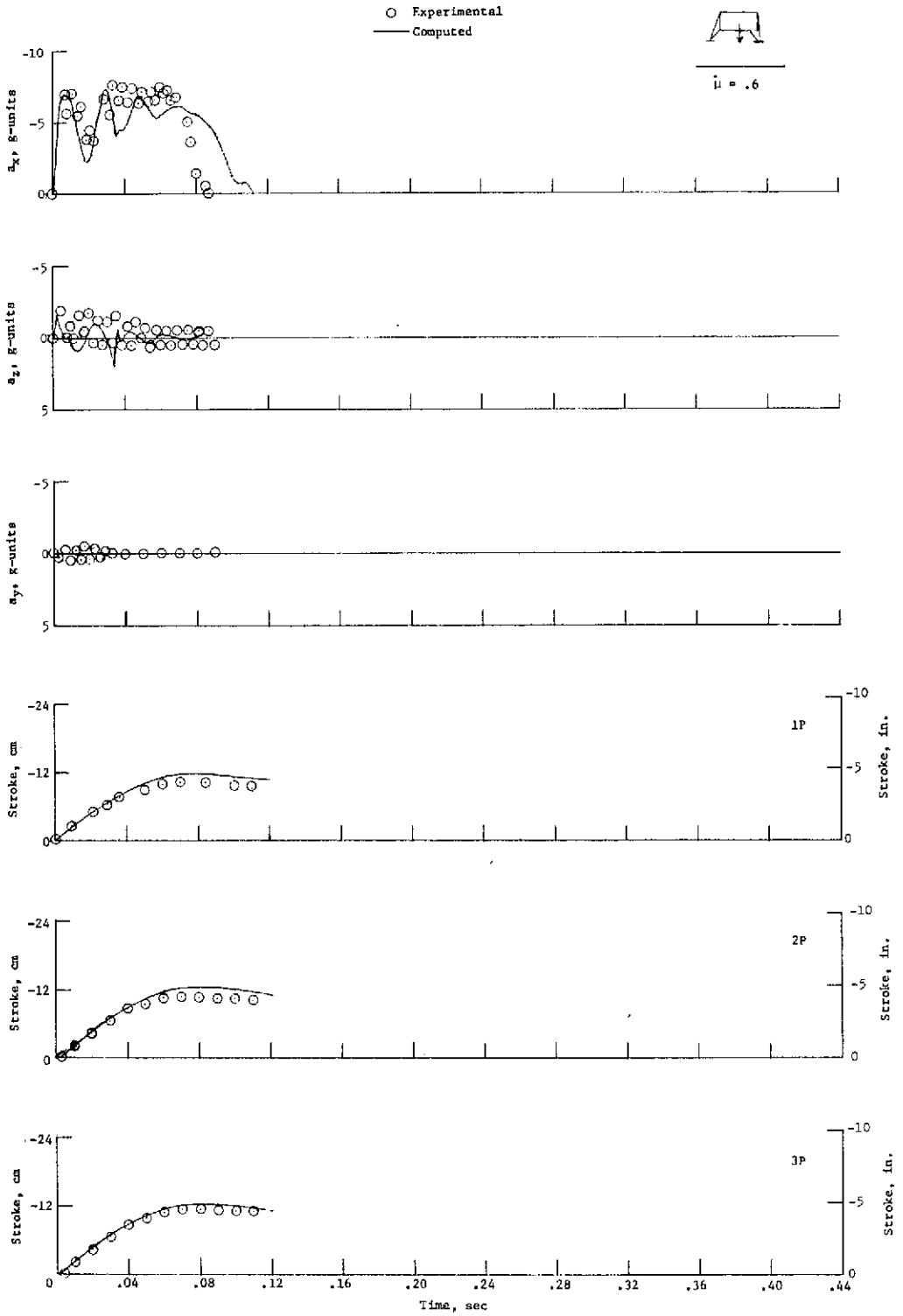

(a) Accelerations and primary-strut strokes for case 1.

Figure A1.- Experimental and analytical time histories of center-of-gravity accelerations, primary strut strokes, and strut forces. All values are full scale.

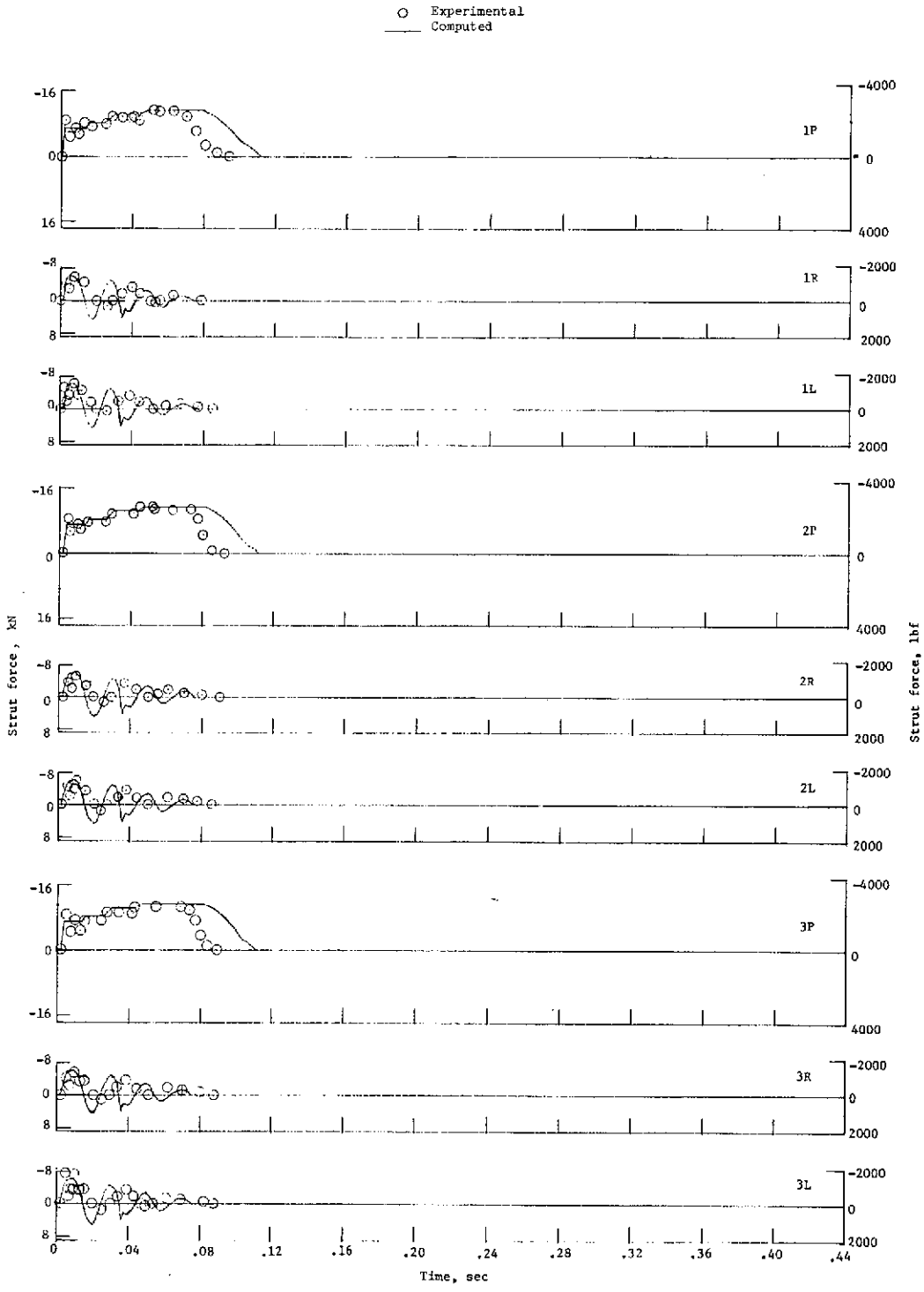

(b) Strut forces for case 1.

Figure A1.- Continued.

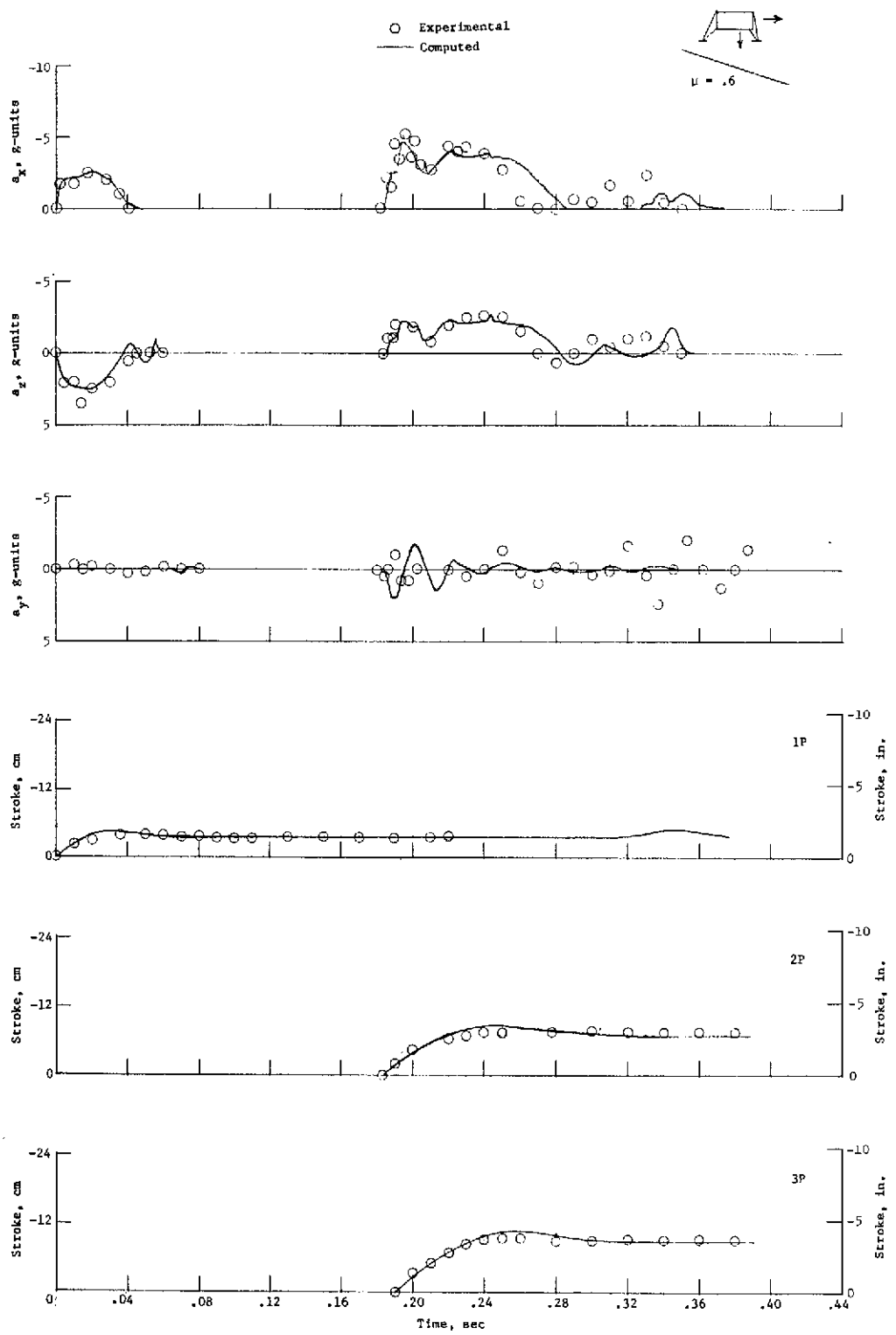

(c) Accelerations and primary strut strokes for case 2.

Figure A1.- Continued.

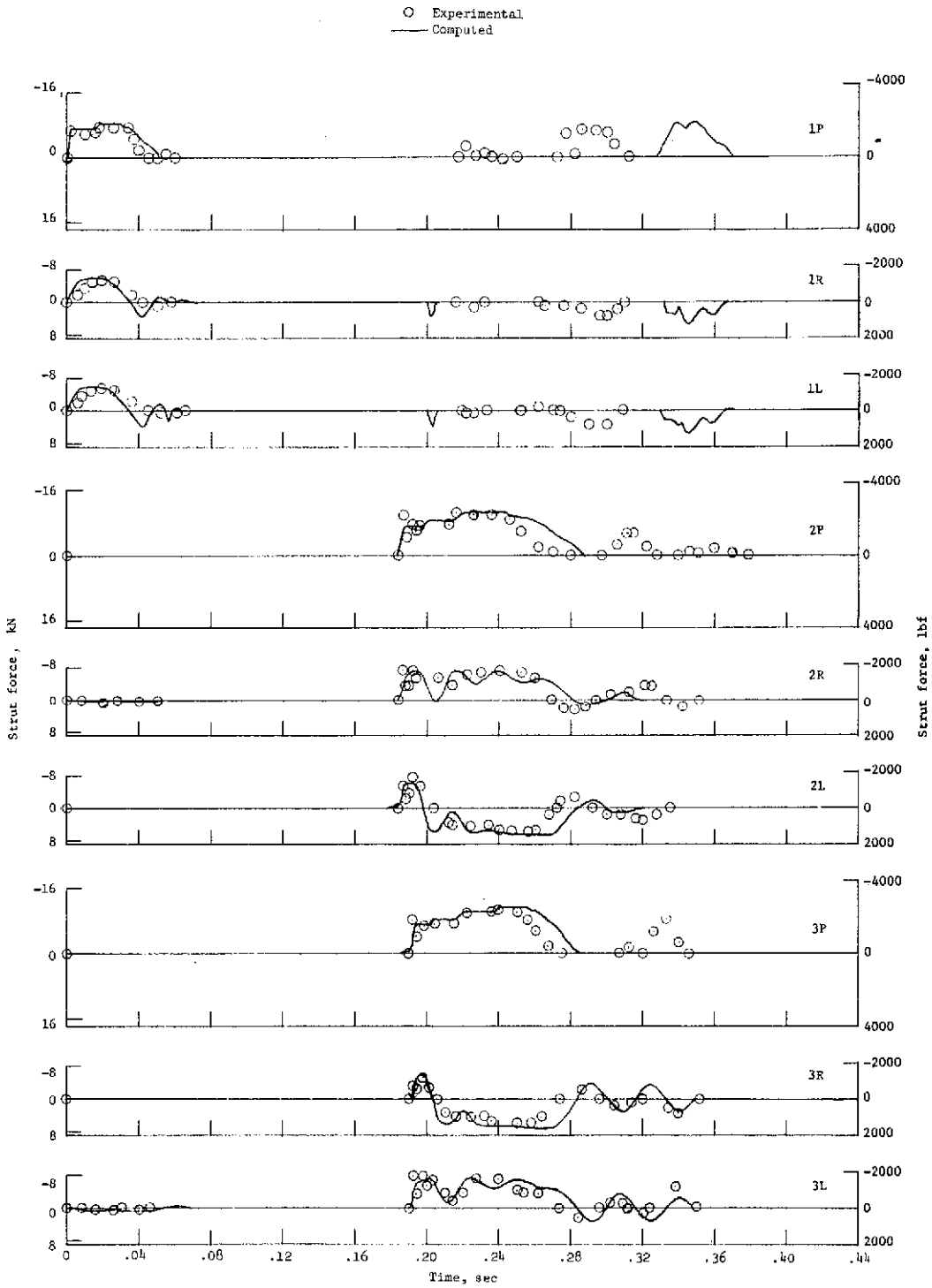

(d) Strut forces for case 2.

Figure A1.- Continued.

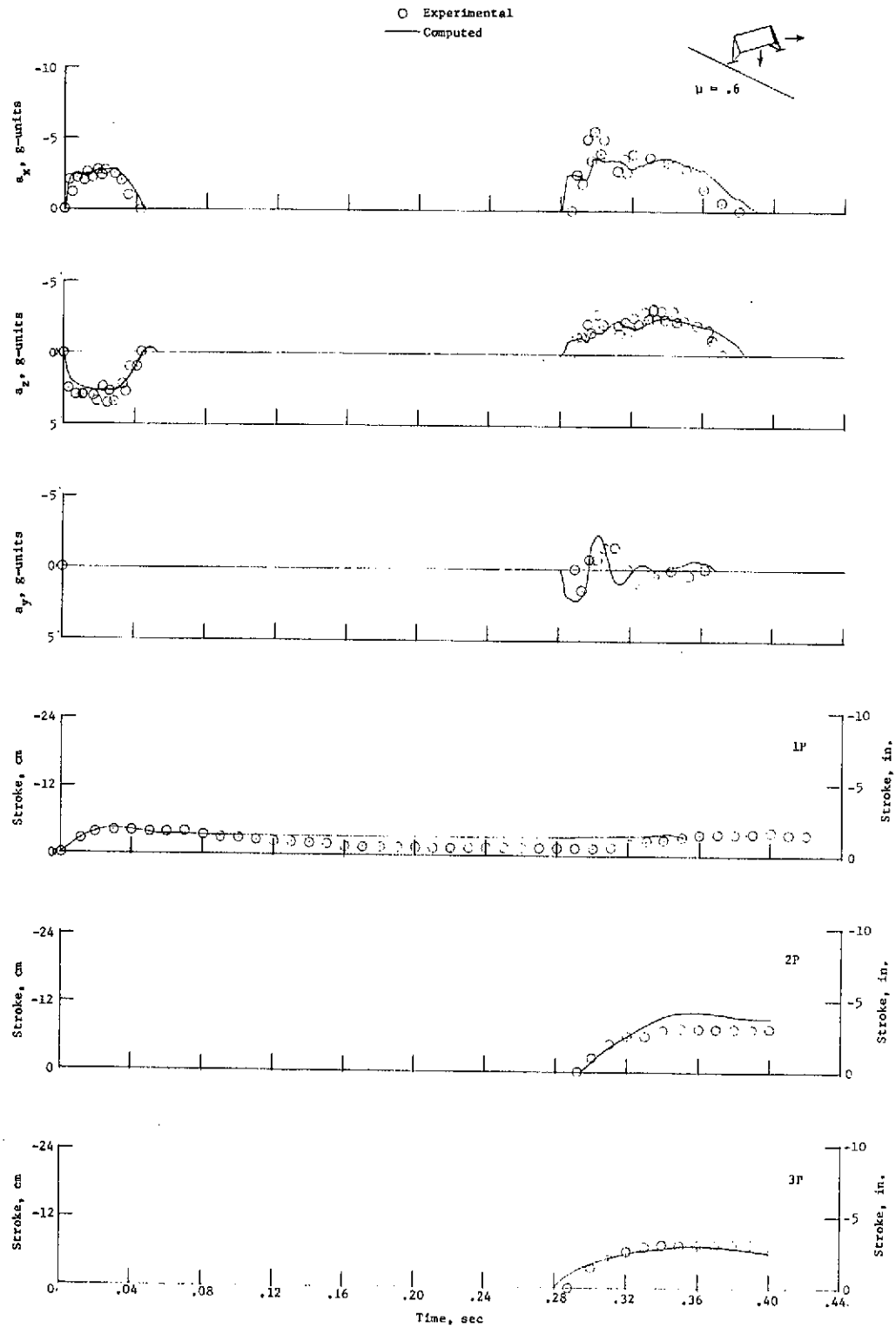

(e) Accelerations and primary-strut strokes for case 4.

Figure A1.- Continued.

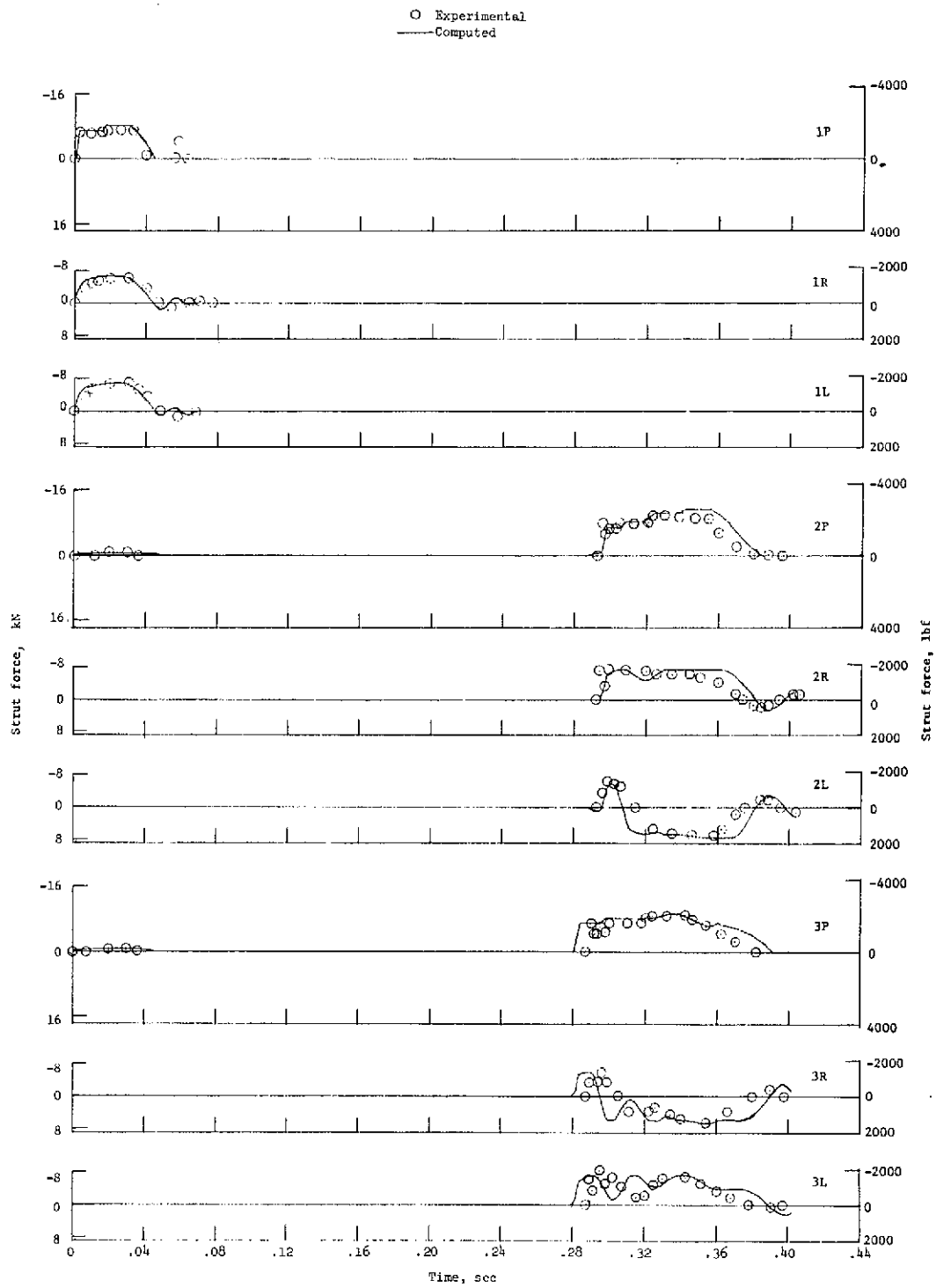

(f) Strut forces for case 4.

Figure A1.- Continued.

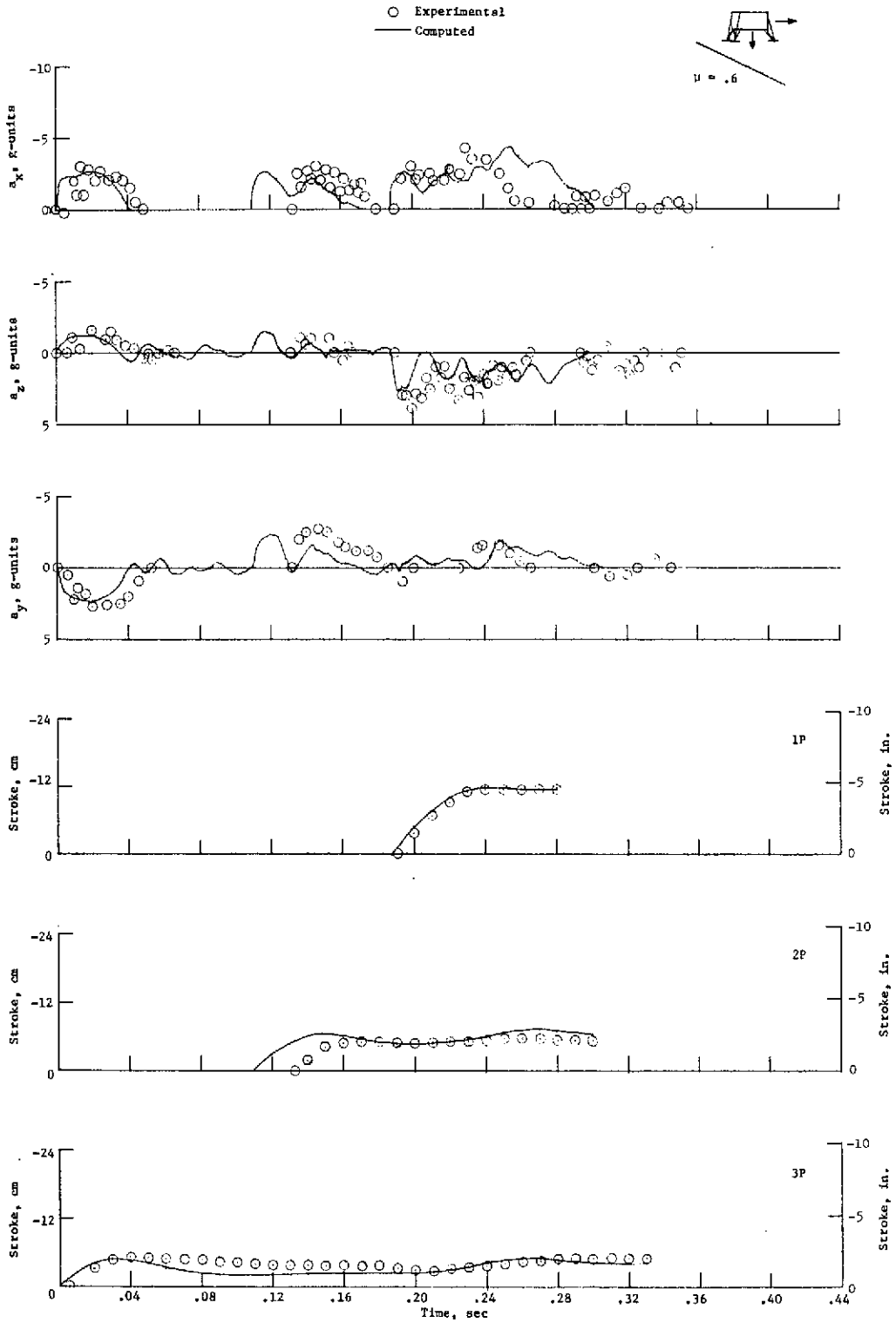

(g) Accelerations and primary-strut strokes for case 5.

Figure A1.- Continued.

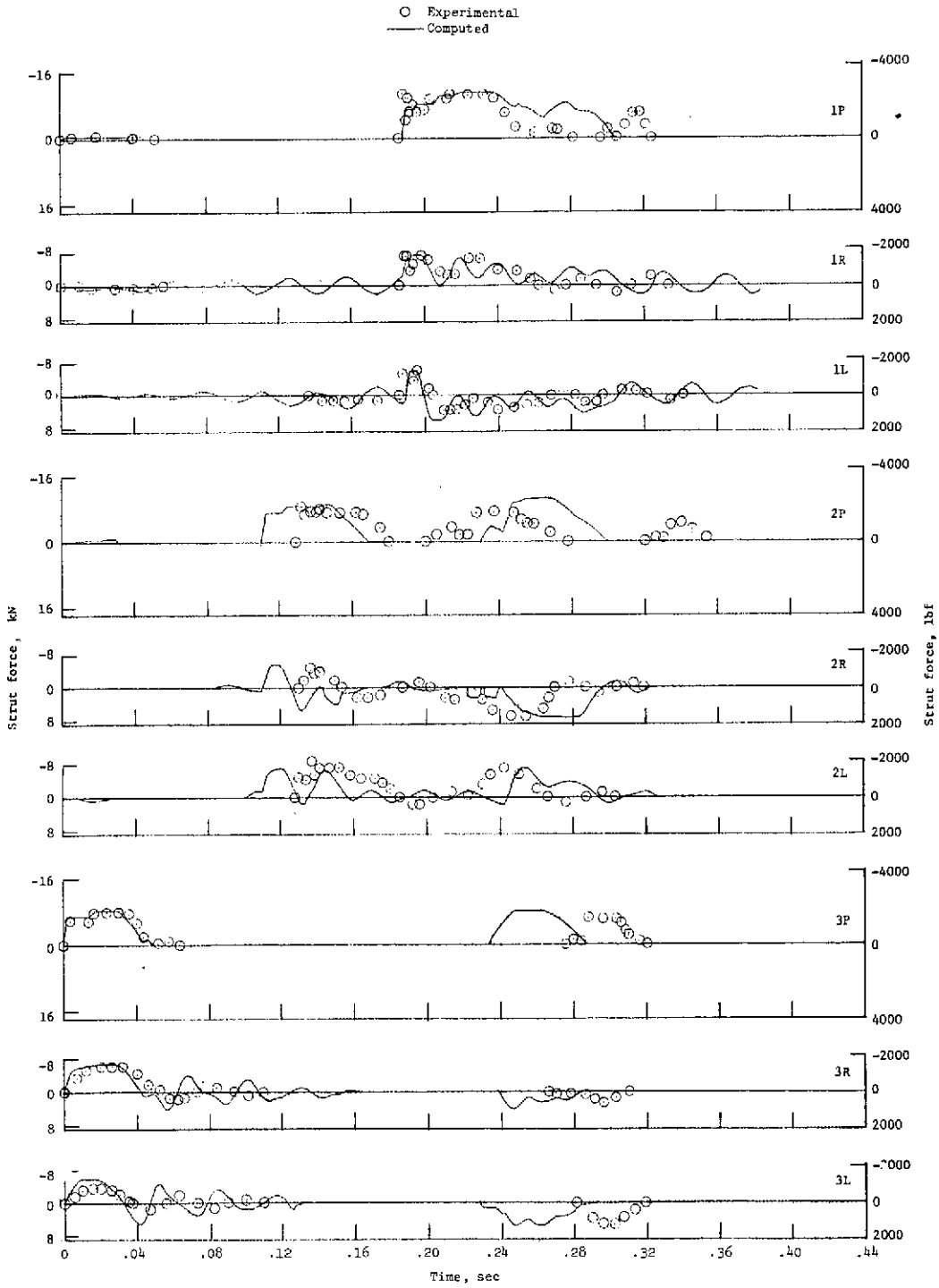

(h) Strut forces for case 5.

Figure A1.- Continued.

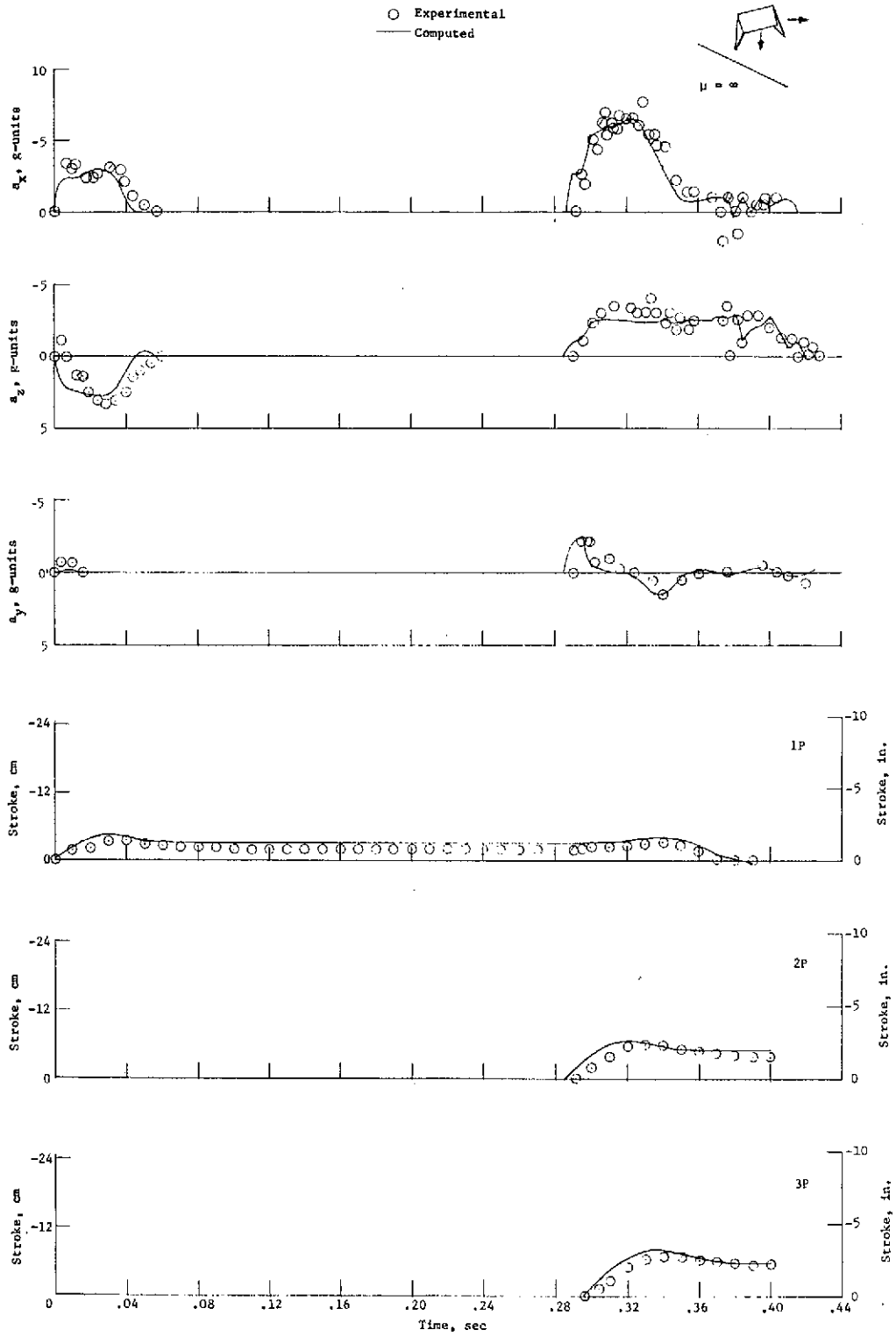

(i) Accelerations and primary-strut strokes for case 6.

Figure A1.- Continued.

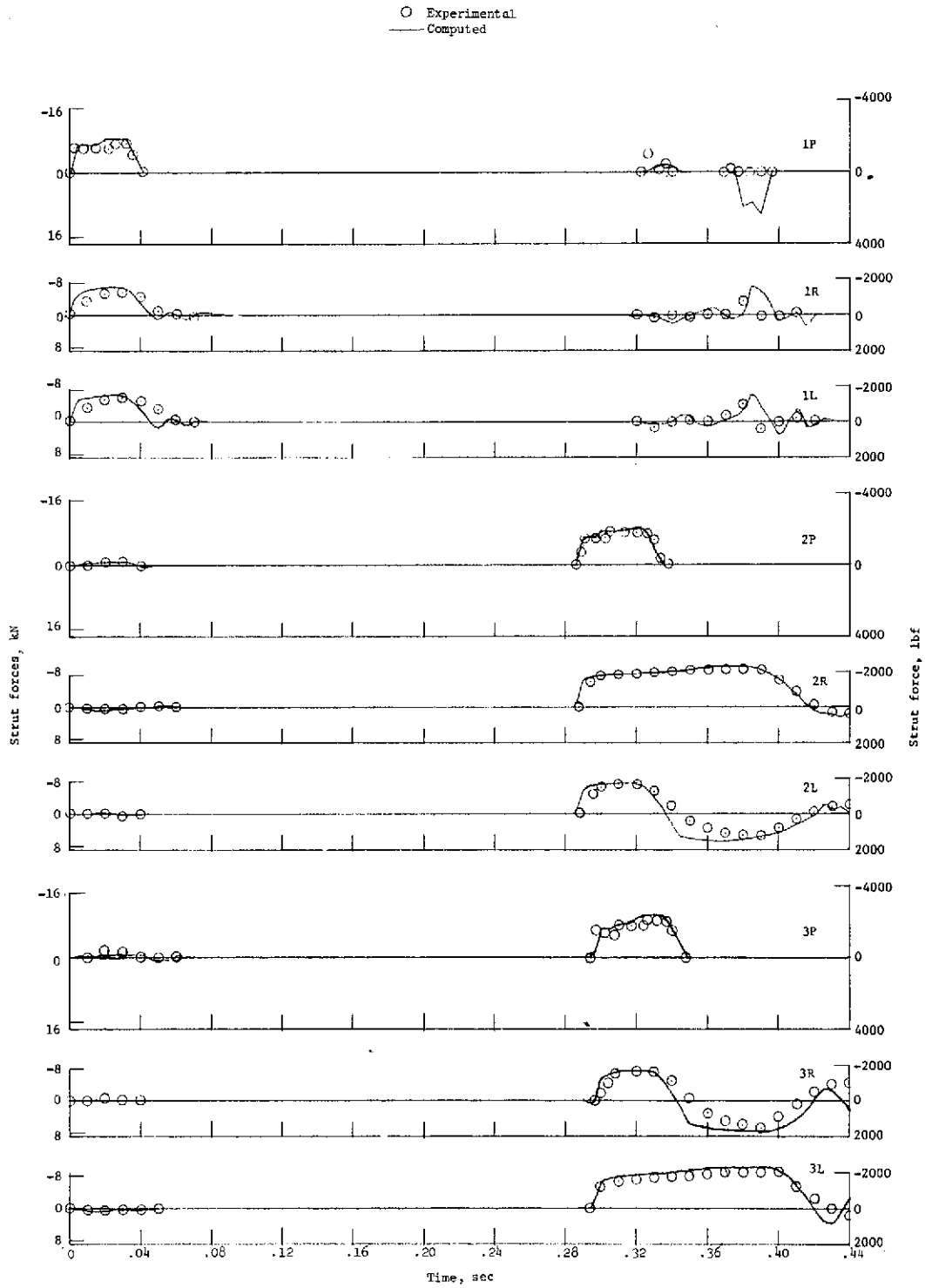

(j) Strut forces for case 6.

Figure A1.- Continued.

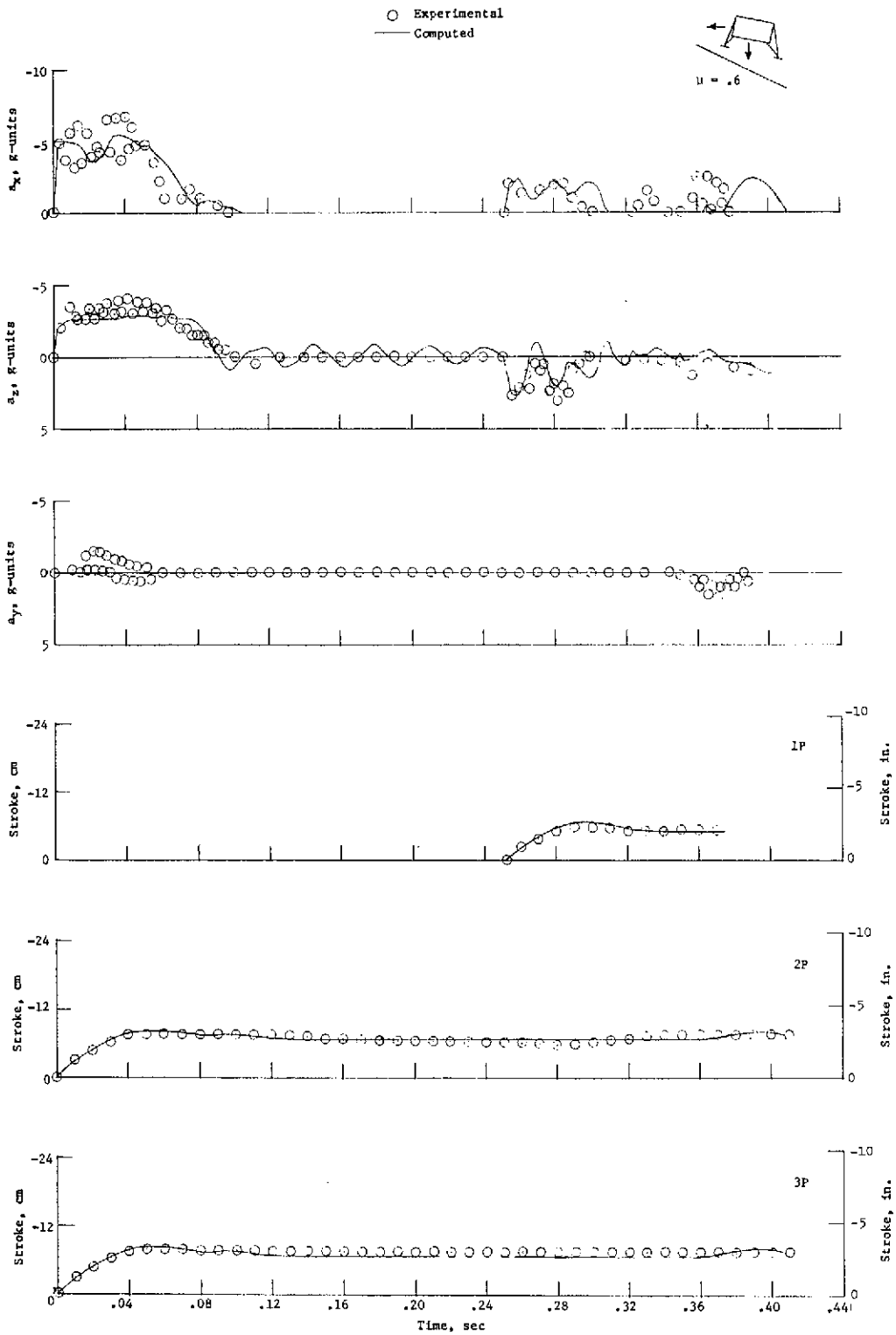

(k) Accelerations and primary-strut strokes for case 7.

Figure A1.- Continued.

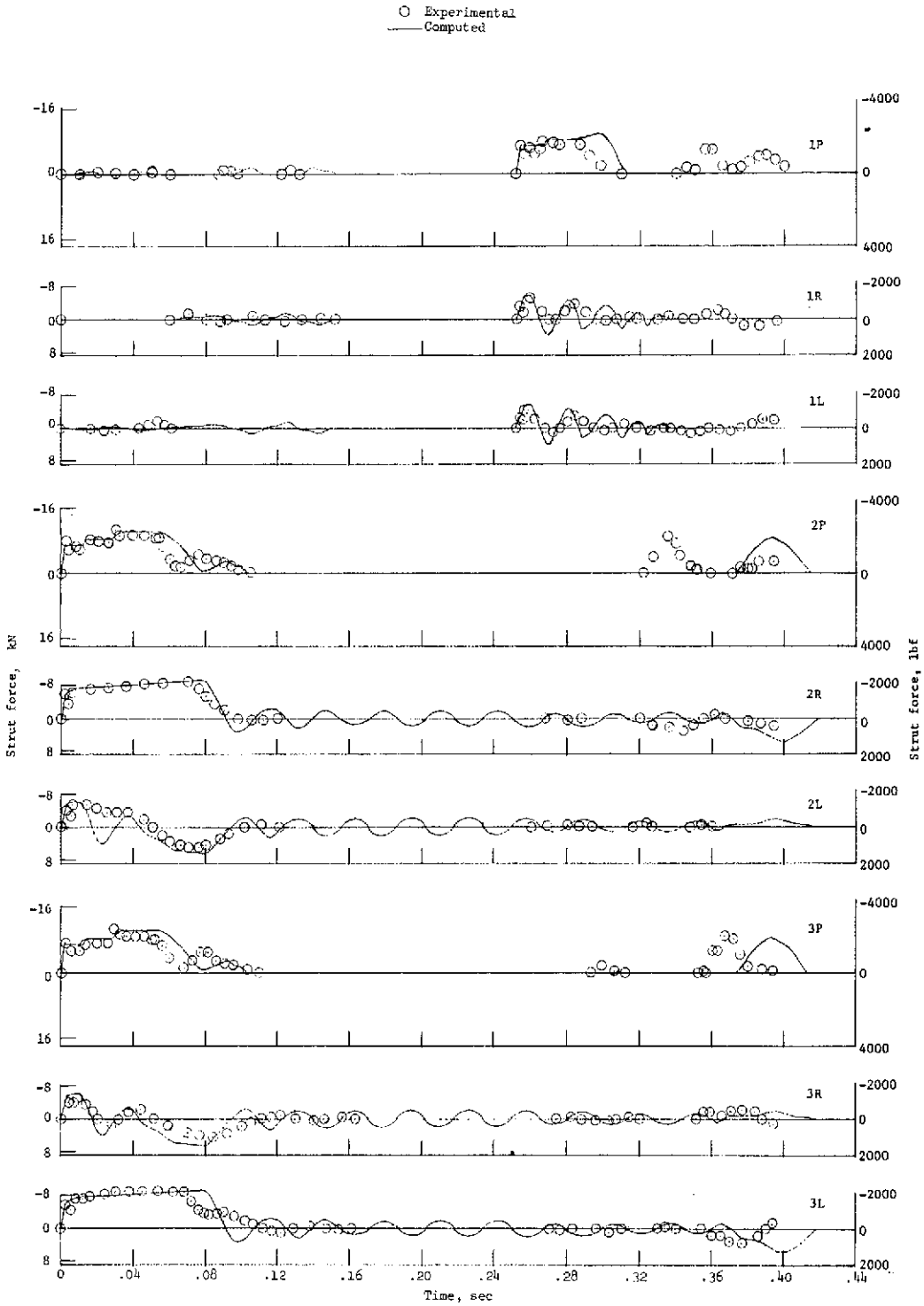

(l) Strut forces for case 7.

Figure A1.- Continued.

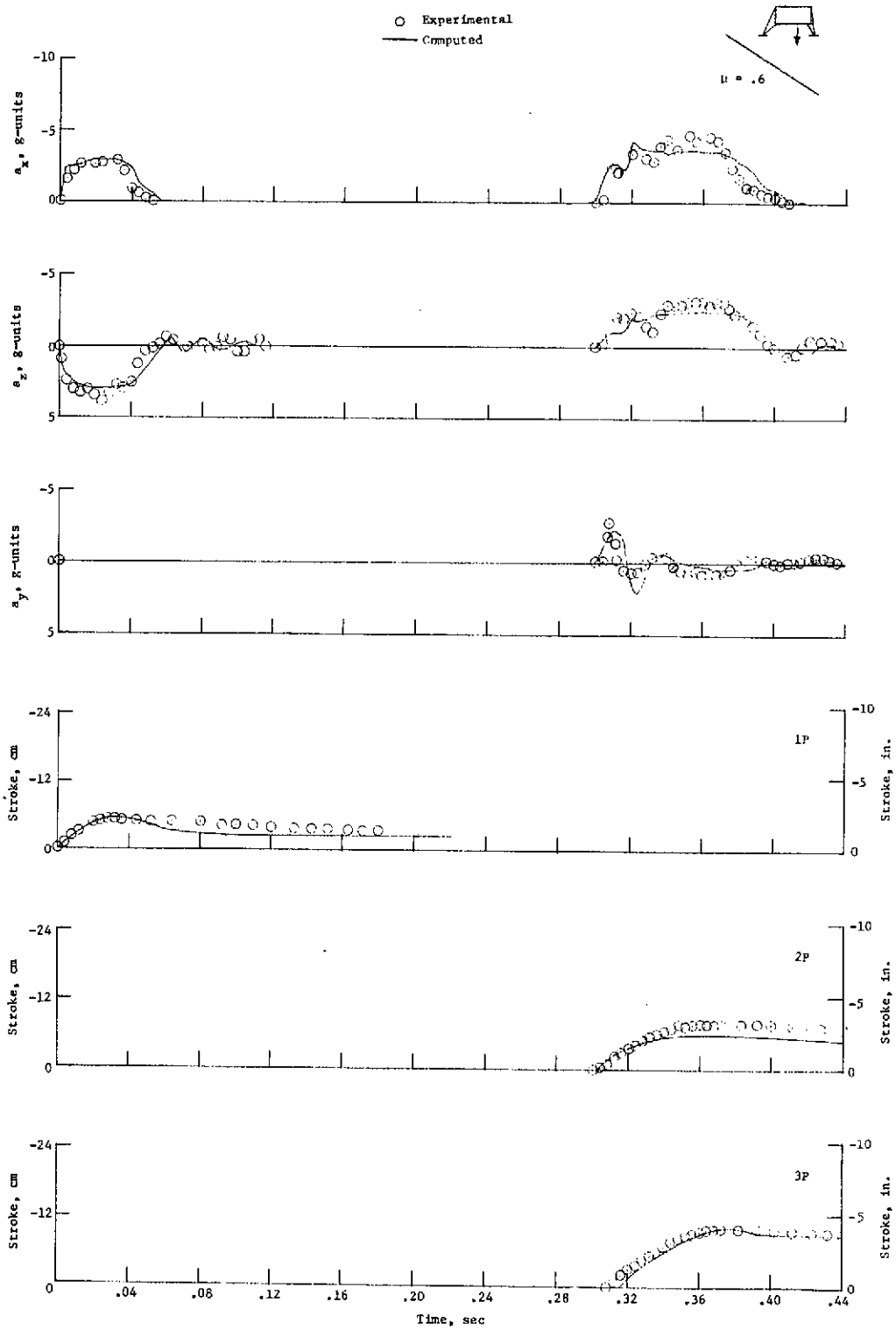

(m) Accelerations and primary-strut strokes for case 8.

Figure A1.- Continued.

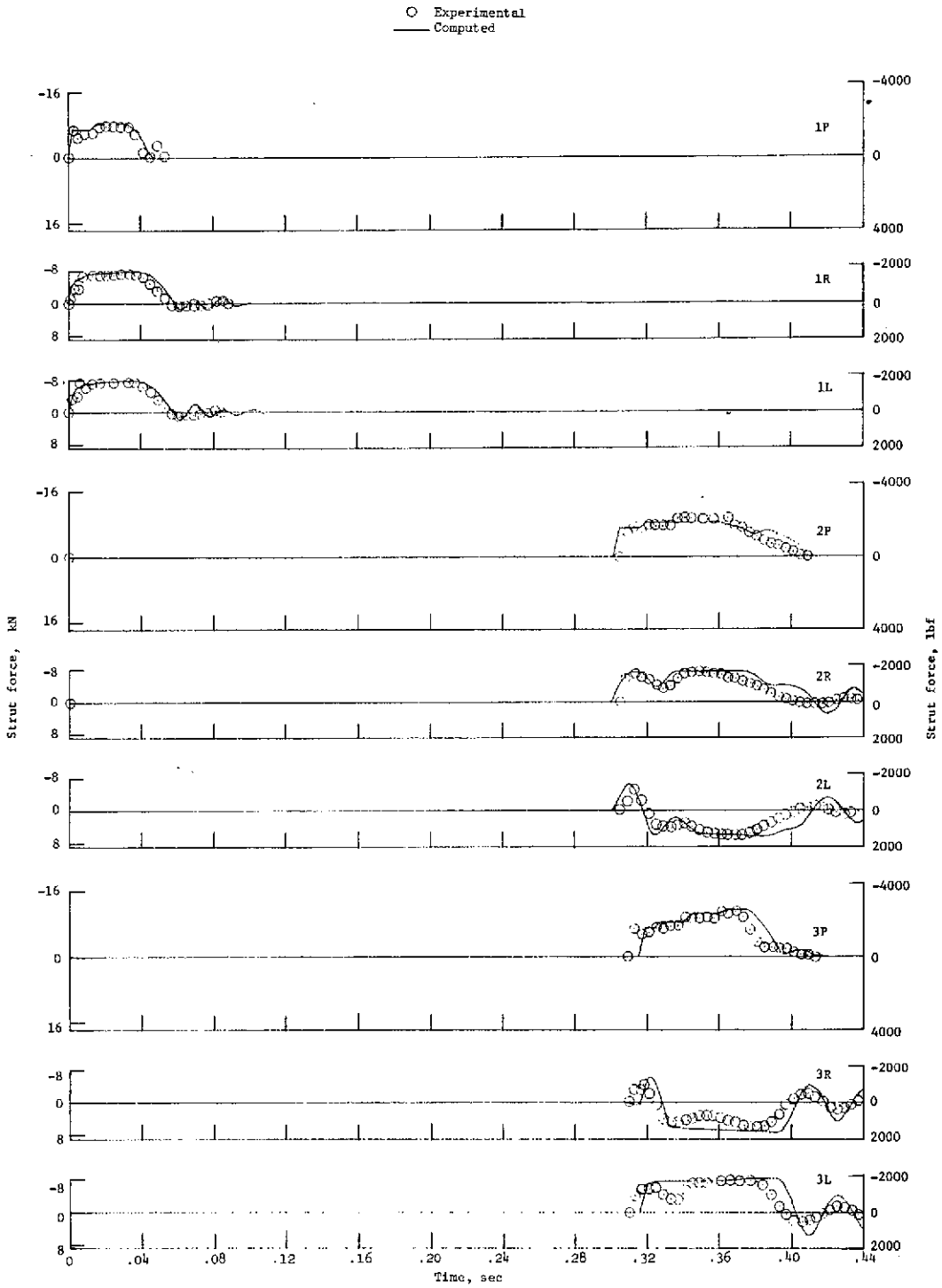

(n) Strut forces for case 8.

Figure A1.- Continued.

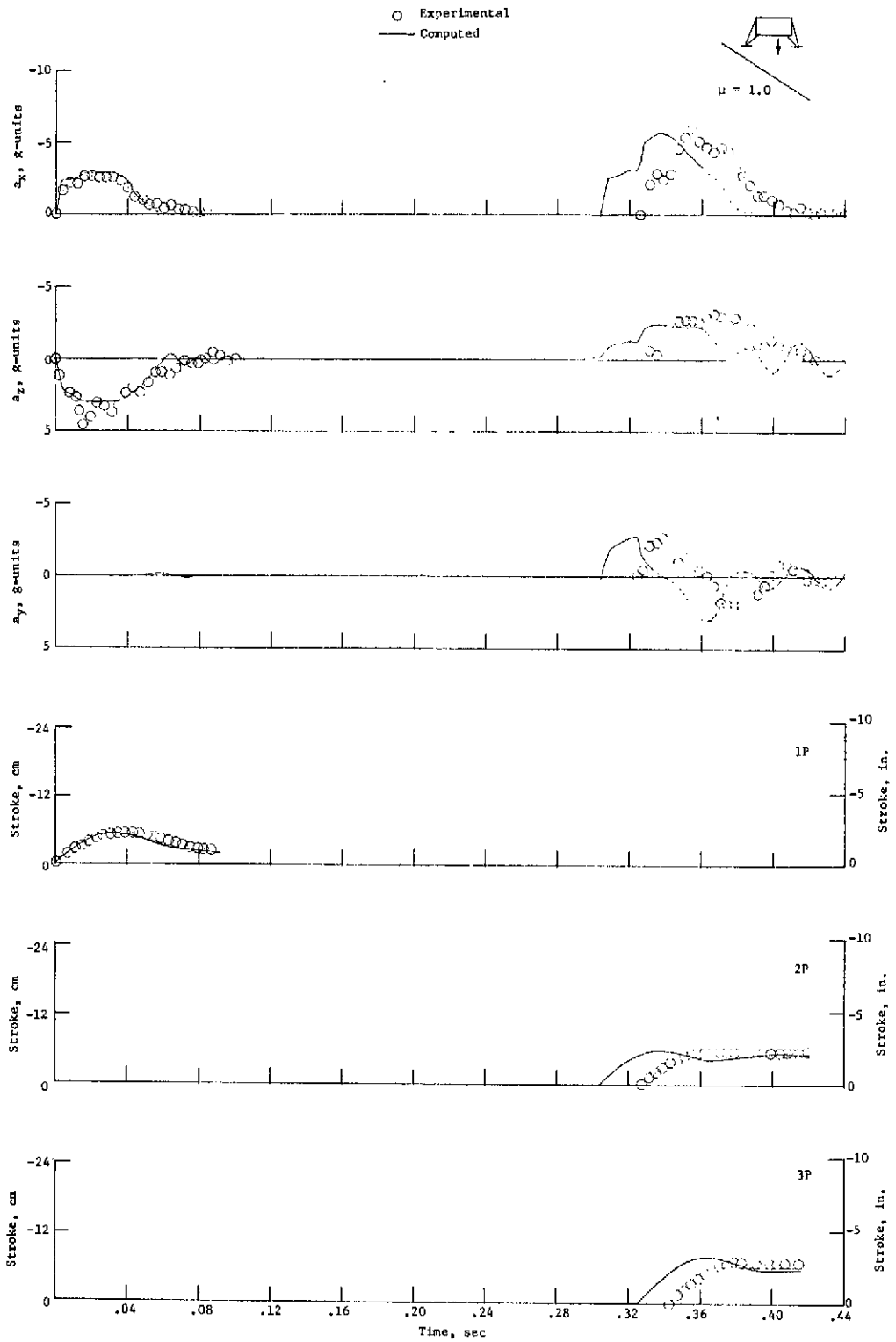

(o) Accelerations and primary-strut strokes for case 9.

Figure A1.- Continued.

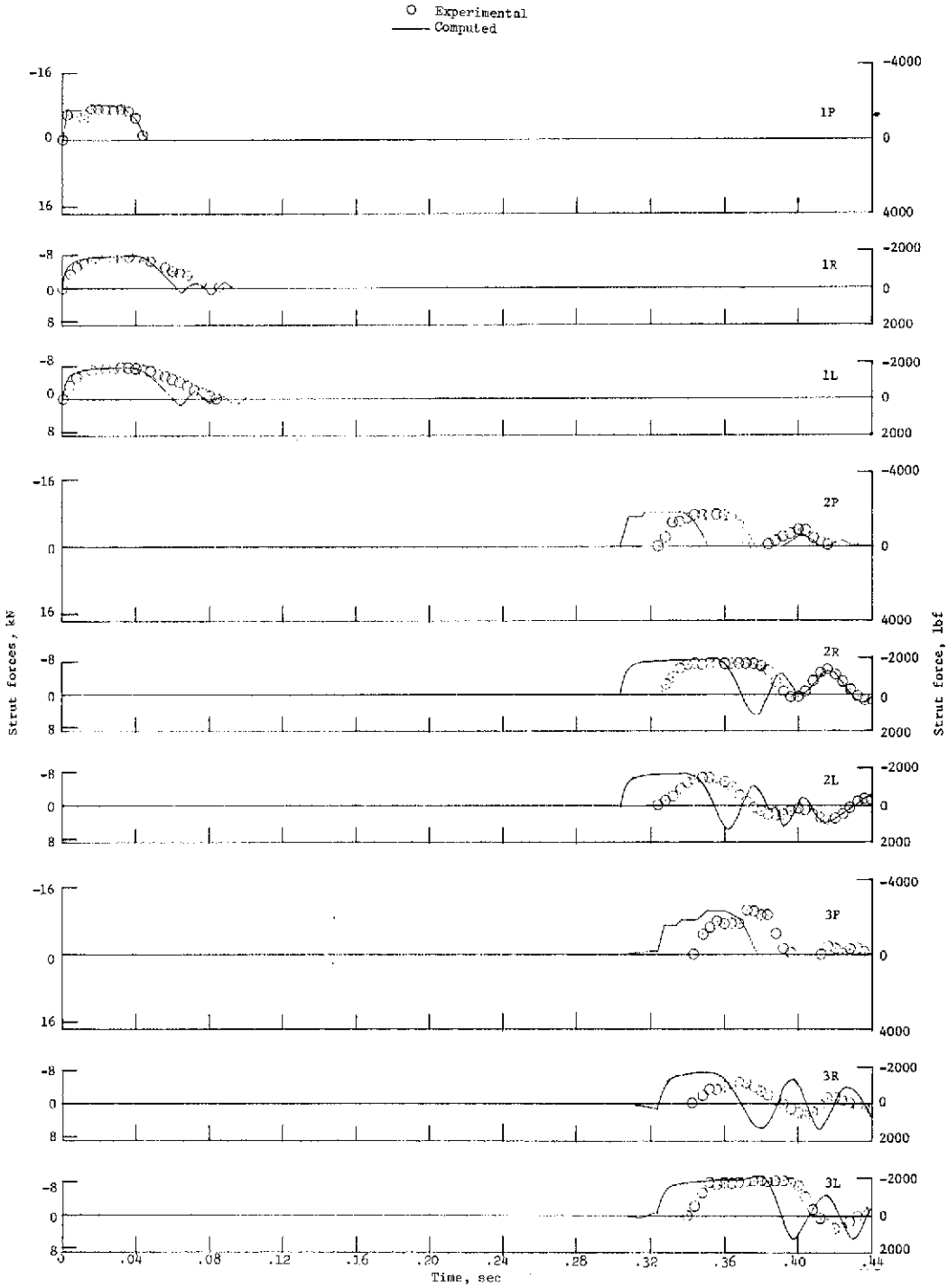

(p) Strut forces for case 9.

Figure A1.- Continued.

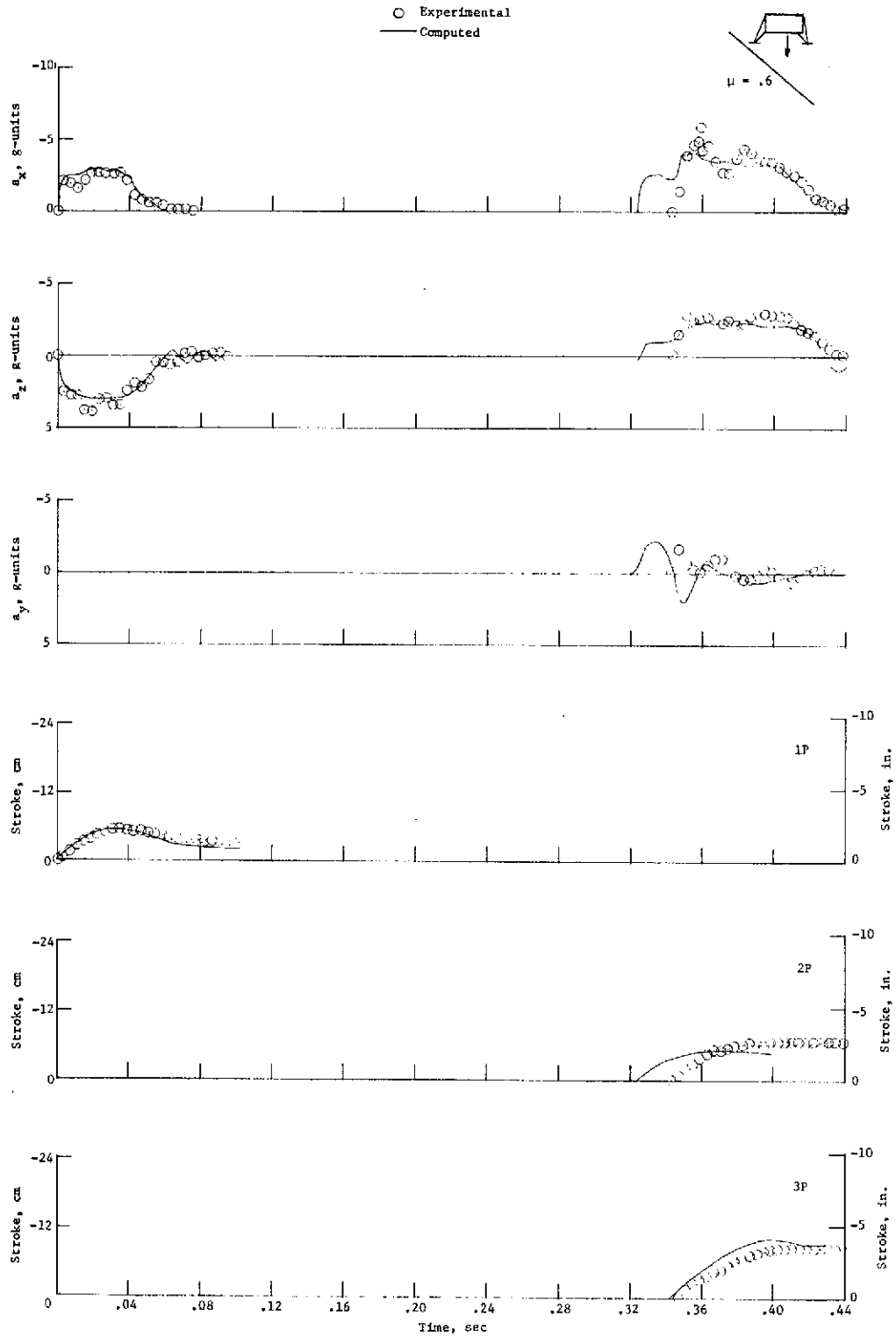

(q) Accelerations and primary-strut strokes for case 10.

Figure A1.- Continued.

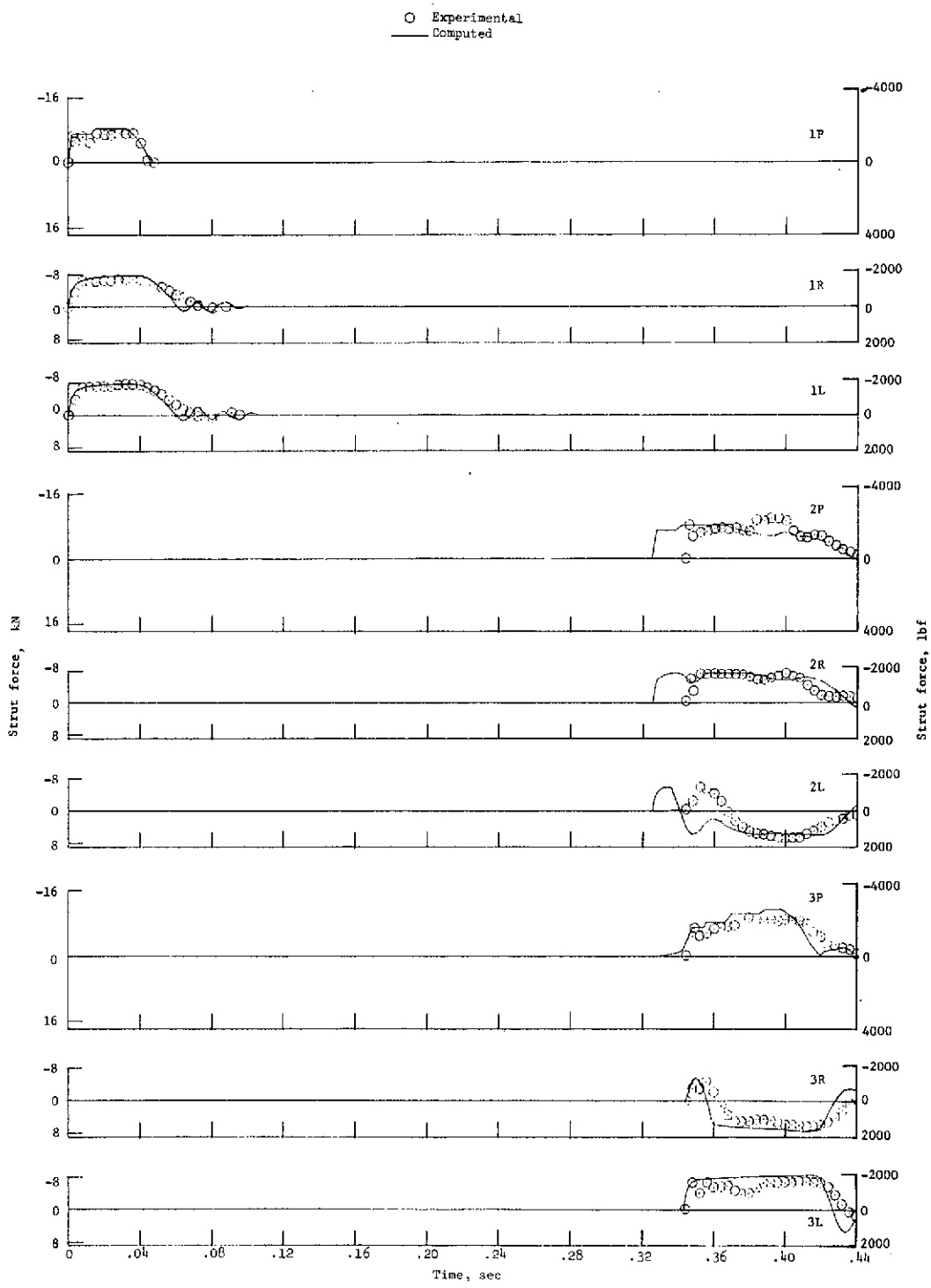

(r) Strut forces for case 10.

Figure A1.- Continued.

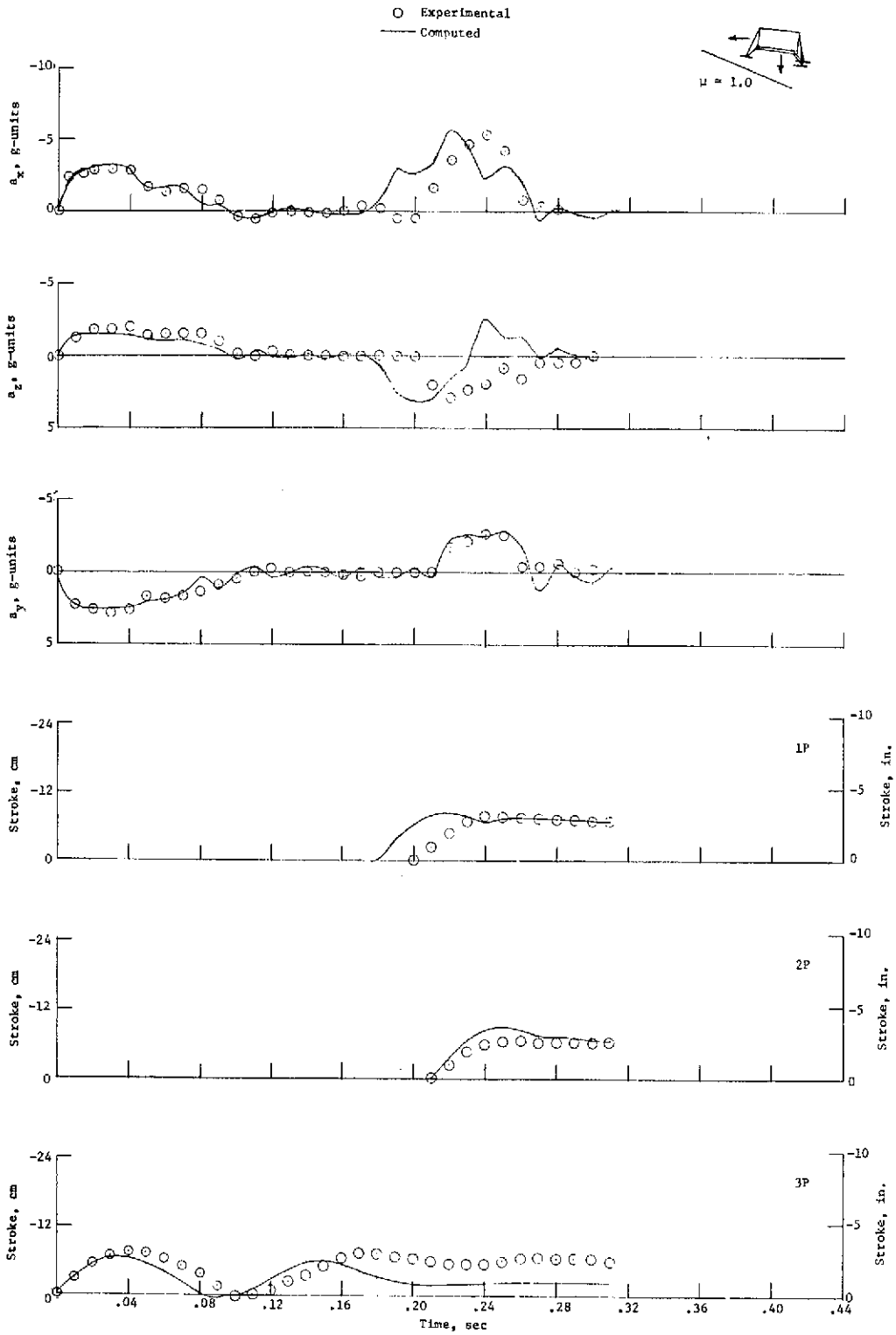

(s) Accelerations and primary-strut strokes for case 13.

Figure A1.- Continued.

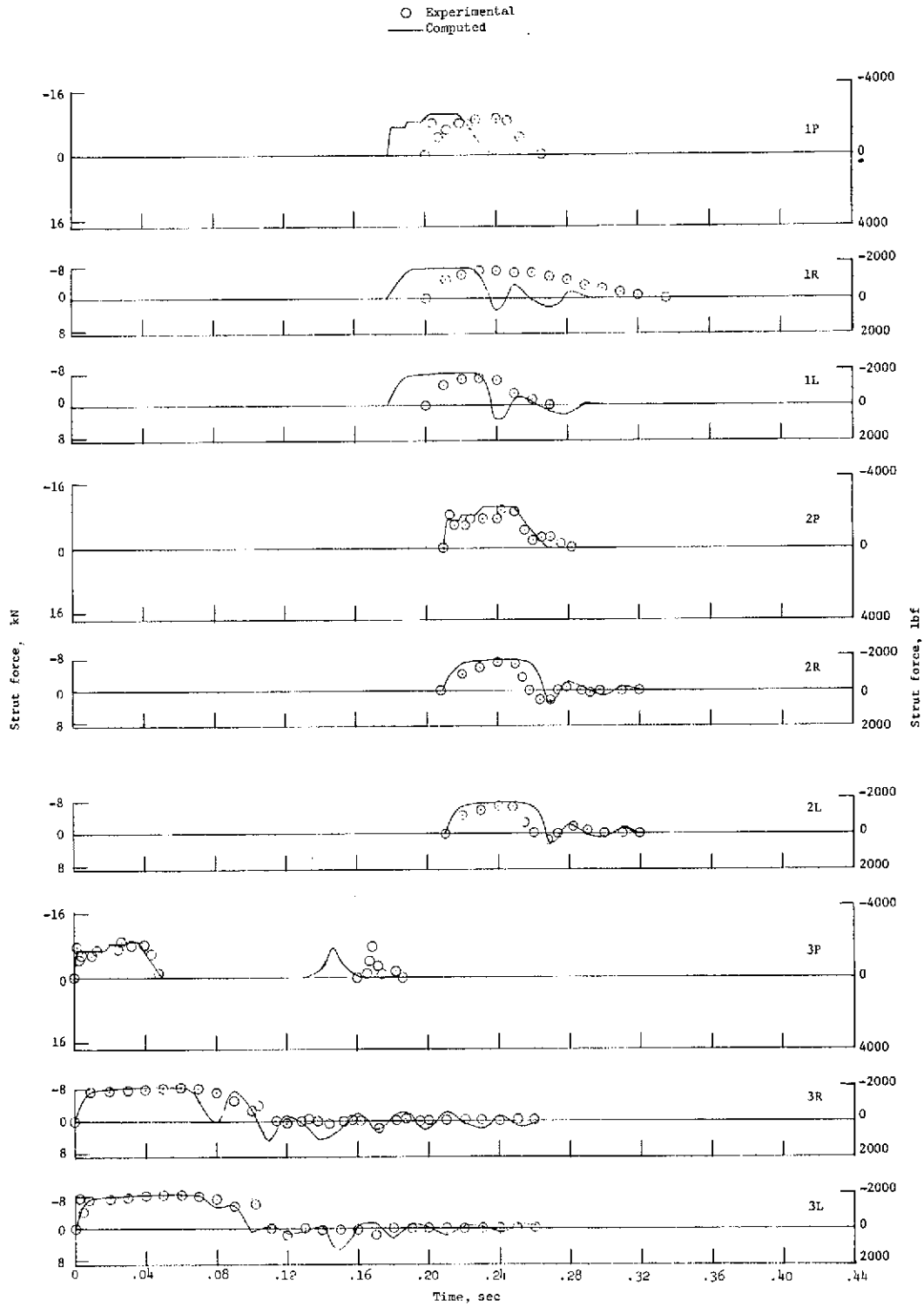

(t) Strut forces for case 13.

Figure A1.- Continued.

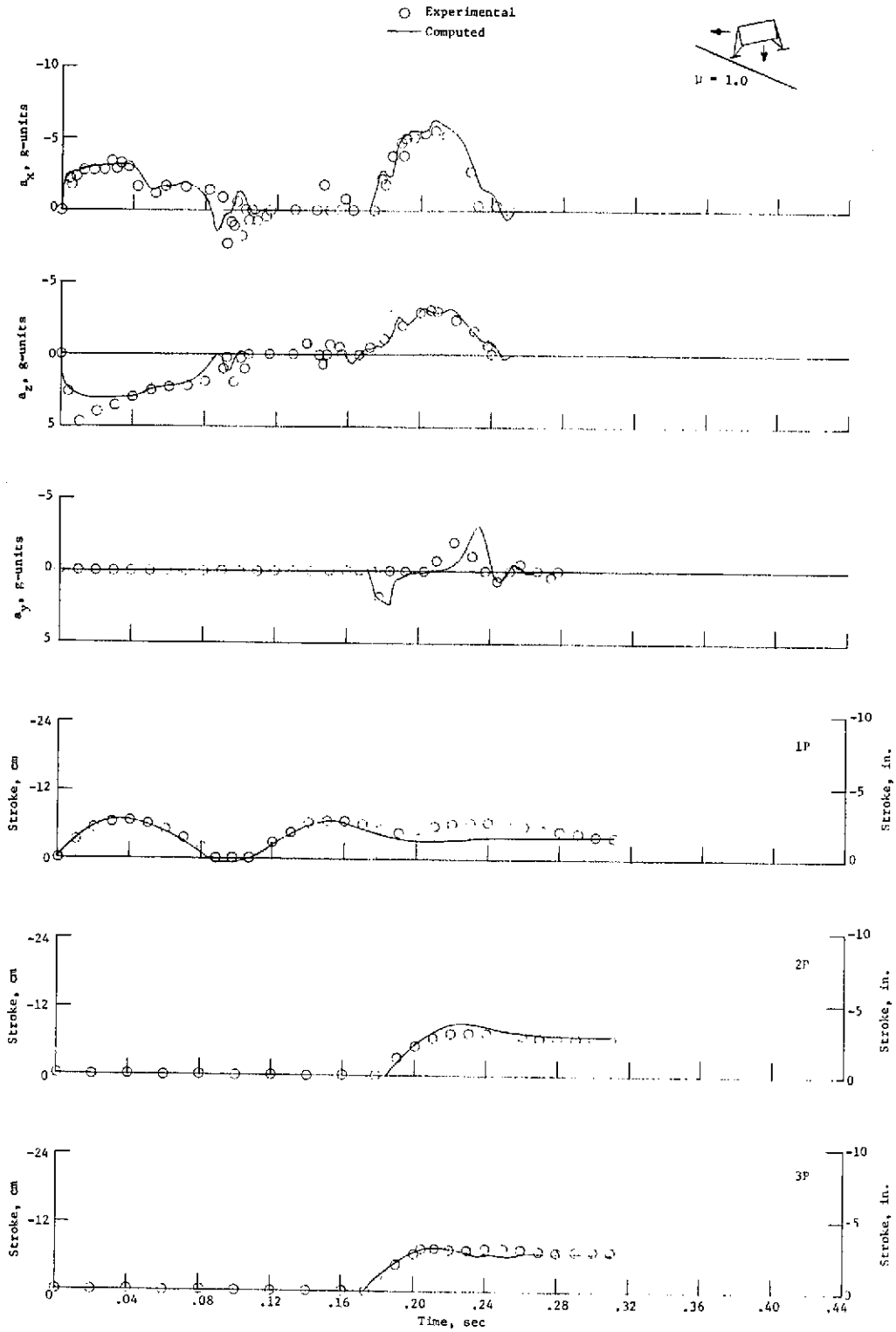

(u) Accelerations and primary-strut strokes for case 16.

Figure A1.- Continued.

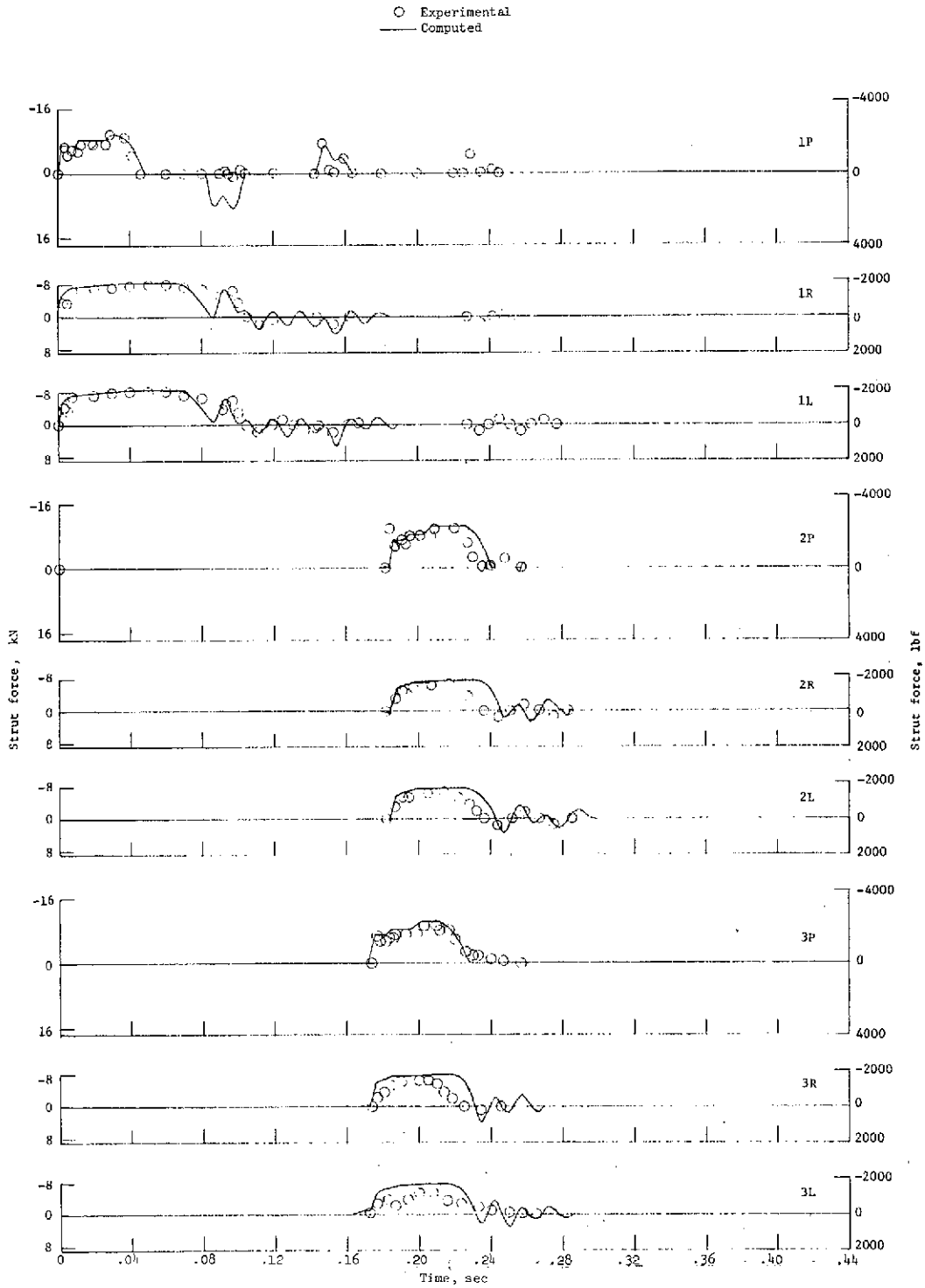

(v) Strut forces for case 16.

Figure A1.- Concluded.

REFERENCES

1. Mantus, M.; Lerner, E.; and Elkins, W.: Landing Dynamics of the Lunar Excursion Module (Method of Analysis). LED-520-6 (Contract NAS 9-1100), Grumman Aircraft Engineering Corp., Mar. 6, 1964.

2. Anon.: Summary Report of Lunar Landing Dynamics Systems Investigation. Rept. No. MM-64-10 (Dept 870), Bendix Products Aerospace Div., Bendix Corp., Oct. 1964.

3. Garba, J. A.; and Bookstein, D.: Surveyor Lunar Touchdown Computer Program: Rigid-Surface Version Usage Document. Tech Mem. 33-360 (Contract No. NAS 7-100), Jet Propulsion Lab., California Inst. Technol., Aug. 1967.

4. Herr, Robert W.; and Leonard, H. Wayne: Dynamic Model Investigation of Touchdown Stability of Lunar-Landing Vehicles. NASA TN D-4215, 1967.

5. Walton, William C., Jr.; and Durling, Barbara J.: A Procedure for Computing the Motion of a Lunar-Landing Vehicle During the Landing Impact. NASA TN D-4216, 1967.

6. Walton, W. C., Jr.; Herr, R. W.; and Leonard, H. W.: Studies of Touchdown Stability for Lunar Landing Vehicles. J. Spacecraft, vol. 1, no. 5, Sept.-Oct. 1964, pp. 552-556.

7. Zupp, George A., Jr.; and Doiron, Harold H.: A Mathematical Procedure for Predicting the Touchdown Dynamics of a Soft-Landing Vehicle. NASA TN D-7045, 1971.

8. Otto, O. R.; Laurenson, R. M.; Melliere, R. A.; and Moore, R. L.: Master Agreement Task Order Five – Analyses and Limited Evaluation of Payload and Legged Landing System Structures for the Survivable Soft Landing of Instrument Payloads. Contract No. NAS 1-8137, McDonnell Douglas Astronautics Company-East, July 1971. (Available as NASA CR-111919.)

9. Laurenson, R. M.: Master Agreement Task Order Six – Analytical Determination of the Effect of Structural Elasticity on Landing Stability of a Version of the Viking Lander. Contract No. NAS 1-8137, McDonnell Douglas Astronautics Company-East, Aug. 1972. (Available as NASA CR-112115.)

10. Stubbs, Sandy M.: Investigation of Technique for Conducting Landing-Impact Tests at Simulated Planetary Gravity. NASA TN D-6459, 1971.

11. Laurenson, Robert M.; Melliere, Ronald A.; and McGehee, John R.: Analysis of Legged Landers for the Survivable Soft Landing of Instrument Payloads. AIAA Paper No. 72-371, Apr. 1972.

TABLE I.- SCALE RELATIONSHIPS FOR SCALING MODEL RESULTS OBTAINED IN EARTH'S GRAVITY FIELD TO PREDICT FULL-SCALE RESULTS IN MARS' GRAVITY FIELD

[Gravitational[a] scale factor, $\beta = 8/3$; geometric scale factor, $\lambda = 3/8$]

Quantity	Earth 3/8-scale model	Scale factor	Mars full-scale model
Length[b]	l	$1/\lambda$	l/λ
Stress[b]	σ	1	σ
Linear acceleration[b]	a	$1/\beta$	a/β
Area	A	$1/\lambda^2$	A/λ^2
Force	F	$1/\lambda^2$	F/λ^2
Friction coefficient	μ	1	μ
Mass	m	β/λ^2	$\beta m/\lambda^2$
Linear velocity	V	$1/\sqrt{\beta\lambda}$	$V/\sqrt{\beta\lambda}$
Time	t	$\sqrt{\beta/\lambda}$	$t\sqrt{\beta/\lambda}$
Inertia	I	β/λ^4	$\beta I/\lambda^4$
Angular velocity	Ω	$1/\sqrt{\beta/\lambda}$	$\Omega/\sqrt{\beta/\lambda}$
Angular acceleration	α	λ/β	$\lambda\alpha/\beta$
Mass density	ρ	$\beta\lambda$	$\beta\lambda\rho$
Energy	E	$1/\lambda^3$	E/λ^3
Elastic spring rate	K	$1/\lambda$	K/λ

[a]The acceleration of gravity on Mars was assumed to be 3.69 m/s^2 (12.1 ft/sec^2) and that on earth to be 9.82 m/s^2 (32.2 ft/sec^2) for this investigation.

[b]Scale factors determining remaining scale relationships.

TABLE II.- PERTINENT MEASURED AND FULL-SCALE PARAMETERS

Parameter	3/8-scale experimental model	Full-scale model
Mass, kg (slugs)	30.1 (2.06)	570 (39.1)
Mass moments of inertia, kg-m^2 (slug-ft^2):		
Vehicle I_X, roll	2.17 (1.60)	293 (216)
Vehicle I_Y, pitch	1.29 (0.950)	174 (128)
Vehicle I_Z, yaw	1.50 (1.11)	202 (150)
Center body I_X, roll	1.57 (1.16)	212 (156)
Center body I_Y, pitch	1.11 (0.820)	150 (111)
Center body I_Z, yaw	0.94 (0.69)	126 (93.0)
Landing gear unsprung mass, kg (slugs)	0.803 (0.055)	15.0 (1.03)
Center-of-gravity location:		
Height, m (ft)	0.29 (0.94)	0.76 (2.50)
y-coordinate from vertical axis of symmetry, m (ft)	0 (0)	0 (0)
z-coordinate from vertical axis of symmetry, m (ft)	0 (0)	0 (0)
Elastic spring rates of primary struts, kN/m (lbf/ft)	421.76 (28 900)	1123.7 (77 000)
Elastic spring rates of drag strut and load alleviator, kN/m (lbf/ft)	421.76 (28 900)	1123.7 (77 000)

TABLE III.- MAXIMUM ACCELERATIONS, STROKES, AND FORCES FOR 3/8-SCALE EXPERIMENTAL MODEL

[All values are full scale]

(a) SI Units

Case no.	V_V, m/s	V_H, m/s	Landing attitude in –			ζ, deg	μ	Maximum acceleration at center of gravity, earth g units			Maximum strut strokes in centimeters for –			Maximum strut forces in kN for –									Stability
			Roll, deg	Pitch, deg	Yaw, deg			a_x	a_z	a_y	1P	2P	3P	Leg 1			Leg 2			Leg 3			
														1P	1R	1L	2P	2R	2L	3P	3R	3L	
1	4.017	0	180	-0.5	0	0	0.6	-7.1	1.1, -0.5	0.2, -0.2	-9.9	-10.7	-11.2	-12	-4.9, 1.3	-4.9, 0.9	-12	-4.4, 1.3	-4.9, 1.3	-10.7	-4.9, 1.3	-5.8, 1.3	Stable
2	3.420	1.2	0	0	0	20	.6	-4.5	3.2, -2.9	-2.4, 1.2	-3.8	-7.6	-9.7	-7.1	-5.3, 3.6	-5.3, 4.0	-9.8	-6.7, 2.7	-5.8, 6.2	-9.8	-4.9, 6.2	-7.1, 2.7	Stable
3	3.438	1.2	0	9.5	-.5	20	.6	-4.8	1.5, -3.5	-2.5, 1.2	-4.3	-8.6	-11.4	-7.1	4.4, -1.3	4.4, -1.3	-9.8	-7.1, 2.7	-5.3, 5.3	-10.7	-4.9, 4.4	-7.1, 1.3	Stable
4	3.106	1.2	0	-9.0	1.0	20	.6	-4.7	4.0, -2.9	2.2, -1.8	-4.6	-7.9	-7.9	-7.1	-6.2, 1.3	-6.7, 1.3	-9.3	-7.6, 1.8	-6.2, 6.7	-8.9	-4.9, 6.2	-6.7, 0.9	Stable
5	3.548	1.2	150	[a]0	[a]0	20	.6	-4.0	-1.4, 3.5	2.4, -2.7	-11.4	-5.8	-5.1	-11	-6.7, 1.8	-4.9, 3.6	-7.1	-4.4, 7.1	-7.1, 1.8	-8.0	-6.2, 2.7	-3.6, 4.9	Stable
6	3.066	1.2	0	-8.5	0	20	∞	-7.0	3.0, -3.5	-2.3, 1.5	-3.6	-5.8	-7.1	-7.1	-6.2, 1.3	-6.2, 1.8	-8.0	-9.8, 3.1	-7.6, 5.3	-8.9	-7.6, 7.6	-8.9, 2.7	Unstable
7	3.655	-1.2	180	9.0	0	20	.6	-5.6	-3.6, 2.6	-0.8, 1.4	-5.6	-8.6	-8.1	-7.6	-4.4, 1.8	-4.0, 0.9	-9.3	-8.9, 2.7	-5.3, 5.3	-9.3	-4.4, 4.4	-8.9, 3.6	Stable
8	3.353	0	0	.5	-1.0	33	.6	-4.6	3.6, -3.2	-2.5, 0.7	-5.3	-7.9	-10.2	-7.6	-7.1, 0.9	-7.1, 0.9	-9.8	-7.1, 0.4	-4.4, 5.8	-10.7	-4.0, 5.8	-8.0, 2.2	Stable
9	3.322	0	0	.3	-1.5	33	1.0	-5.4	4.1, -3.0	-2.6, 2.0	-5.8	-5.8	-7.1	-7.1	-7.6, 1.8	-7.6, 1.8	-7.6	-7.6, 1.8	-6.2, 3.6	-10.7	-4.9, 2.7	-8.0, 3.1	Unstable
10	3.353	0	0	.3	-1.3	35	.6	-4.8	3.5, -3.0	-1.3, 0.5	-5.3	-6.6	-8.6	-7.1	-6.7, 0.9	-7.1, 0.9	-9.8	-7.1, 0.9	-5.3, 6.7	-8.9	-4.4, 6.2	-7.1, 1.8	Stable
11	3.353	-1.2	0	-5.5	.8	19	1.0	-5.2	3.5, -2.8	1.4, -1.7	-6.9	-8.4	-6.9	-7.6	-8.0, 2.2	-8.5, 1.8	-8.9	-7.1, 1.3	-5.8, 1.3	-9.3	-2.7, 1.3	-4.4, 0.9	Unstable
12	3.353	-1.2	0	-5.5	0	30	1.0	-6.0	4.0, -3.0	-2.5, 3.5	-6.9	-7.4	-8.6	-9.8, 13	-7.6, 2.2	-8.9, 2.2	-9.3	-7.6, 1.3	-7.6, 3.1	-8.9	-6.7, 3.1	-7.6, 1.3	Stable
[b]13	3.359	-1.2	120	[a]2.3	[a]4.5	18	1.0	-5.2	-2.0, 2.7	2.8, -3.0	-8.1	-6.6	-7.6	-8.9	-6.7, 0	-6.7, 0.9	-8.9	-7.1, 2.7	-6.7, 1.3	-8.5	-8.0, 1.8	-7.6, 2.2	Unstable
14	3.359	-1.2	0	-4.3	0	19	Soil	-3.4	0.7, -0.5	0.5, -0.4	-1.0	-3.6	-3.8	-5.3	-0.9, 1.8	-0.9, 1.8	-7.6	2.7, -0.9	1.3	-7.1	1.8	3.1	Stable
15	3.359	1.2	0	10.0	-1.0	20	∞	-6.8	1.5, -4.2	-3.0, 1.5	-2.3	-8.1	-8.4	-7.1	4.4, -2.7	4.4, -2.7	-9.3	-9.3, 0.9	-7.1, 3.1	-8.9	-7.6, 4.4	-8.9, 2.7	Unstable
16	3.353	-1.2	0	-4.8	0	16	1.0	2.3, -5.5	4.3, -3.2	1.8, -2.1	-6.6	-7.4	-7.4	-9.8	-8.5, 1.8	-8.9, 1.8	-9.8	-6.2, 1.8	-6.7, 1.8	-9.3	-6.7, 0.9	1.8, -5.3	Stable

(b) U.S. Customary Units

Case no.	V_V, ft/sec	V_H, ft/sec	Landing attitude in –			ζ, deg	μ	Maximum acceleration at center of gravity, earth g units			Maximum strut strokes in inches for –			Maximum strut forces in lbf × 10^{-3} for –									Stability
			Roll, deg	Pitch, deg	Yaw, deg			a_x	a_z	a_y	1P	2P	3P	Leg 1			Leg 2			Leg 3			
														1P	1R	1L	2P	2R	2L	3P	3R	3L	
1	13.18	0	180	-0.5	0	0	0.6	-7.1	1.1, -0.5	0.2, -0.2	-3.9	-4.2	-4.4	-2.6	-1.1, 0.3	-1.1, 0.2	-2.6	-1.0, 0.3	-1.1, -0.3	-2.4	-1.1, 0.3	-1.3, 0.3	Stable
2	11.22	4.0	0	0	0	20	.6	-4.5	3.2, -2.9	-2.4, 1.2	-1.5	-3.0	-3.8	-1.6	-1.2, 0.8	-1.2, 0.9	-2.2	-1.5, 0.6	-1.3, 1.4	-2.2	-1.1, 1.4	-1.6, 0.6	Stable
3	11.28	4.0	0	9.5	-.5	20	.6	-4.8	1.5, -3.5	-2.5, 1.2	-1.7	-3.4	-4.5	-1.6	1.0, -0.3	1.0, -0.3	-2.2	-1.6, 0.6	-1.2, 1.2	-2.4	-1.1, 1.0	-1.6, 0.3	Stable
4	10.19	4.0	0	-9.0	1.0	20	.6	-4.7	4.0, -2.9	2.2, -1.8	-1.8	-3.1	-3.1	-1.6	-1.4, 0.3	-1.5, 0.3	-2.1	-1.7, 0.4	-1.4, 1.5	-2.0	-1.1, 1.4	-1.5, 0.2	Stable
5	11.64	4.0	150	[a]0	[a]0	20	.6	-4.0	-1.4, 3.5	2.4, -2.7	-4.5	-2.3	-2.0	-2.4	-1.5, 0.4	-1.1, 0.8	-1.6	-1.0, 1.6	-1.6, 0.4	-1.8	-1.4, 0.6	-0.8, 1.1	Stable
6	10.06	4.0	0	-8.5	0	20	∞	-7.0	3.0, -3.5	-2.3, 1.5	-1.4	-2.3	-2.8	-1.6	-1.4, 0.3	-1.4, 0.4	-1.8	-2.2, 0.7	-1.7, 1.2	-2.0	-1.7, 1.7	-2.0, 0.6	Unstable
7	11.99	-4.0	180	9.0	0	20	.6	-5.6	-3.6, 2.6	-0.8, 1.4	-2.2	-3.4	-3.2	-1.7	-1.0, 0.4	-0.9, 0.2	-2.1	-2.0, 0.6	-1.2, 1.2	-2.1	-1.0, 1.0	-2.0, 0.8	Stable
8	11.00	0	0	.5	-1.0	33	.6	-4.6	3.6, -3.2	-2.5, 0.7	-2.1	-3.1	-4.0	-1.7	-1.6, 0.2	-1.6, 0.2	-2.2	-1.6, 0.1	-1.0, 1.3	-2.4	-0.9, 1.3	-1.8, 0.5	Stable
9	10.90	0	0	.3	-1.5	33	1.0	-5.4	4.1, -3.0	-2.6, 2.0	-2.3	-2.3	-2.8	-1.6	-1.7, 0.4	-1.7, 0.4	-1.7	-1.7, 0.4	-1.4, 0.8	-2.4	-1.1, 0.6	-1.8, 0.7	Unstable
10	11.00	0	0	.3	-1.3	35	.6	-4.8	3.5, -3.0	-1.3, 0.5	-2.1	-2.6	-3.4	-1.6	-1.5, 0.2	-1.6, 0.2	-2.2	-1.6, 0.2	-1.2, 1.5	-2.0	-1.0, 1.4	-1.6, 0.4	Stable
11	11.00	-4.0	0	-5.5	.8	19	1.0	-5.2	3.5, -2.8	1.4, -1.7	-2.7	-3.3	-2.7	-1.7	-1.8, 0.5	-1.9, 0.4	-2.0	-1.6, 0.3	-1.3, 0.3	-2.1	-0.6, 0.3	-1.0, 0.2	Unstable
12	11.00	-4.0	0	-5.5	0	30	1.0	-6.0	4.0, -3.0	-2.5, 3.5	-2.7	-2.9	-3.4	-2.2, 2.9	-1.7, 0.5	-2.0, 0.5	-2.1	-1.7, 0.3	-1.7, 0.7	-2.0	-1.5, 0.7	-1.7, 0.3	Stable
[b]13	11.02	-4.0	120	[a]2.3	[a]4.5	18	1.0	-5.2	-2.0, 2.7	2.8, -3.0	-3.2	-2.6	-3.0	-2.0	-1.5, 0	-1.5, 0.2	-2.0	-1.6, 0.6	-1.5, 0.3	-1.9	-1.8, 0.4	-1.7, 0.5	Unstable
14	11.02	-4.0	0	-4.3	0	19	Soil	-3.4	0.7, -0.5	0.5, -0.4	-0.4	-1.4	-1.5	-1.2	-0.2, 0.4	-0.2, 0.4	-1.7	0.6, -0.2	0.3, 0	-1.6	0.4, 0	0.7, 0	Stable
15	11.03	4.0	0	10.0	-1.0	20	∞	-6.8	1.5, -4.2	-3.0, 1.5	-1.3	-3.2	-3.3	-1.6	1.0, -0.6	1.0, -0.6	-2.1	-2.1, 0.2	-1.6, 0.7	-2.0	-1.7, 1.0	-2.0, 0.6	Unstable
16	11.00	-4.0	0	-4.8	0	16	1.0	2.3, -5.5	4.3, -3.2	1.8, -2.1	-2.6	-2.9	-2.9	-2.2	-1.9, 0.4	-2.0, 0.4	-2.2, 0.2	-1.4, 0.4	-1.5, 0.4	-2.1	-1.5, 0.2	0.4, -1.2	Stable

[a]Preset values.

[b]Center of gravity is offset -0.040 m (-0.133 ft) along $Z\text{-axis}_{VCS}$ toward leg 1. Mass moments of inertia about the new axes changed 2 percent less.

TABLE IV.- MAXIMUM COMPUTED VALUES OF ACCELERATIONS, STROKES, AND FORCES FOR ANALYTICAL MODEL

[All values are full scale]

(a) SI Units

Case	V_V, m/s	V_H, m/s	Landing attitude in –			ζ, deg	μ	Maximum acceleration at center of gravity, earth g units			Maximum strut strokes in centimeters for –			Maximum strut forces in kN for –									Stability
														Leg 1			Leg 2			Leg 3			
			Roll, deg	Pitch, deg	Yaw, deg			a_x	a_z	a_y	1P	2P	3P	1P	1R	1L	2P	2R	2L	3P	3R	3L	
1	4.023	0	180	-0.3	0	0	0.6	-6.9	2.0, -1.7	0, 0	-11.9	-12.4	-12.4	-12	-5.8, 4.4	-5.8, 4.4	-12	-5.8, 4.9	-5.8, 4.4	-12	-5.8, 4.4	-5.8, 4.9	Stable
2	3.414	1.2	0	0	.5	20	.6	-4.6	2.5, -2.2	-2.0, 1.7	-4.8	-8.6	-10.9	-8.5	-5.8, 3.6	-5.8, 4.0	-11	-7.1, 1.3	-6.2, 6.7	-12	-5.8, 7.1	-7.1, 3.1	Stable
3	3.444	1.2	0	9.5	-.5	20	.6	-4.6	1.1, -2.5	-2.0, 2.0	-4.8	-9.4	-11.2	-8.5	4.9, -1.8	4.9, -1.8	-11	-7.1, 2.2	-6.2, 6.7	-12	-5.8, 6.7	-7.1, 3.6	Stable
4	3.109	1.2	0	-9.0	1.0	20	.6	-3.7	2.7, -2.6	2.2, -2.4	-4.6	-10.7	-7.4	-8.5	-6.7, 1.8	-6.7, 0.9	-12	-7.6, 2.7	-5.8, 6.2	-9.3	-6.2, 5.8	-7.1, 2.2	Stable
5	3.536	1.2	150	0	0	20	.6	-4.2	-1.5, 2.6	2.3, -2.3	-11.9	-7.4	-5.1	-12	-7.6, 2.2	-5.8, 6.2	-11	-5.8, 7.1	-7.1, 1.8	-8.5	-7.1, 4.0	-6.2, 5.3	Stable
6	3.078	1.2	0	-9.0	-1.0	20	1000.0	-6.4	2.8, -2.8	-2.4, 1.5	-3.6	-6.4	-7.1	-8.5, 11	-7.1, 2.7	-7.1, 3.1	-8.9	-10, 2.7	-7.6, 6.7	-11	-7.1, 7.6	-10, 3.6	Unstable
7	3.655	-1.2	180	9.0	0	20	.6	-5.5	-2.9, 2.6	0, 0	-6.9	-8.4	-8.4	-9.8	-5.8, 3.6	-5.3, 4.0	-11	-9.3, 5.8	-6.2, 6.2	-11	-6.2, 6.7	-8.9, 5.3	Stable
8	3.353	0	0	.5	-1.3	33	.6	-4.2	3.0, -2.5	-2.3, 1.6	-5.6	-6.1	-10.9	-8.5	-8.0, 1.3	-7.6, 1.8	-8.0	-7.1, 2.7	-6.2, 6.2	-12	-6.2, 7.1	-7.6, 5.8	Stable
9	3.322	0	0	.3	-1.5	33	1.0	-5.7	3.0, -2.5	-2.8, 3.0	-5.6	-6.1	-8.1	-8.5	-8.0, 1.8	-7.6, 1.8	-8.5	-8.9, 4.9	-8.0, 5.8	-11	-7.1, 6.2	-9.3, 5.3	Unstable
10	3.353	0	0	.3	0	35	.6	-4.1	3.0, -2.4	-2.2, 2.0	-5.6	-5.1	-10.4	-8.5	-8.0, 1.3	-7.6, 1.3	-8.5	-7.6, 1.3	-5.8, 5.8	-12	-5.3, 7.1	-8.9, 5.3	Stable
11	3.353	-1.2	0	-5.5	.8	19	1.0	-6.2	3.2, -3.2	2.1, -2.6	-6.9	-8.9	-7.6	-9.8, 8.0	-8.5, 4.0	-8.9, 4.0	-11	-8.0, 3.1	-7.6, 3.6	-11	-8.0, 4.4	-7.6, 3.1	Unstable
12	3.353	-1.2	0	-5.5	0	30	1.0	-6.3, 2.0	3.0, -3.0	0, 0	-6.9	-9.4	-9.4	-8.9, 13	-8.9, 6.2	-8.9, 6.2	-11, 4.9	-8.0, 5.8	-8.0, 5.3	-11, 4.9	-8.0, 4.0	-8.5, 5.8	Stable
[a]13	3.353	-1.2	120	2.3	4.5	18	1.0	-5.6, 0.5	3.2, -2.5	2.6, -2.8	-8.4	-6.6	-9.1	-10	-7.6, 2.7	-8.0, 3.6	-11	-8.0, 2.7	-8.0, 2.7	-8.9	-8.5, 4.4	-8.5, 5.3	Unstable
14	3.359	-1.2	0	-4.3	0	19	Soil	-3.2	0.9, -0.7	0, 0	-.8	-3.8	-3.8	-7.1	-1.8, 3.1	-1.8, 3.1	-8.0	-2.7, 0	-2.2, 0	-8.0	-2.2, 0	-2.7, 0	Stable
15	3.359	1.2	0	10.0	-1.0	20	1000.0	-6.5	0.8, -3.6	-2.3, 1.6	-4.3	-9.1	-10.9	-8.5	6.7, -1.8	7.1, -1.8	-11	-8.5, 4.4	-8.0, 4.9	-12	-8.0, 5.3	-8.9, 5.3	Unstable
16	3.353	-1.2	0	-5.0	-1.0	16	1.0	1.5, -6.3	3.1, -3.2	2.3, -3.1	-6.8, 0.8	-9.1	-7.6	-9.8, 8.9	-8.5, 4.0	-8.9, 5.3	-11	-7.6, 3.6	-7.6, 3.6	-10	-8.0, 4.0	-7.6, 3.1	Stable

(b) U.S. Customary Units

Case no.	V_V, ft/sec	V_H, ft/sec	Landing attitude in –			ζ, deg	μ	Maximum acceleration at center of gravity, earth g units			Maximum strut strokes in inches for –			Maximum strut forces in lbf × 10^{-3} for –									Stability
														Leg 1			Leg 2			Leg 3			
			Roll, deg	Pitch, deg	Yaw, deg			a_x	a_z	a_y	1P	2P	3P	1P	1R	1L	2P	2R	2L	3P	3R	3L	
1	13.20	0	180	-0.3	0	0	0.6	-6.9	2.0, -1.7	0, 0	-4.7	-4.9	-4.9	-2.6	-1.3, 1.0	-1.3, 1.0	-2.6	-1.3, 1.1	-1.3, 1.0	-2.6	-1.3, 1.0	-1.3, 1.1	Stable
2	11.20	4.0	0	0	.5	20	.6	-4.6	2.5, -2.2	-2.0, 1.7	-1.9	-3.4	-4.3	-1.9	-1.3, 0.8	-1.3, 0.9	-2.4	-1.6, 0.3	-1.4, 1.5	-2.6	-1.3, 1.6	-1.6, 0.7	Stable
3	11.30	4.0	0	9.5	-.5	20	.6	-4.6	1.1, -2.5	-2.0, 2.0	-1.9	-3.7	-4.4	-1.9	1.1, -0.4	1.1, -0.4	-2.4	-1.6, 0.5	-1.4, 1.5	-2.6	-1.3, 1.5	-1.6, 0.8	Stable
4	10.20	4.0	0	-9.0	1.0	20	.6	-3.7	2.7, -2.6	2.2, -2.4	-1.8	-4.2	-2.9	-1.9	-1.5, 0.4	-1.5, 0.2	-2.6	-1.7, 0.6	-1.3, 1.4	-2.1	-1.4, 1.3	-1.6, 0.5	Stable
5	11.60	4.0	150	0	0	20	.6	-4.2	-1.5, 2.6	2.3, -2.3	-4.7	-2.9	-2.0	-2.6	-1.7, 0.5	-1.3, 1.4	-2.4	-1.3, 1.6	-1.6, 0.4	-1.9	-1.6, 0.9	-1.4, 1.2	Stable
6	10.10	4.0	0	-9.0	-1.0	20	1000.0	-6.4	2.8, -2.8	-2.4, 1.5	-1.4	-2.5	-2.8	-1.9, 2.4	-1.6, 0.6	-1.6, 0.7	-2.0	-2.3, 0.6	-1.7, 1.5	-2.4	-1.6, 1.7	-2.3, 0.8	Unstable
7	11.99	-4.0	180	9.0	-1.5	20	.6	-5.5	-2.9, 2.6	0, 0	-2.7	-3.3	-3.3	-2.2	-1.3, 0.8	-1.2, 0.9	-2.4	-2.1, 1.3	-1.4, 1.4	-2.4	-1.4, 1.5	-2.0, 1.2	Stable
8	11.00	0	0	.5	-1.3	33	.6	-4.2	3.0, -2.5	-2.3, 1.6	-2.2	-2.4	-4.3	-1.9	-1.8, 0.3	-1.7, 0.4	-1.8	-1.6, 0.6	-1.4, 1.4	-2.6	-1.4, 1.6	-1.7, 1.3	Stable
9	10.90	0	0	.3	-1.5	33	1.0	-5.7	3.0, -2.5	-2.8, 3.0	-2.2	-2.4	-3.2	-1.9	-1.8, 0.4	-1.7, 0.4	-1.9	-2.0, 1.1	-1.8, 1.3	-2.4	-1.6, 1.4	-2.1, 1.2	Unstable
10	11.00	0	0	.3	0	35	.6	-4.1	3.0, -2.4	-2.2, 2.0	-2.2	-2.0	-4.1	-1.9	-1.8, 0.3	-1.7, 0.3	-1.9	-1.7, 0.3	-1.3, 1.3	-2.6	-1.2, 1.6	-2.0, 1.2	Stable
11	11.00	-4.0	0	-5.5	.8	19	1.0	-6.2	3.2, -3.2	2.1, -2.6	-2.7	-3.5	-3.0	-2.2, 1.8	-1.9, 0.9	-2.0, 0.9	-2.4	-1.8, 0.7	-1.7, 0.8	-2.4	-1.8, 1.0	-1.7, 0.7	Unstable
12	11.00	-4.0	0	-5.5	0	30	1.0	-6.3, 2.0	3.0, -3.0	0, 0	-2.7	-3.7	-3.7	-2.0, 2.9	-2.0, 1.4	-2.0, 1.4	-2.4, 1.1	-1.8, 1.3	-1.8, 0.9	-2.4, 1.1	-1.8, 0.9	-1.9, 1.3	Stable
[a]13	11.00	-4.0	120	2.3	4.5	18	1.0	-5.6, 0.5	3.2, -2.5	2.6, -2.8	-3.3	-2.6	-3.6	-2.3	-1.7, 0.6	-1.8, 0.8	-2.4	-1.8, 0.6	-1.8, 0.6	-2.0	-1.9, 1.0	-1.9, 1.2	Unstable
14	11.02	-4.0	0	-4.3	0	19	Soil	-3.2	0.9, -0.7	0, 0	-.3	-1.5	-1.5	-1.6	-0.4, 0.7	-0.4, 0.7	-1.8	0.6, 0	0.5, 0	-1.8	0.5, 0	0.6, 0	Stable
15	11.03	4.0	0	10.0	-1.0	20	1000.0	-6.5	0.8, -3.6	-2.3, 1.6	-1.7	-3.6	-4.3	-1.9	1.5, -0.4	1.6, -0.4	-2.4	-1.9, 1.0	-1.8, 1.1	-2.6	-1.8, 1.2	-2.0, 1.2	Unstable
16	11.00	-4.0	0	-5.0	-1.0	16	1.0	1.5, -6.3	3.1, -3.2	2.3, -3.1	-2.7, 0.3	-3.6	-3.0	-2.2, 2.0	-1.9, 0.9	-2.0, 1.2	-2.4	-1.7, 0.8	-1.7, 0.8	-2.3	-1.8, 0.9	-1.7, 0.7	Stable

[a]Center of gravity is offset -0.040 m (-0.133 ft) along Z-axis$_{VCS}$ toward leg 1. Mass moments of inertia about the new axes changed 2 percent less.

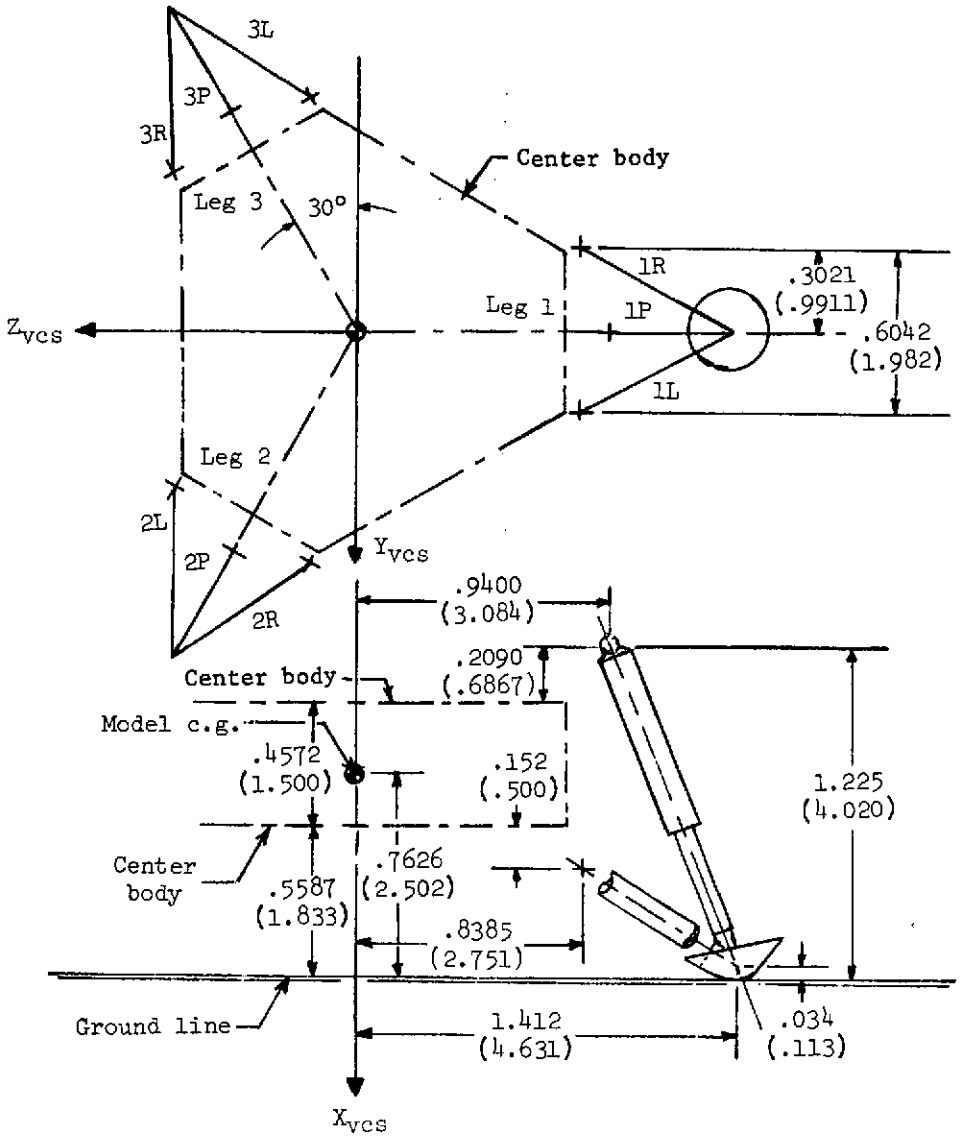

Figure 1.- General arrangement of lander. Dimensions are in m (ft). All values are full scale.

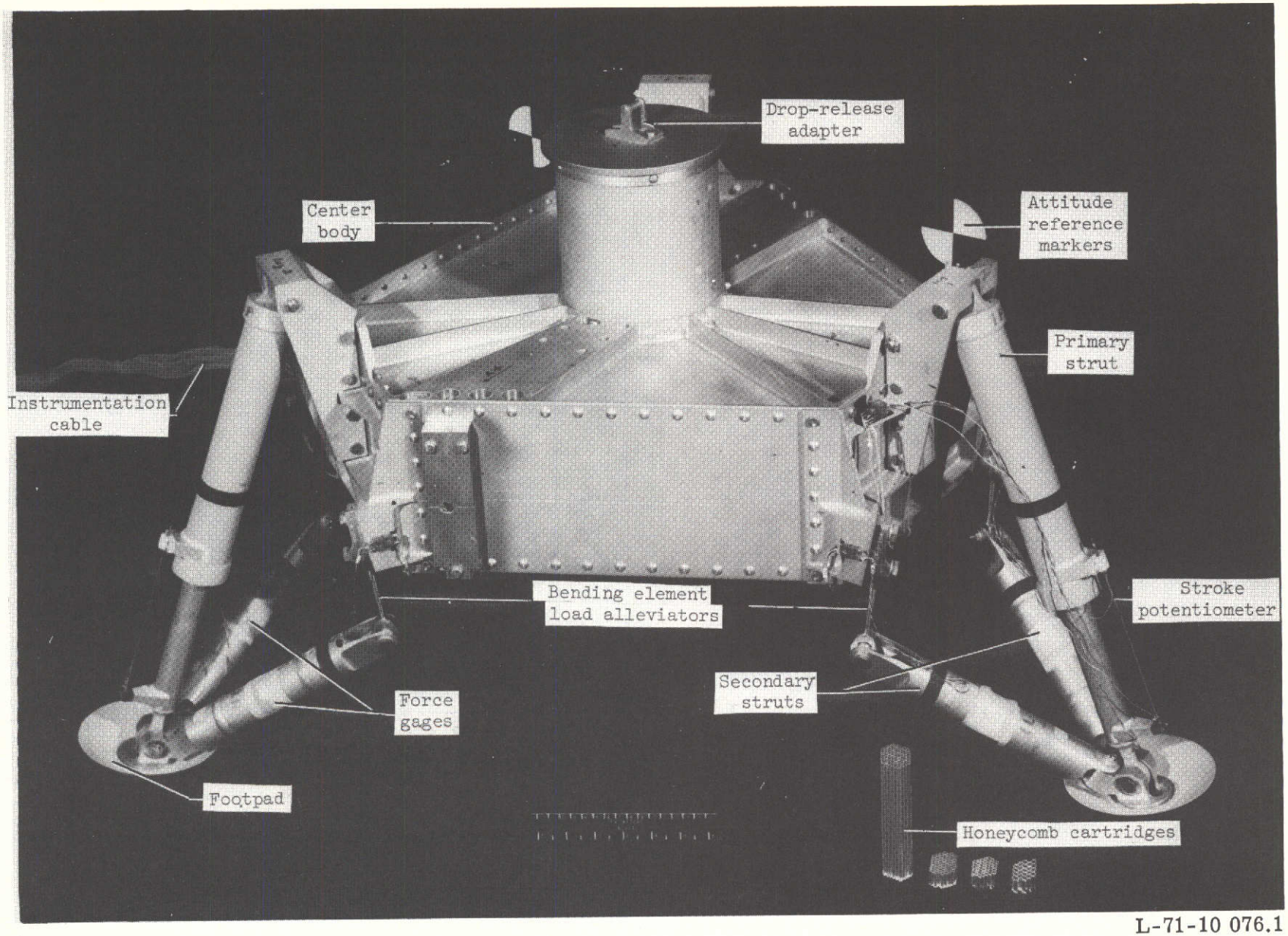

L-71-10 076.1

Figure 2.- Photograph of 3/8-scale experimental model.

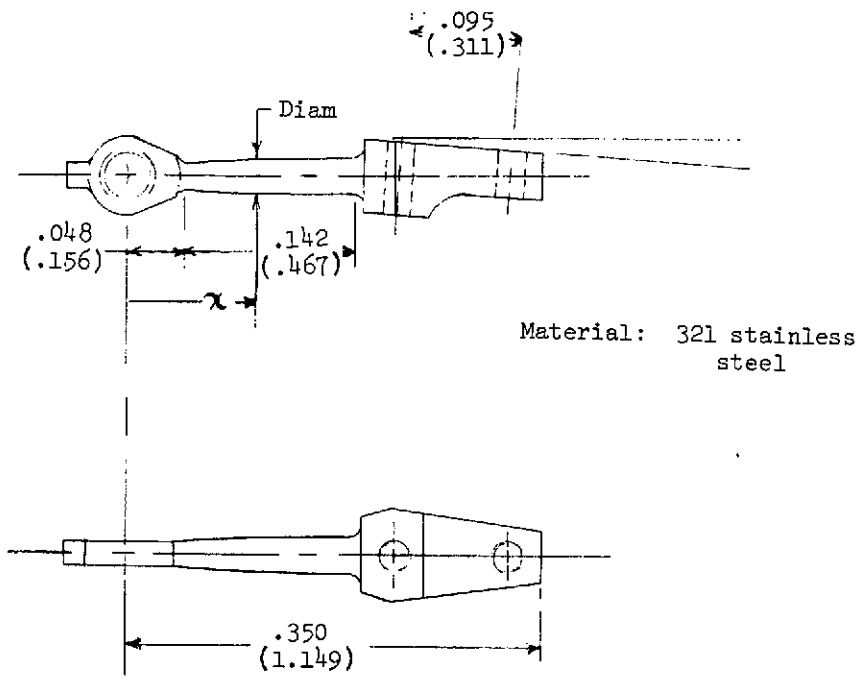

Distance, x	Diameter ±0.0001 (±0.0004)	Distance, x	Diameter ±0.0001 (±0.0004)
0.048 (0.156)	0.0170 (0.0558)	0.122 (0.400)	0.0219 (0.0720)
.054 (.177)	.0177 (.0580)	.129 (.422)	.0222 (.0729)
.061 (.200)	.0183 (.0600)	.135 (.444)	.0225 (.0738)
.068 (.222)	.0188 (.0618)	.142 (.467)	.0227 (.0746)
.074 (.244)	.0193 (.0633)	.149 (.489)	.0230 (.0756)
.081 (.267)	.0198 (.0649)	.156 (.511)	.0232 (.0762)
.088 (.289)	.0202 (.0662)	.162 (.533)	.0235 (.0771)
.095 (.311)	.0206 (.0676)	.169 (.556)	.0237 (.0778)
.101 (.333)	.0210 (.0689)	.176 (.578)	.0239 (.0784)
.109 (.356)	.0213 (.0700)	.183 (.600)	.0241 (.0791)
.115 (.378)	.0216 (.0709)	.190 (.622)	.0243 (.0796)

Figure 3.- Secondary-strut bending-element load alleviators. Dimensions are in m (ft). All values are full scale.

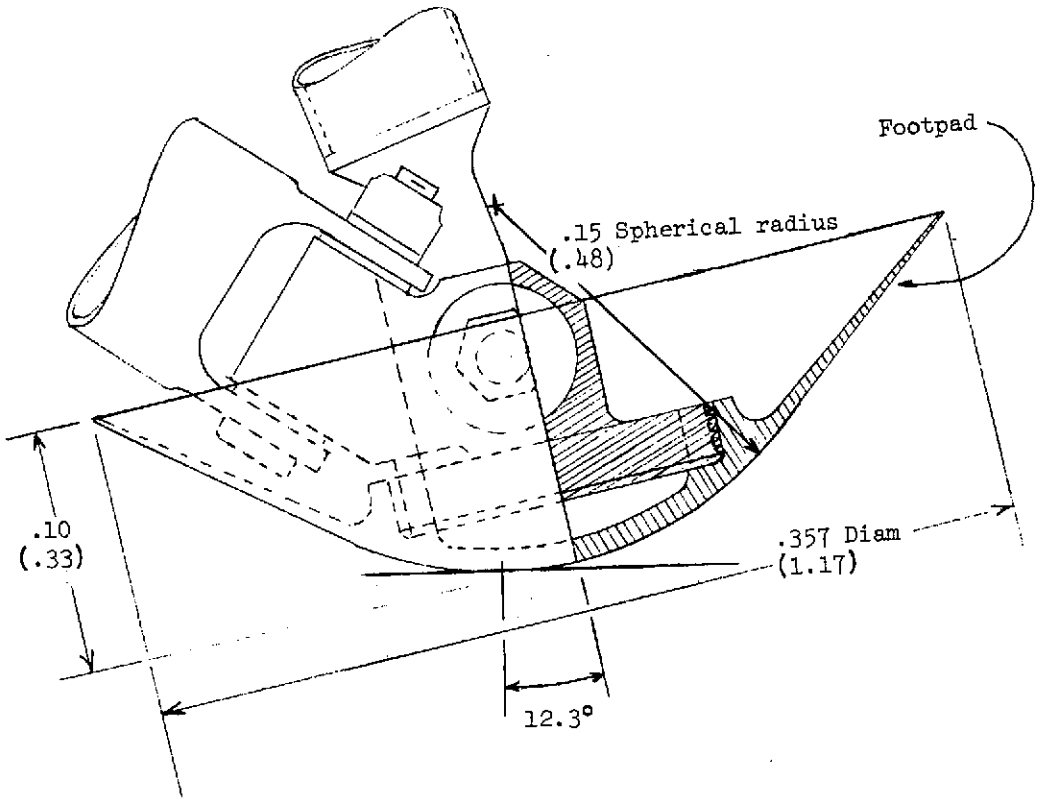

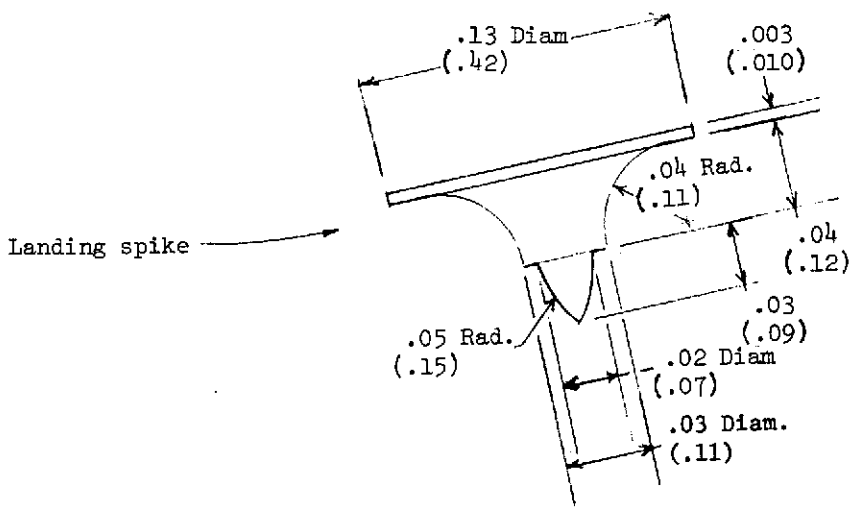

Figure 4.- Schematic drawing of footpad and landing spike. Dimensions are shown in m (ft). All values are full scale.

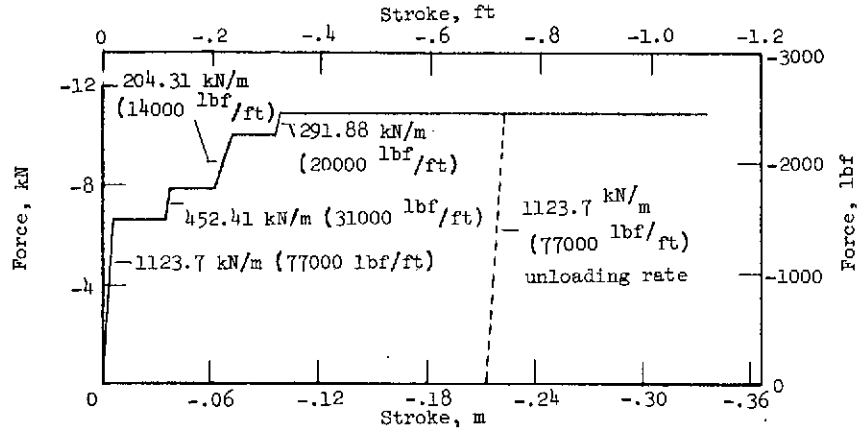

(a) Nominal force-stroke characteristics of primary struts.

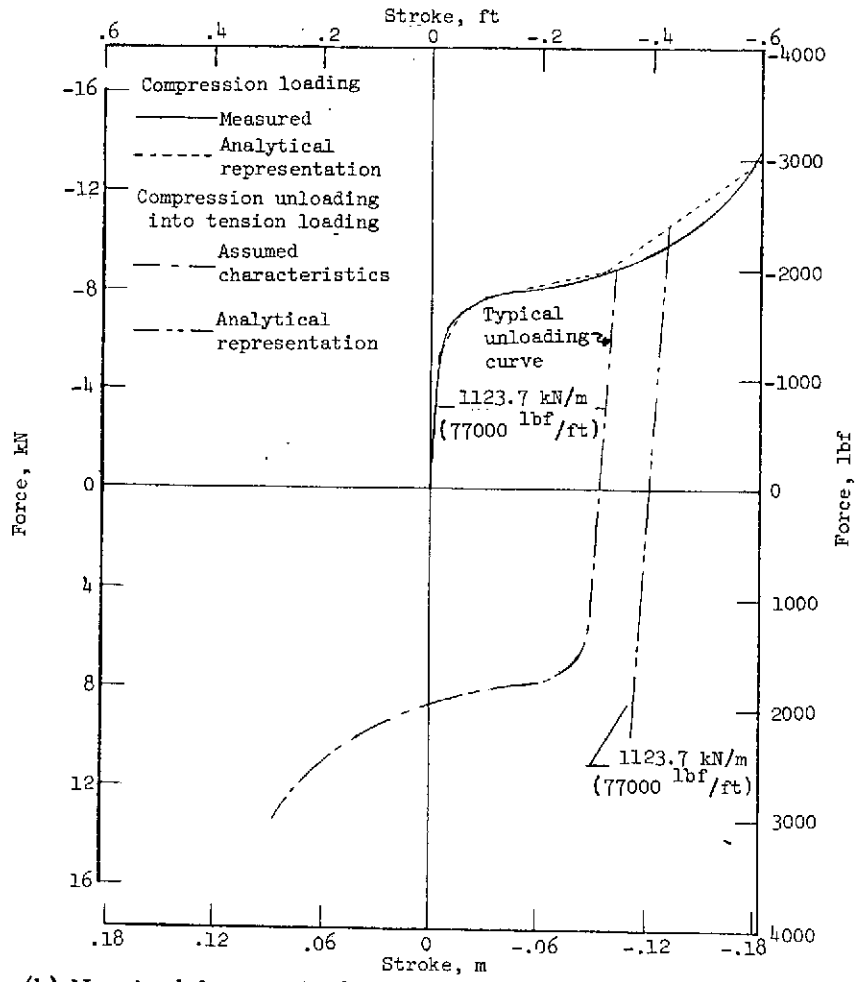

(b) Nominal force-stroke characteristics of secondary struts and load alleviators.

Figure 5.- Experimental and analytical force-stroke characteristics of primary and secondary struts. All values are full scale.

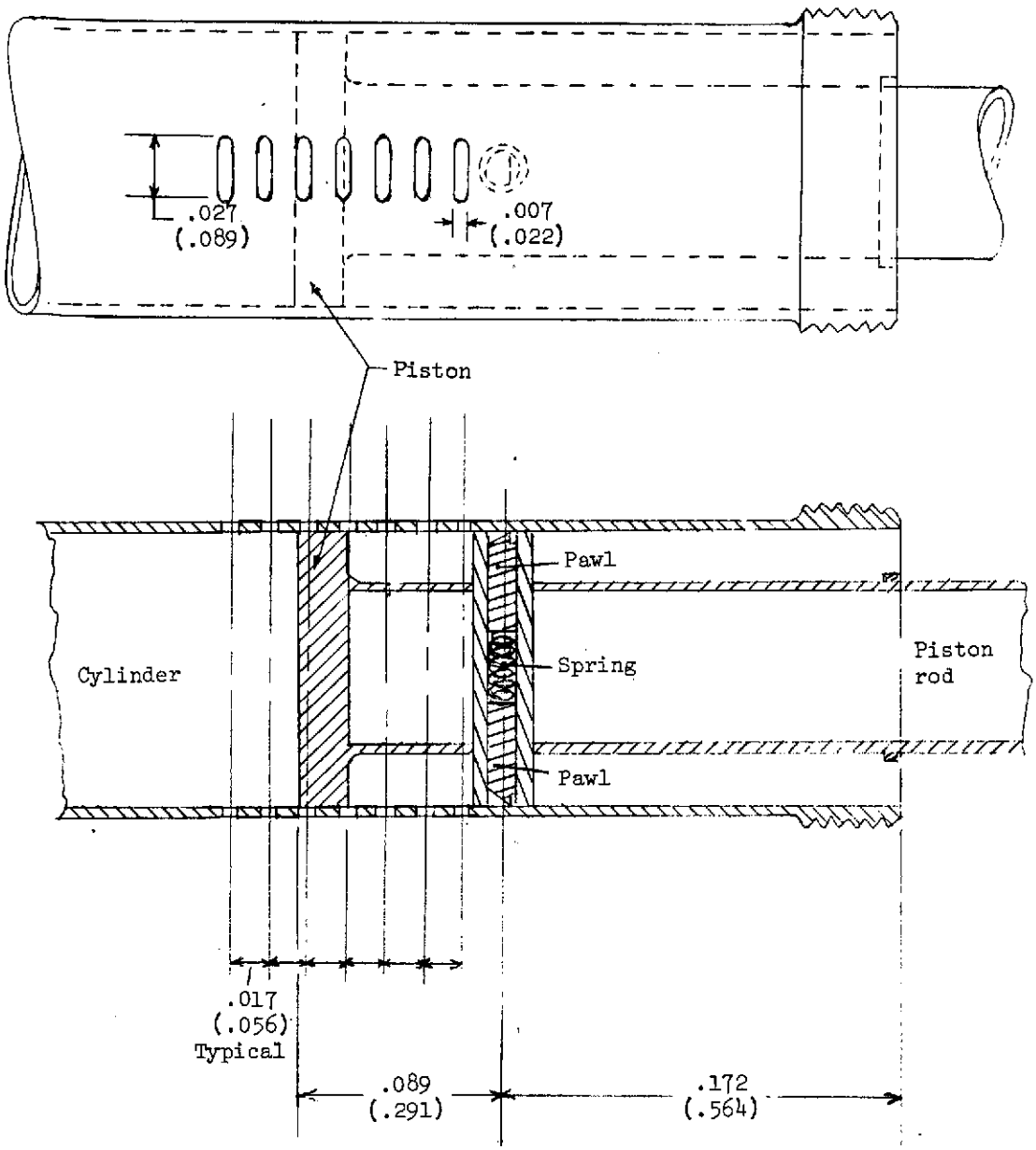

Figure 6.- Ratchet mechanism used for eliminating primary-strut deadband. Dimensions are shown in m (ft). All values are full scale.

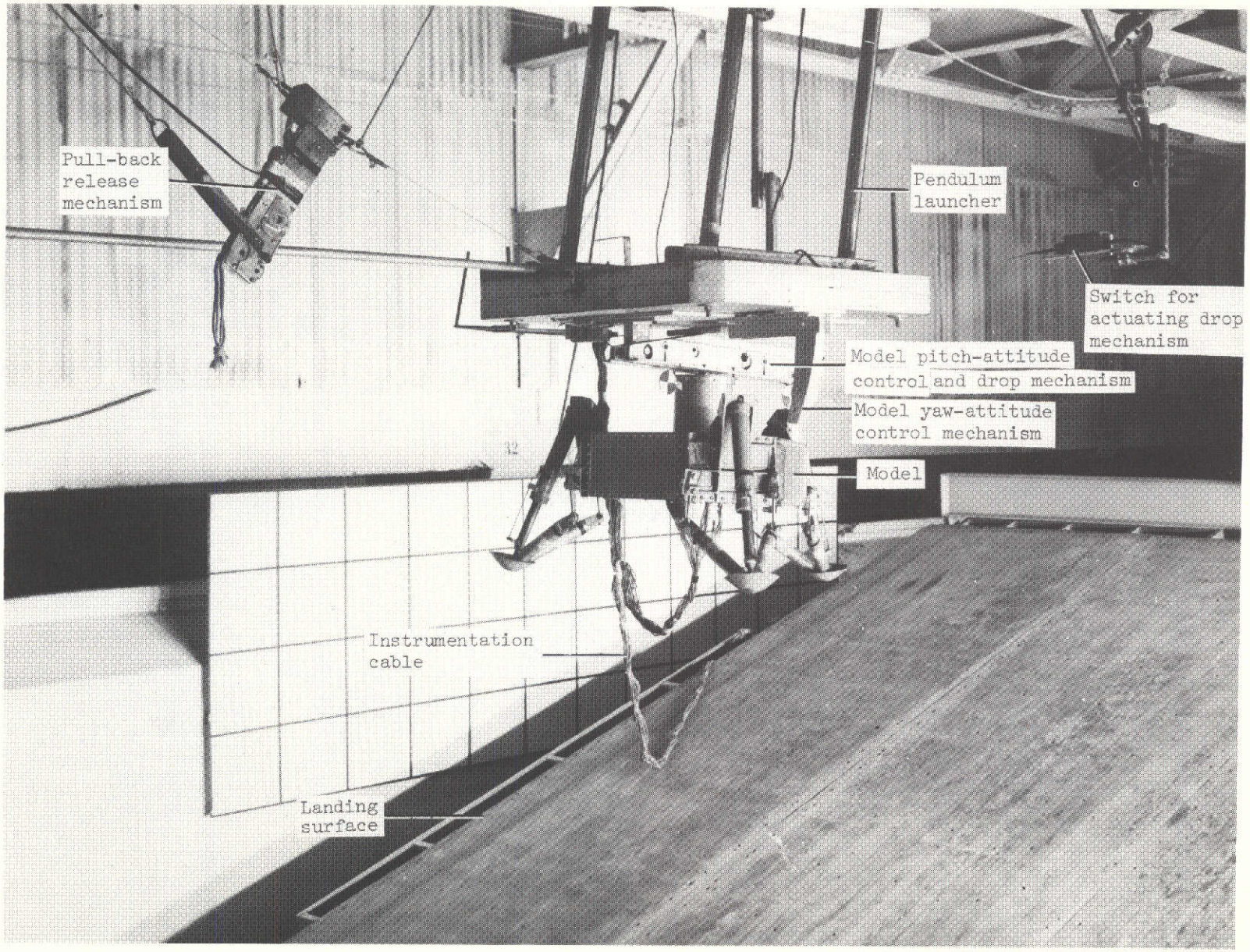

L-72-4346.1

Figure 7.- Photograph of a test setup.

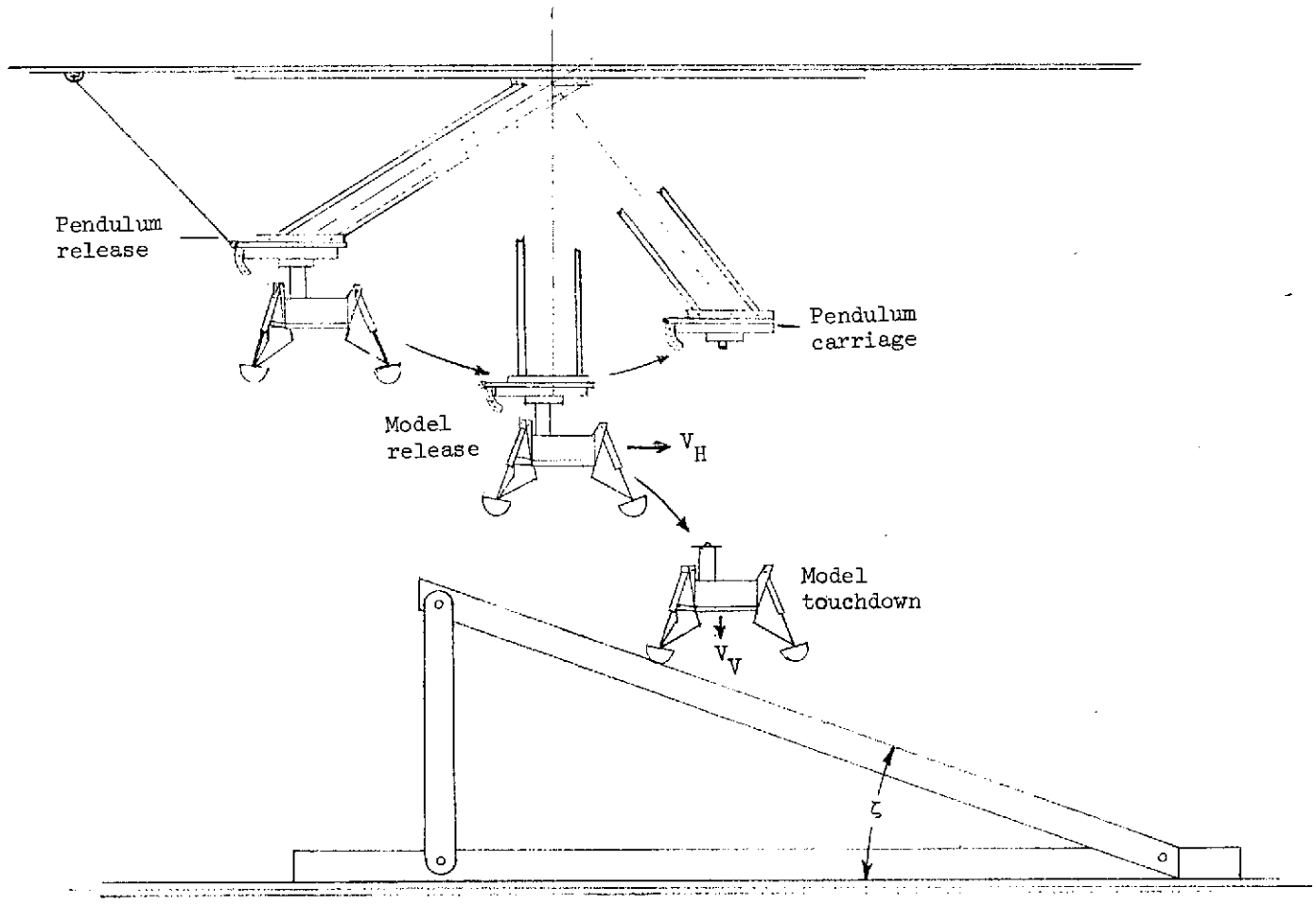

Figure 8.- Sketch illustrating pendulum operation during model launch and landing.

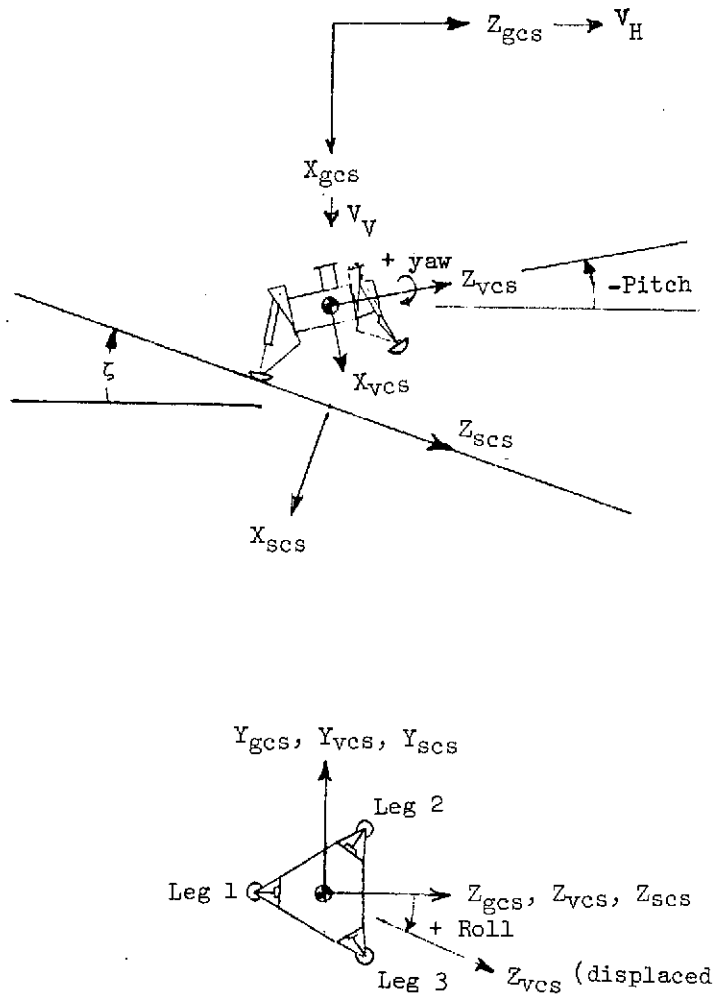

Figure 9.- Sketches identifying coordinate systems, vehicle attitudes, and surface slopes.

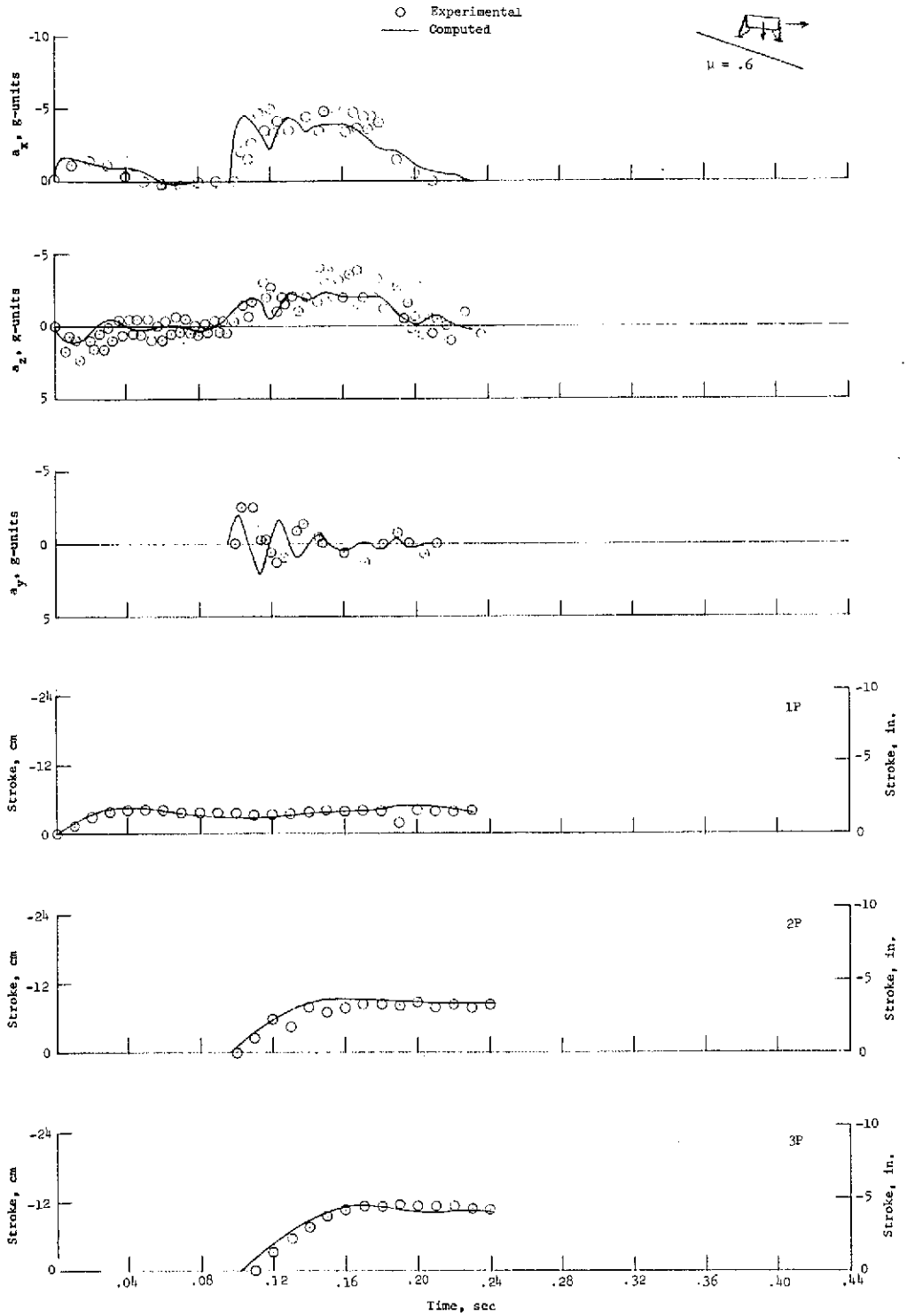

(a) Accelerations and primary-strut strokes for case 3.

Figure 10.- Experimental and analytical time histories showing the effect of friction coefficient. All values are full scale.

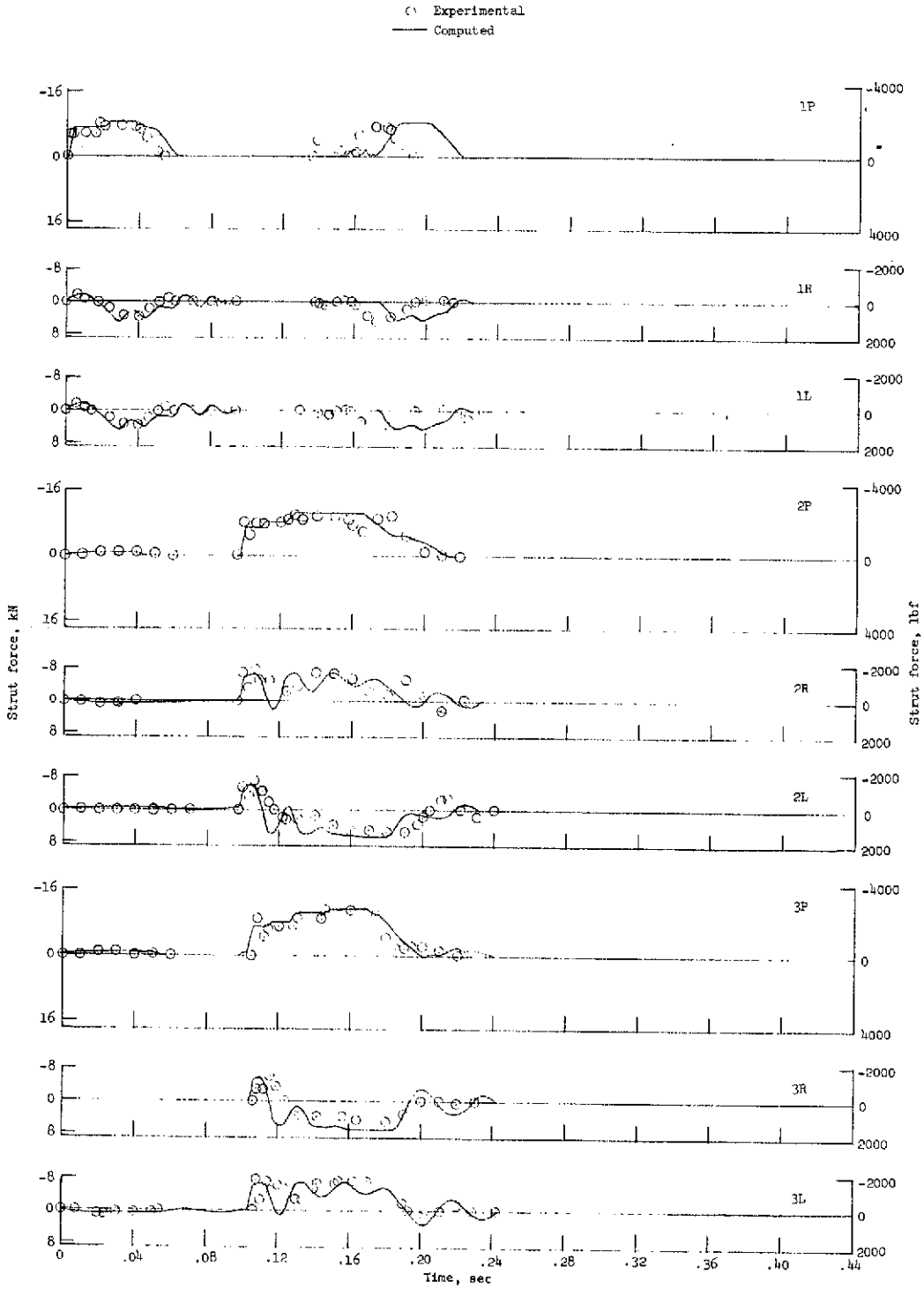

(b) Strut forces for case 3.

Figure 10.- Continued.

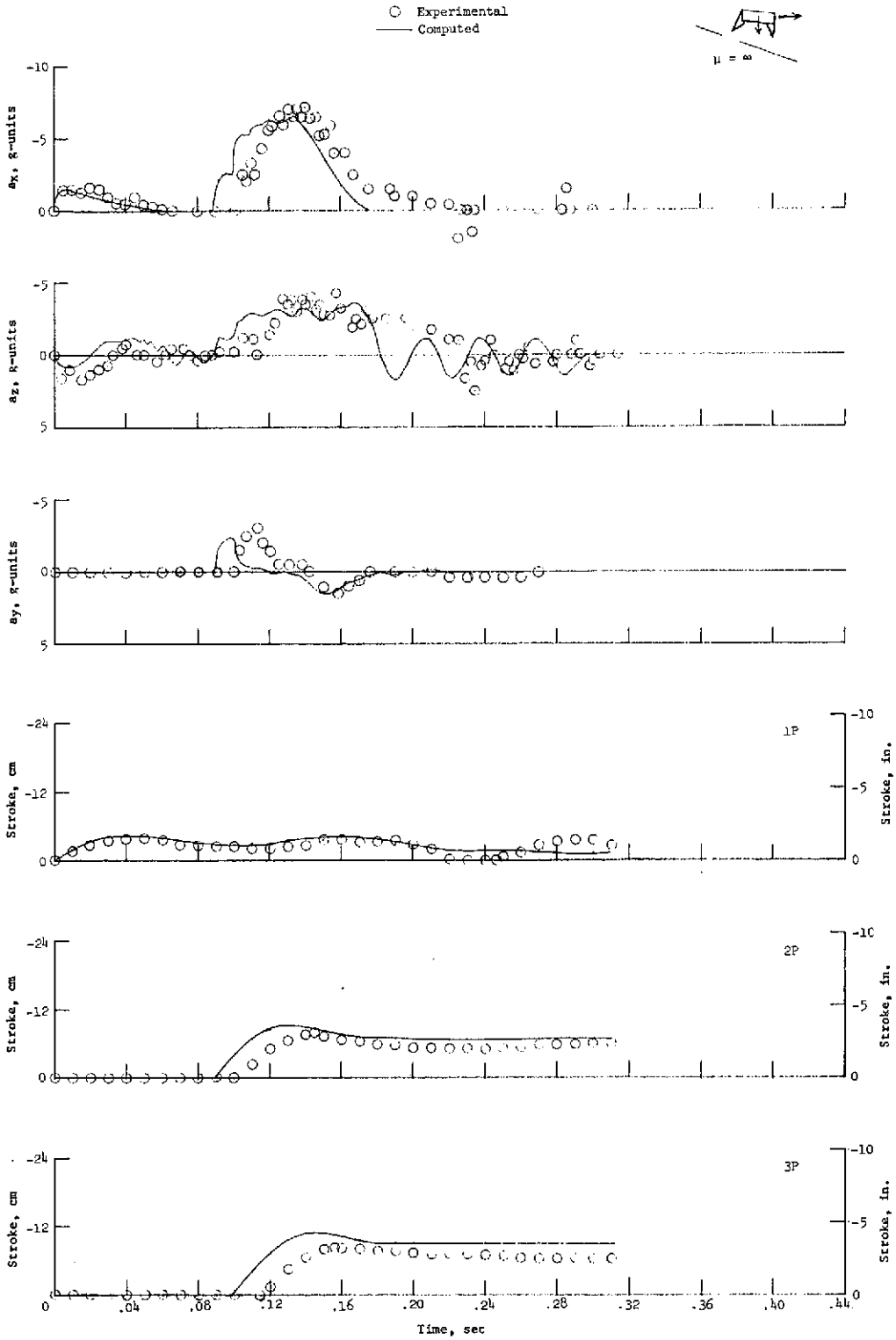

(c) Accelerations and primary-strut strokes for case 15.

Figure 10.- Continued.

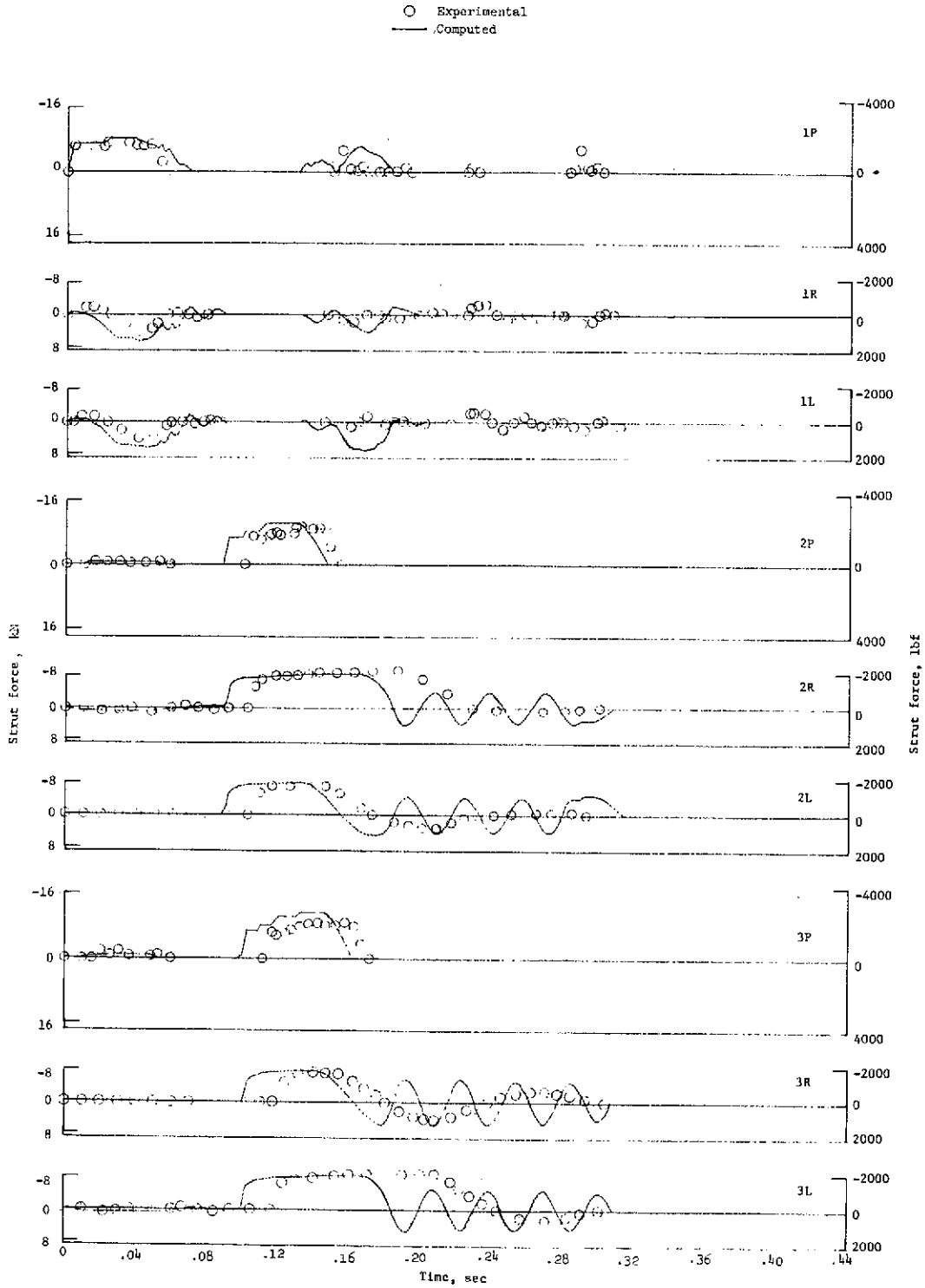

(d) Strut forces for case 15.

Figure 10.- Concluded.

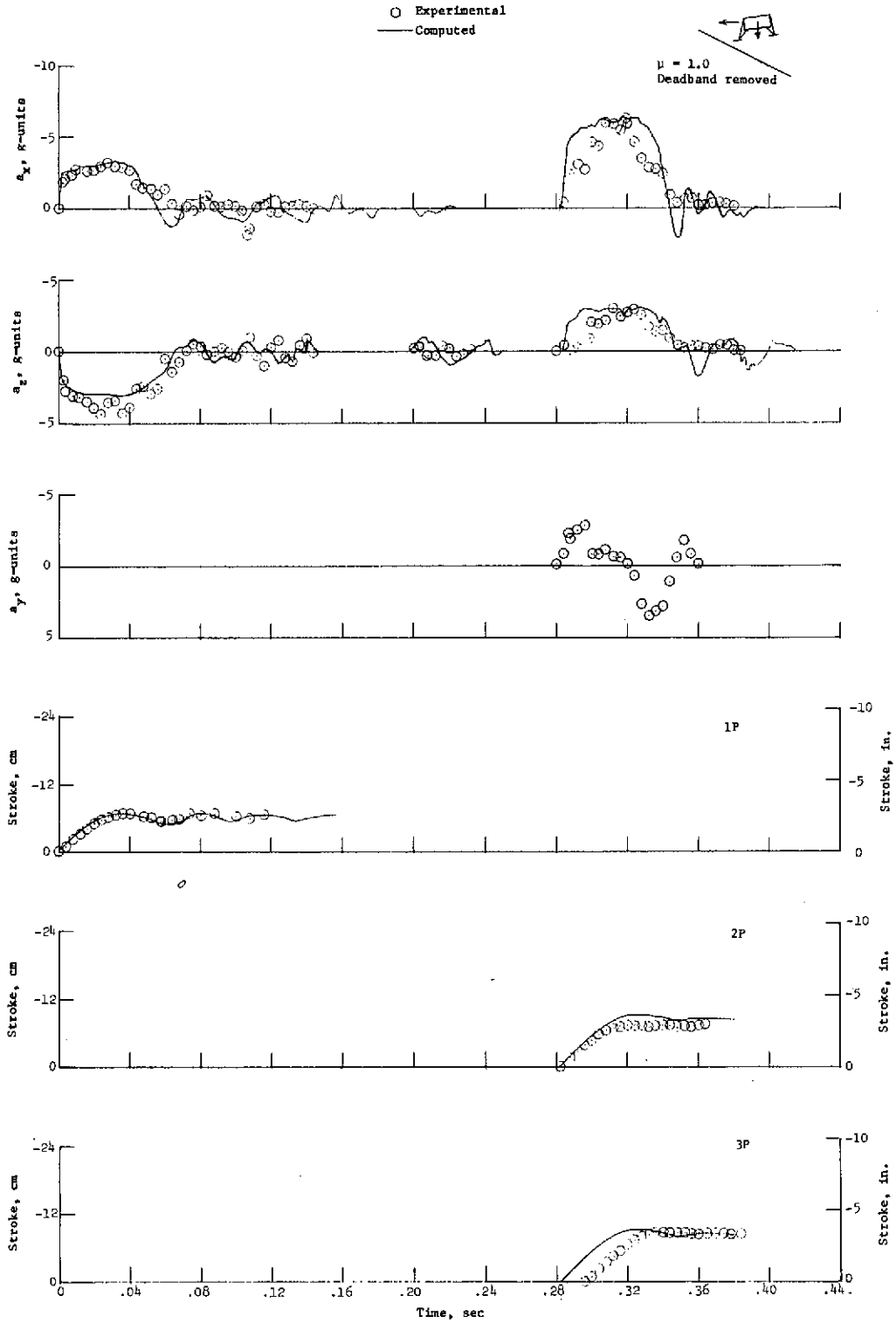

(a) Accelerations and primary-strut strokes for case 12.

Figure 11.- Experimental and analytical time histories showing the effect of removing primary-strut deadband. All values are full scale.

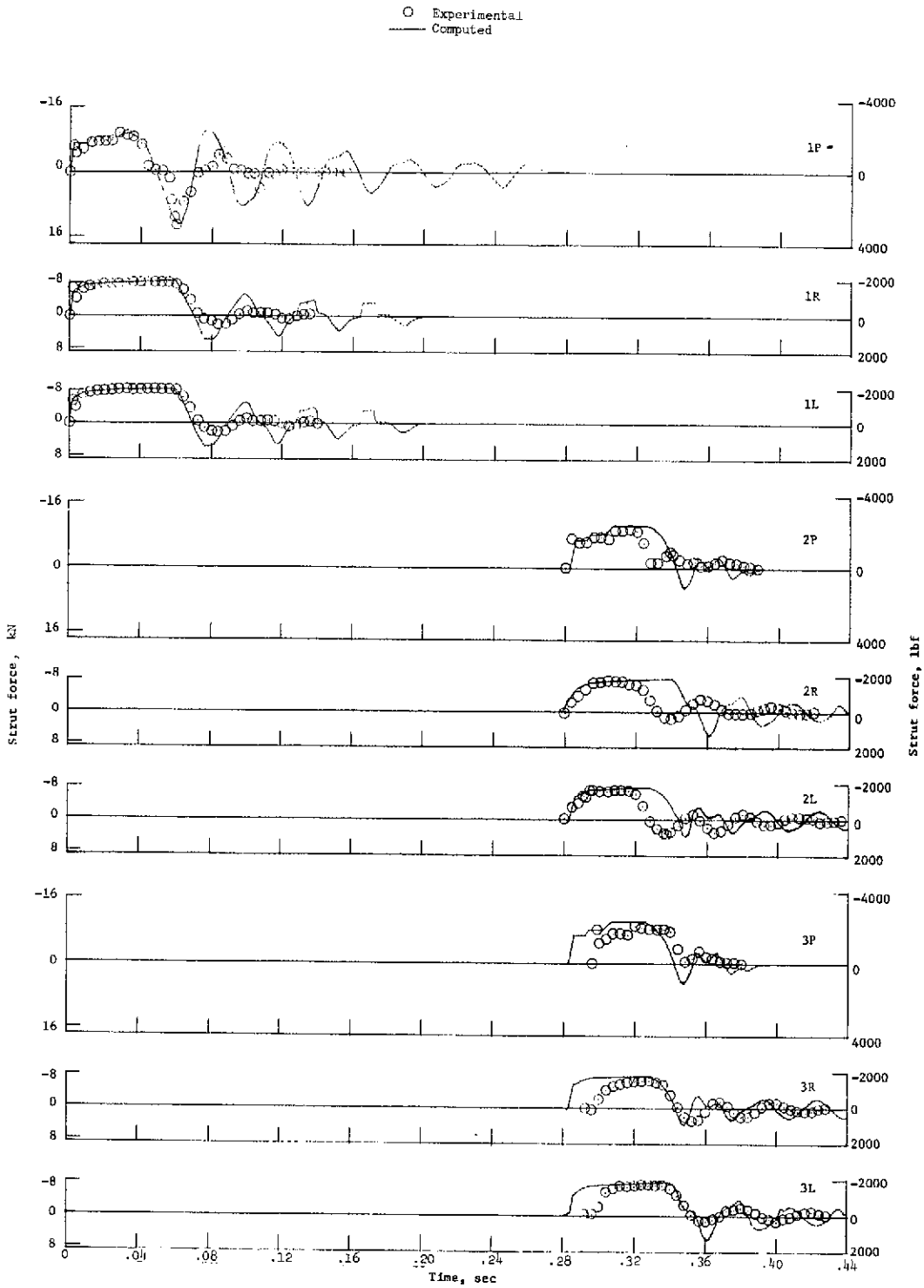

(b) Strut forces for case 12.

Figure 11.- Continued.

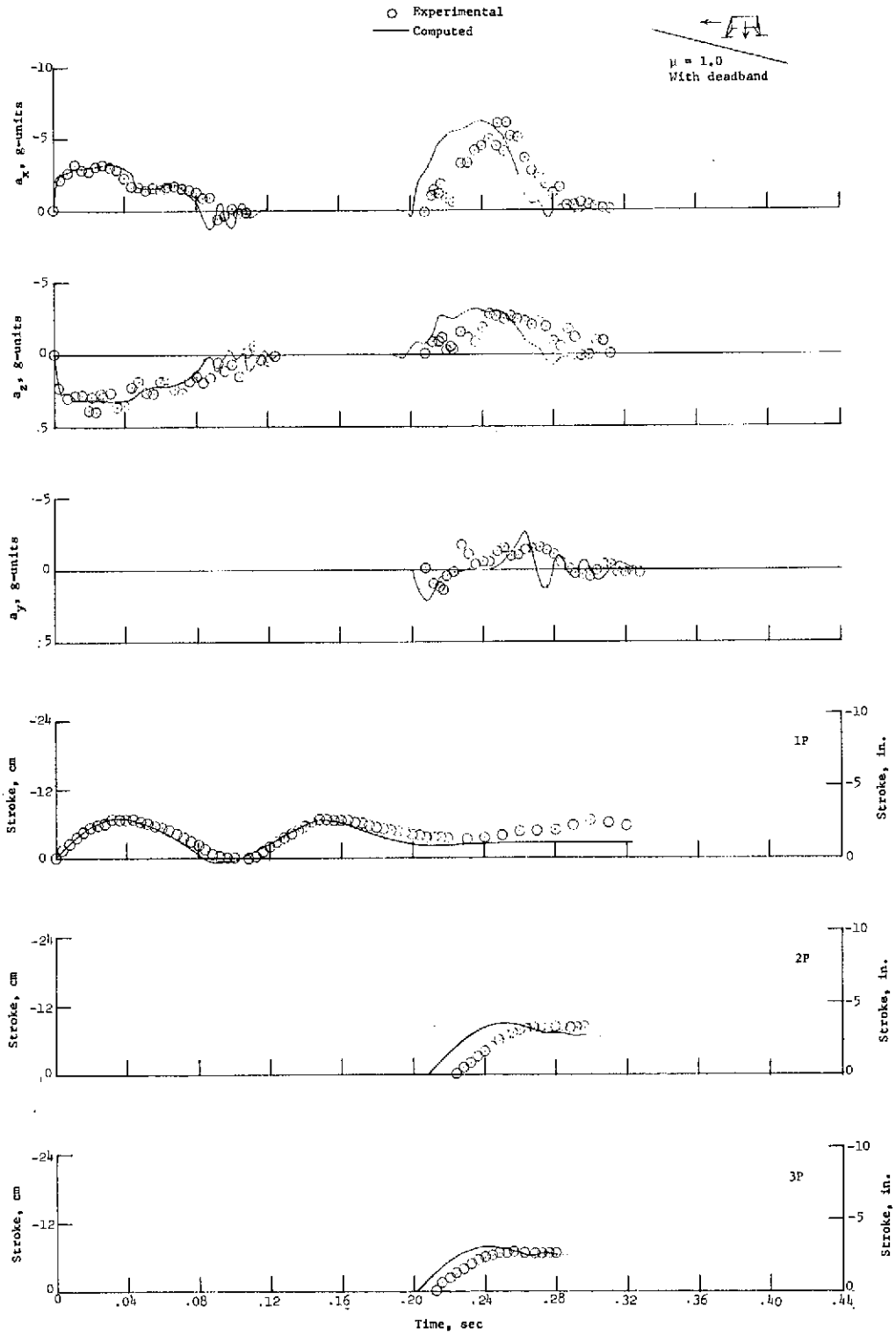

(c) Accelerations and primary-strut forces for case 11.

Figure 11.- Continued.

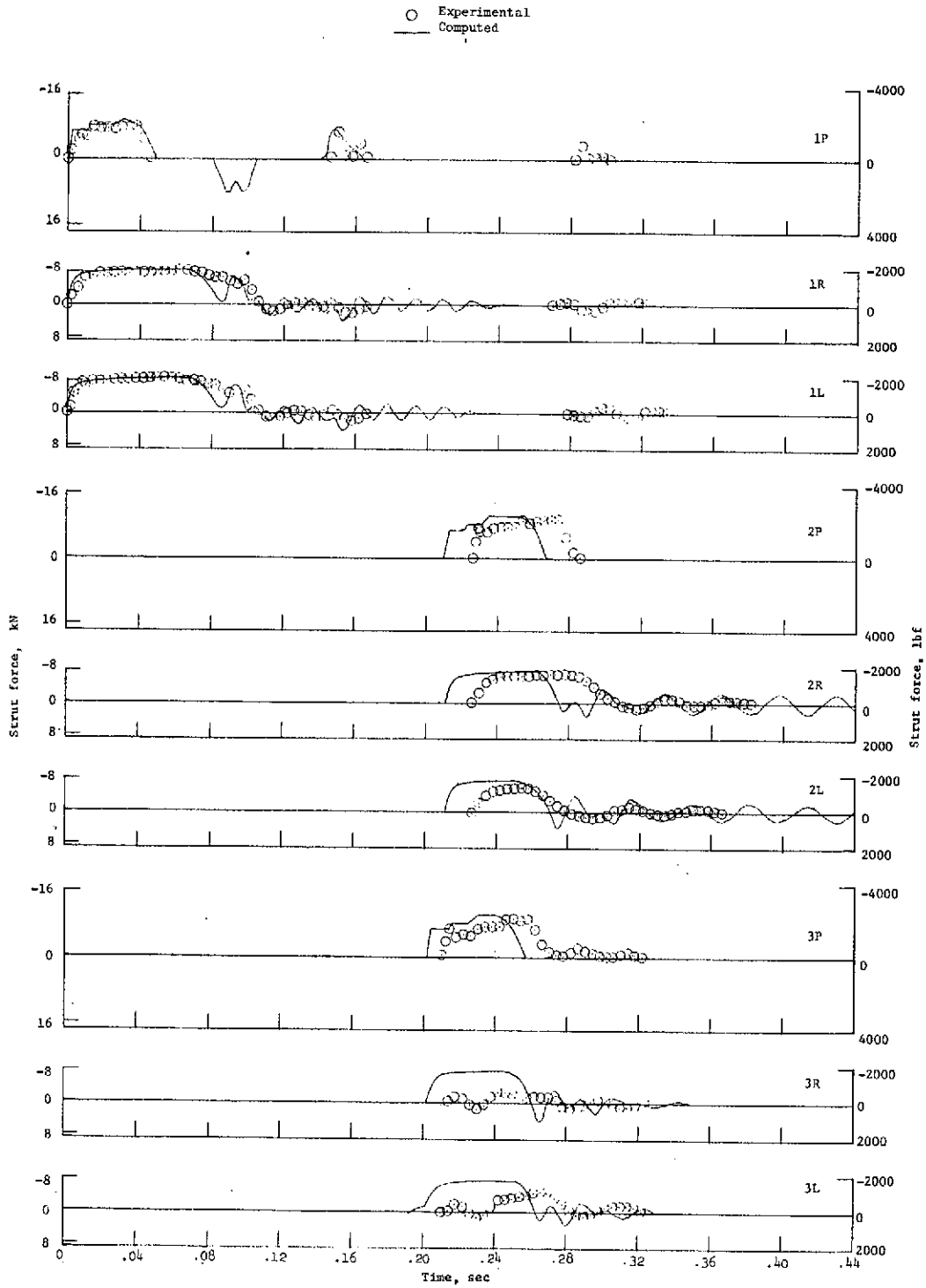

(d) Strut forces for case 11.

Figure 11.- Concluded.

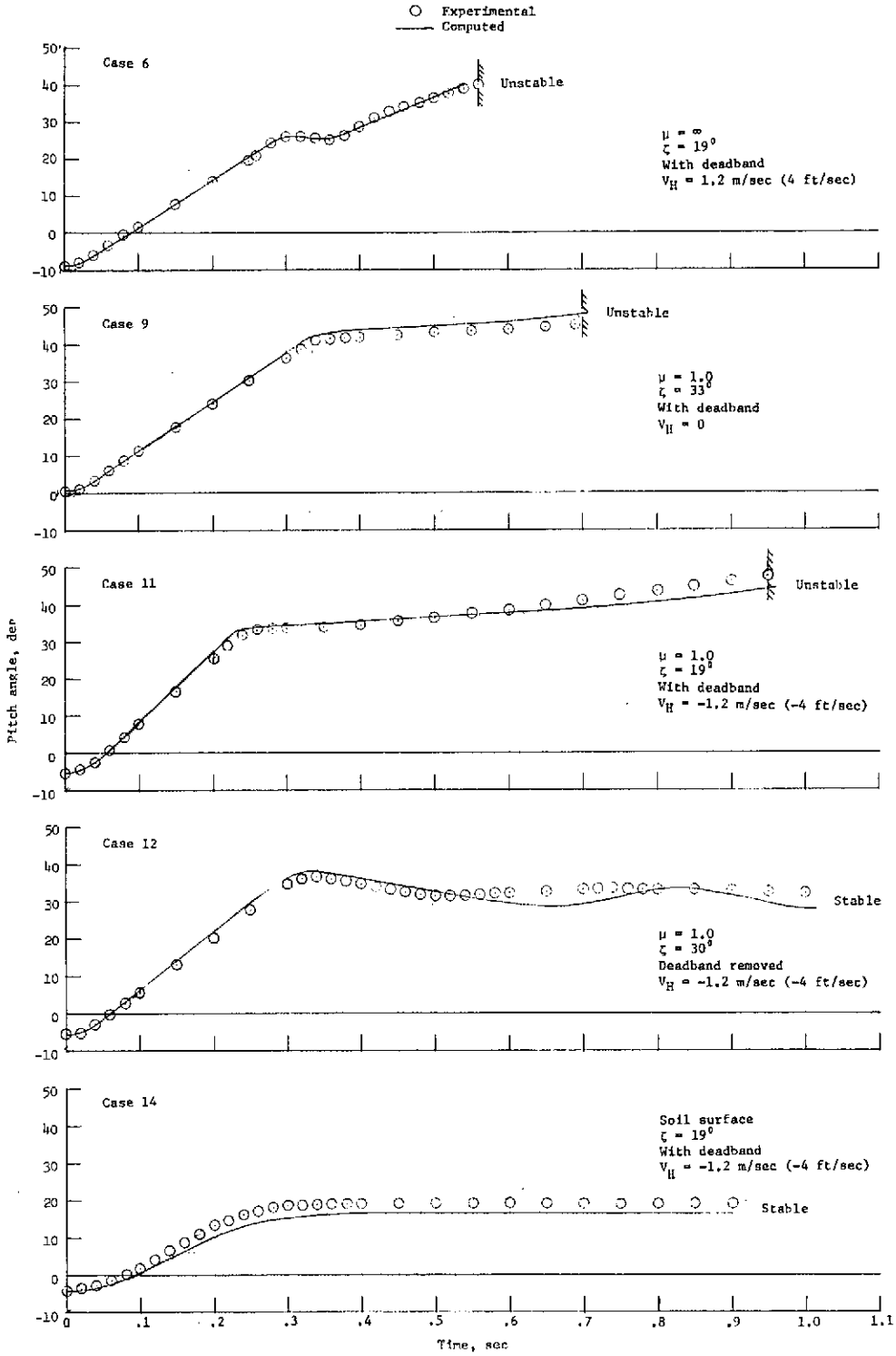

Figure 12.- Experimental and analytical time histories of pitch angle for selected cases. All values are full scale.

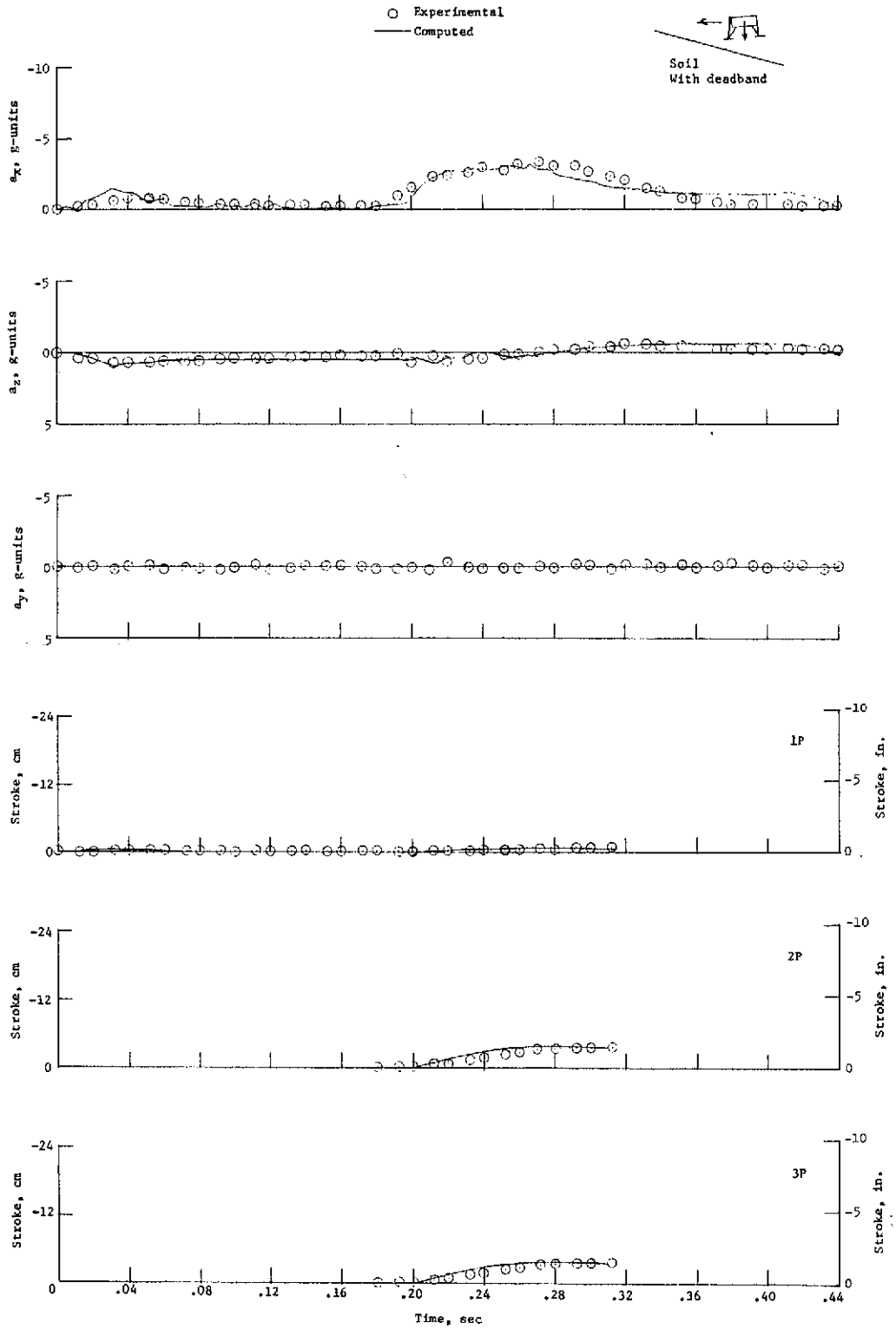

(a) Accelerations and primary-strut strokes for case 14.

Figure 13.- Experimental and analytical time histories for a landing on soft soil. All values are full scale.

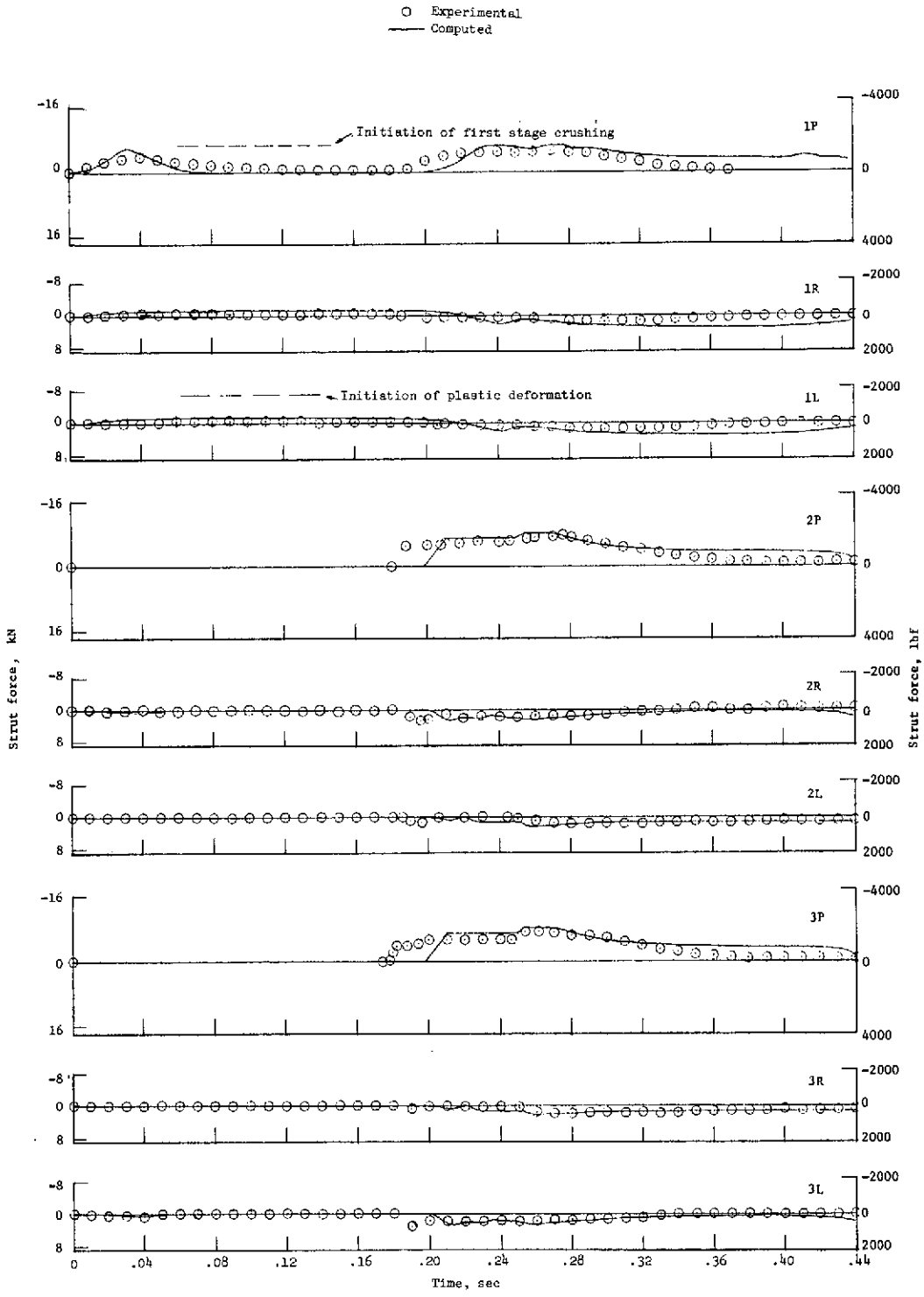

(b) Strut forces for case 14.

Figure 13.- Concluded.

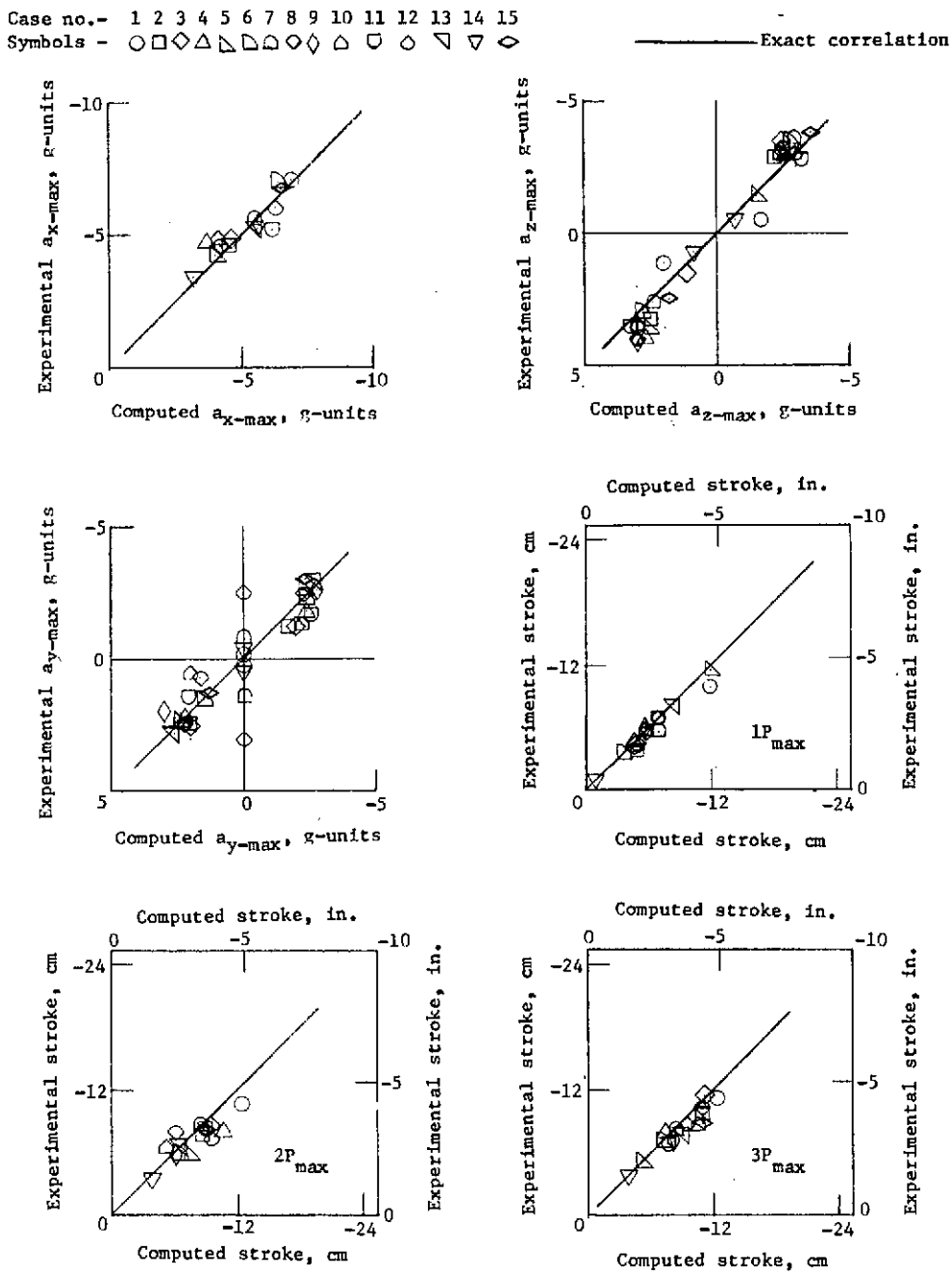

(a) Maximum center-of-gravity accelerations and primary-strut strokes.

Figure 14.- Correlation of experimental and analytical results. All values are full scale.

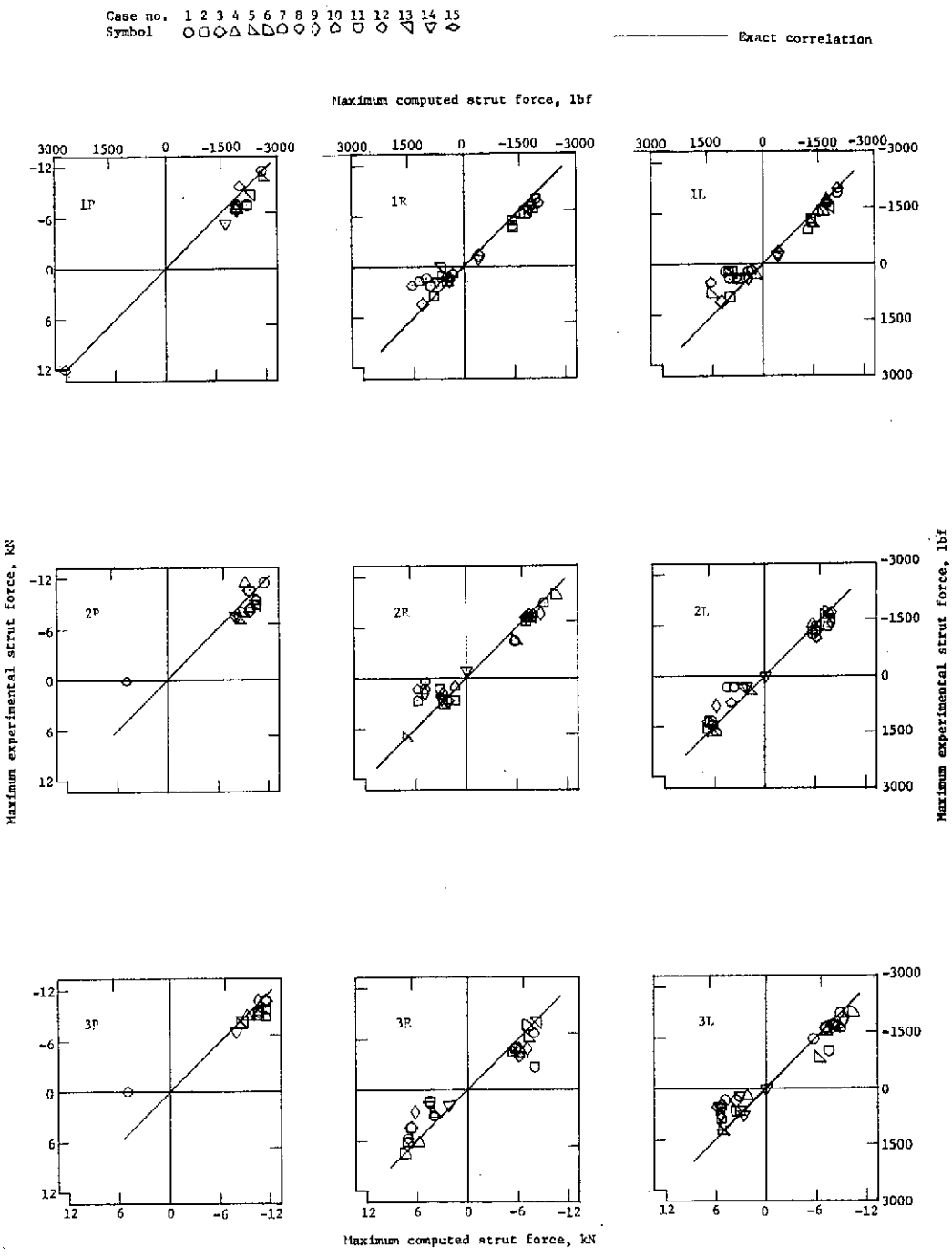

(b) Maximum primary- and secondary-strut forces.

Figure 14.- Concluded.

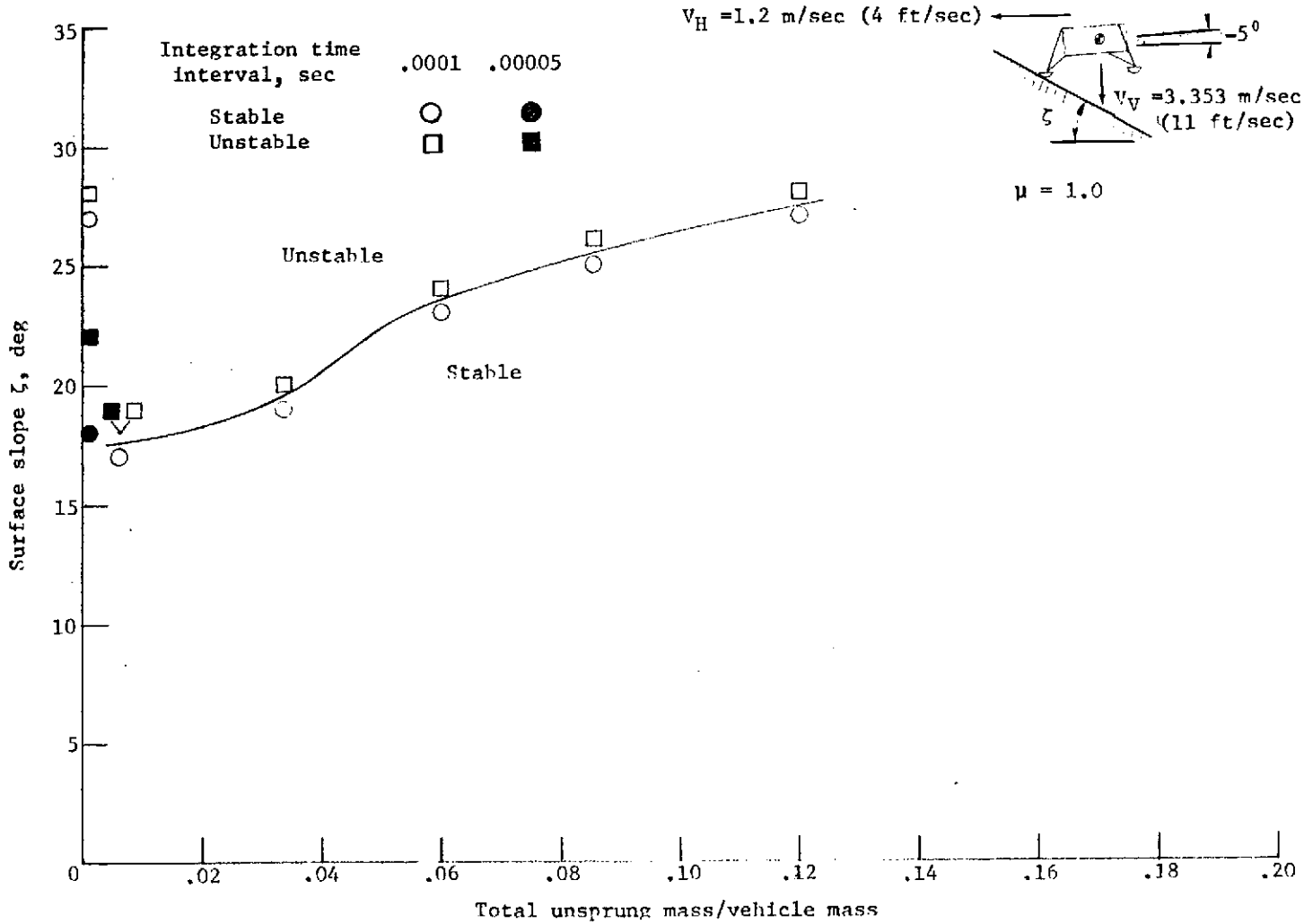

Figure 15.- Calculated stability-critical surface slopes as a function of the ratio of unsprung mass to vehicle mass. Total vehicle mass and moments of inertia are held constant. All values are full scale.

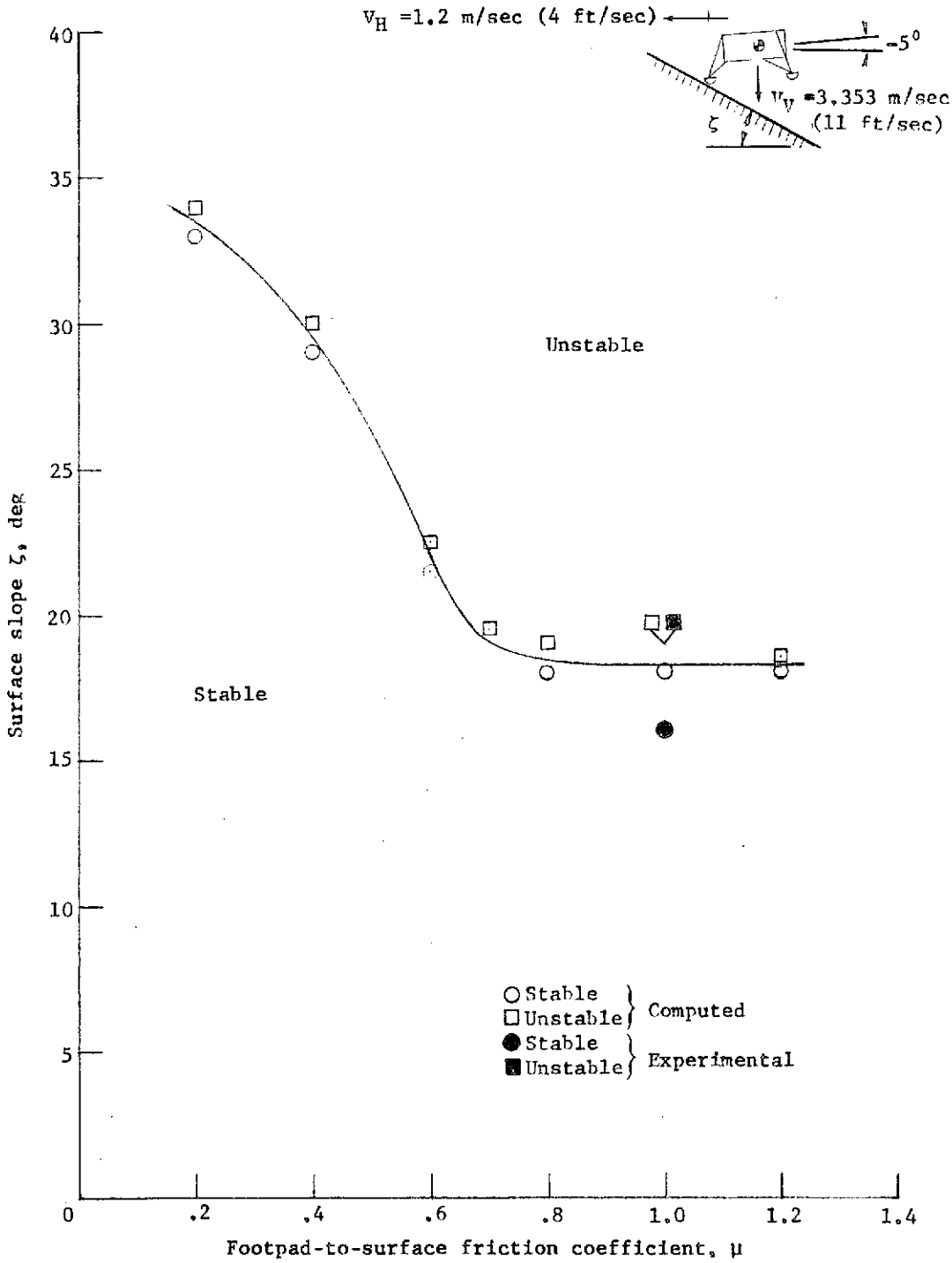

Figure 16.- Stability-critical surface slope as a function of footpad-to-surface friction coefficient. All values are full scale.